(NASA-CR-158851) COMPOSITE STRUCTURAL MATERIALS Semiannual Progress Report, Oct. 1978 - Apr. 1979 (Rensselaer Polytechnic Inst., Troy, N. Y.) 130 p HC A07/MF A01 CSCL 11D G3/24

N79-28235

Unclas
31644

L

RENSSELAER POLYTECHNIC INSTITUTE TROY, N.Y. 12181

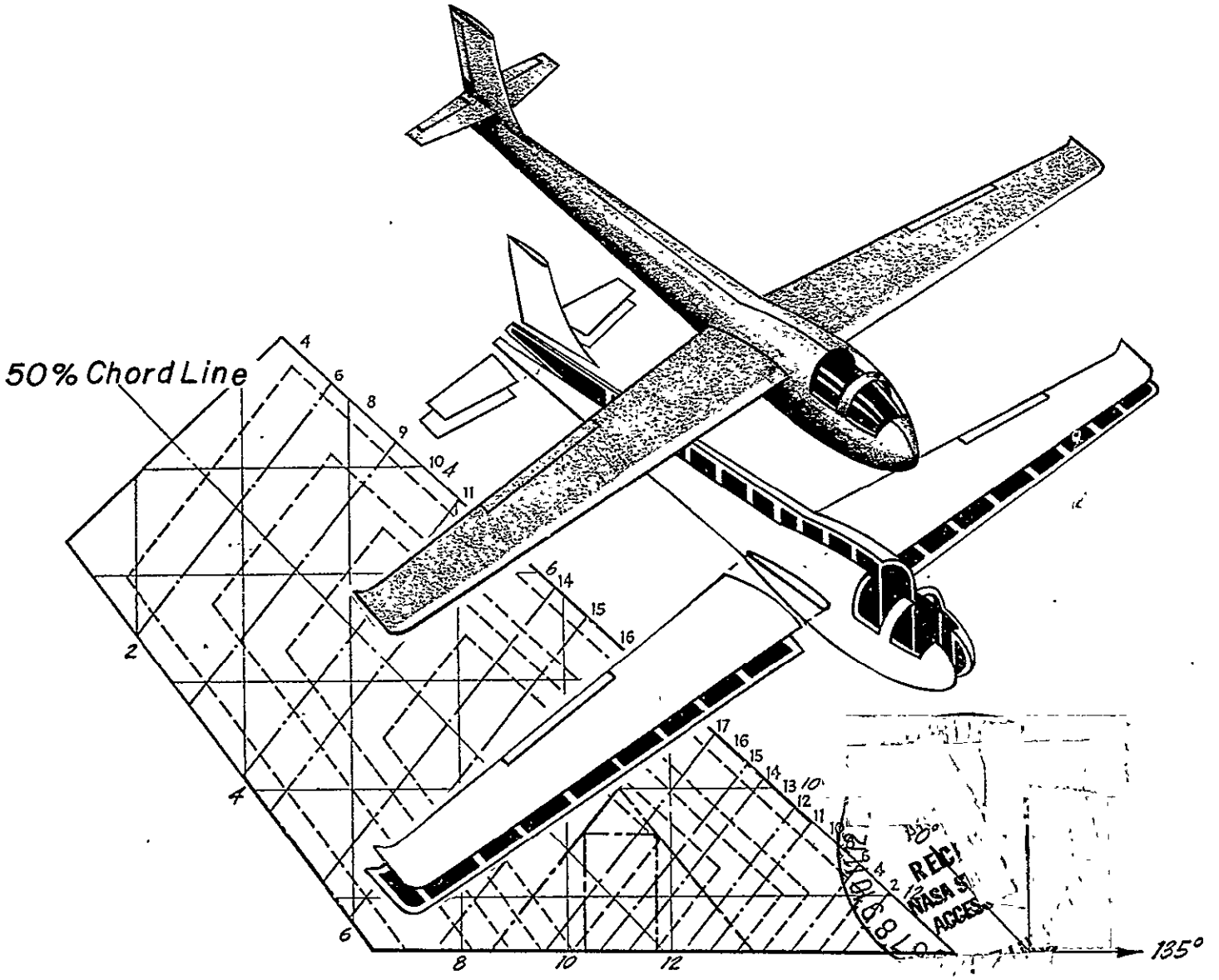

SKIN DESIGN

SPONSORED BY
NASA/AFOSR

Semi-Annual Progress Report

October 1978 - April 1979

COMPOSITE STRUCTURAL MATERIALS

Air Force Office of Scientific Research
and
National Aeronautics and Space Administration
Grant No. NGL 33-018-003

Co-Principal Investigators:

George S. Ansell
Dean, School of Engineering

Robert G. Loewy
Institute Professor

and

Stephen E. Wiberley
Dean, Graduate School and Vice Provost

Rensselaer Polytechnic Institute
Troy, New York 12181

NASA Technical Officer

Leonard A. Harris
Materials and Structures Division
NASA Headquarters

36th Semi-Annual Report

July 1979

CONTENTS

CONTENTS (Continued)

INTRODUCTION

INTRODUCTION

Technological demand for improved performance in materials has always existed. The recent interest in composite materials has been generated by the ability to use brittle materials with high modulus, high strength, but low density in composites which fail in a non-catastrophic manner. These fiber reinforced composite materials offer improved performance and potentially lower costs for aerospace hardware.

However, the application of composite materials to sophisticated aerospace structures requires a strong technology base. NASA and AFOSR have realized that to fully exploit composites the technology base must be improved, both in terms of expanding fundamental knowledge and the means by which it can be successfully applied in design and manufacture and also in the body of engineers and scientists competent in these areas. As part of their approach to accomplishing this, they have funded the current composites program at Rensselaer. The purpose of the RPI composites program is to develop advanced technology in the areas of physical properties, structural concepts and analysis, manufacturing, reliability and life prediction. Concommitant goals are to educate engineers to design and use composite materials as normal or conventional materials. A multifaceted program has been instituted to achieve these objectives.

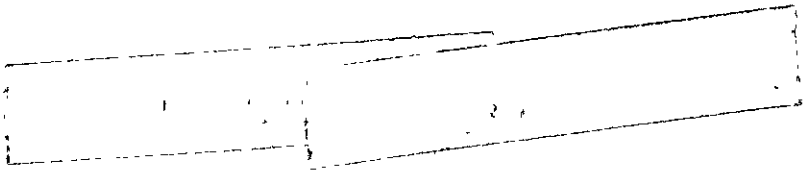

The major elements of the program are:

1. CAPCOMP (Composite Aircraft Program Component). CAPCOMP is primarily a graduate level project being conducted in parallel with a composite structures program sponsored by NASA and performed by a private, aerospace manufacturing contractor, the Boeing Commercial Airplane Company. The main spar/rib region on the Boeing 727 elevator, near its actuator attachment point, has been selected as the first component for study in CAPCOMP. The magnitude of the project - studying, designing, fabricating and testing the most highly stressed region on the elevator - is both consistent with Rensselaer's capabilities, and a significant challenge. The selection of a portion of a full-scale flight hardware structure assures relevance to this project's direction.

Visits to Boeing were conducted in the Fall of 1978 by Professor Hoff and several of his students, and the first serious design work began shortly thereafter. Progress on two alternative designs are reported in Part I.

2. CAPGLIDE (Composite Aircraft Program Glider). This undergraduate demonstration project is to design, fabricate and test a foot-launched, ultralight glider using composite structures. A flight vehicle was selected to maximize student interest and to provide the students with a broad-based engineering experience. For those students continuing with graduate work at RPI, CAPGLIDE is intended to

provide natural progression to CAPCOMP. The progress on the CAPGLIDE project to date has been satisfactory. Four professors and approximately 31 students were actively engaged in the project during the beginning of this period; that is, at the start of the fall semester. A description of the work performed under CAPGLIDE is given in Part II.

3. COMPAD (Computer Aided Design). A major thrust of the composites program is to develop effective and efficient tools for the analysis and design of composite structures. Rensselaer and NASA Langley have jointly implemented the use of the SPAR code on minicomputers. This work has been continued at Rensselaer during the past reporting period to make "virtual memory" available to those using SPAR. More complete details are reported in Part III.

4. Composites Fabrication and Test Facility. Structural design engineers, educated only by course work and design projects limited to paper, often fail to sense or appreciate problems involved in fabrication. The actual fabrication and testing of composite structural components provides this training and the final validation for the designs in our CAP projects. RPI's Composites Fabrication and Test Facility is located in the laboratory and high bay areas of the Jonsson Engineering Center. Equipment is available for compression molding parts as large as 19" x 19" and vacuum bagging parts up to 4' x 8'. Ultimately, panels as large as 5' x 20' will be made by vacuum bagging.

A pressure vessel for small parts and spars has been designed and was built during the last report period. NASA/AFOSR approval to order various pieces of specific test equipment for both materials and components was obtained during the last period and all deliveries have been made, increasing significantly our abilities in fabrication and testing areas. More complete details are reported in Part II under CAPGLIDE.

5. Research Programs. The criteria for selection of research projects to be conducted under this program are (a) that they must anticipate critical problem areas which may occur in the CAP or NASA/AFOSR programs or (b) that solutions to existing problems are not yet satisfactorily in hand. During the reporting period nine programs were funded; one has been phased out as we budget for the coming period. Results from the ongoing projects are reported in Part IV.

6. Curriculum Revisions. The goal of educating engineers to think of composites as normal or conventional materials has required changes in curriculum. Since the initiation of this program, almost all Rensselaer engineers take introductory courses which incorporate the concepts of anisotropy and composite materials. In addition, six specialized courses in composites have been offered during the past three years to develop those special skills required of students involved in the composites program. A new course was introduced in the Fall '78 Semester on composite design

and analysis using programmable hand calculators, a central mini and full frame computers. The additions of the SAP and SPAR computer codes and the growing availability of interactive computer graphics under our COMPAD program element are beginning to reach the point where our engineering students are using these facilities as everyday working tools for design, analysis and visualization purposes.

7. Technical Interchange.

a) As we approached the end of the reporting period Dr. Yoichi Hirano was finishing his research at RPI and preparing for return to the University of Tokyo. His stay at RPI has been most productive, as evidenced by reports on CAPCOMP and INSURE (Innovation and Supporting Research) in this and other progress reports. Dr. Gunter Helwig, our first "NASA/AFOSR Visiting Associate" has been offered and has accepted an appointment as Assistant Research Professor at RPI. With this appointment, he has agreed to lead the CAPGLIDE program element.

b) Technical meetings: Technical meetings, on- and off-campus, provide important opportunities for interchange of technical information. Because of the large number of composites meetings, a central catalog with all upcoming meetings is being maintained and distributed periodically. In this way we help assure that a Rensselaer staff member will participate in important meetings. The calendar for this reporting period is shown in Table I. Meetings attended by RPI composites

TABLE I

CALENDAR OF COMPOSITES-RELATED MEETINGS

for the period October '78 to April '79

1978

10/30-31	Grumman/University Technology Forum, Bethpage, New York. Sponsored by Grumman.
10/29-11/1	Symposium on Future Trends in Computerized Structural Analysis and Synthesis, Marriott Hotel, Washington, D. C. Sponsored by George Washington University and NASA/Langley.
11/7-9	Reinforced Plastics/Composites Institute Corrosion Resistant Structures Conference, Caesars Palace, Las Vegas, Nevada. Sponsored by AIAA.
11/14-17	4th Conference on Fibrous Composites in Structural Design, Sheraton Harbor Island Hotel, San Diego, California. Sponsored by U. S. Army.
11/28-30	Mechanical Failures Prevention Group, Symposium on Detection, Diagnosis and Prognosis, San Antonio, Texas. Sponsored by National Bureau of Standards.
12/6-7	Conference on NDT as Applied to Materials and Energy Conservation, Arlington, Virginia. Sponsored by ASNT.
12/14-15	Composite Materials in Auto Industry, San Francisco, California. Sponsored by AIAA/ASME.

1979

1/15-17	17th Aerospace Sciences Meeting, Grand Hotel, New Orleans, Louisiana. Sponsored by AIAA.
1/15-19	Gordon Research Conference on Polymers, Miramar Hotel, Santa Barbara, California.
1/22-26	Gordon Research Conference on Deformation and Failure Mechanisms in Polymers and Composites, Miramar Hotel, Santa Barbara, California.
2/6-9	34th Annual Reinforced Plastics/Composites Conference and Exhibit, Shoreham Americana Hotel, Washington, D. C. Sponsored by AIAA.
3/20-22	Special Review of ACEE Composites Programs, Huntington-Sheraton Hotel, Pasadena, California. Sponsored by NASA.

program faculty/staff during the reporting period are shown in Table II. Some meetings held on-campus with off-campus speakers, particularly relevant to composites, are listed in Table III. A list of composite-related visits to relevant organizations by RPI faculty/staff/students, with the purpose of each visit outlined, is presented in Table IV.

In summary, the NASA/AFOSR Composites Aircraft Program is a multi-faceted program whereby aeronautical, mechanical and materials engineers must interact to achieve its goals. "Hard-nosed" engineering of composite aircraft structures is balanced against research aimed at solving present and future problems. In the following sections, detailed descriptions of the CAPCOMP, CAPGLIDE, COMPAD and INSURE programs are presented.

TABLE II

COMPOSITES-RELATED TECHNICAL MEETINGS ATTENDED OFF-CAMPUS

for the period October '78 to April '79

1978

9/25-27	1978 Ultrasonic Symposium (Prof. Tiersten), Cherry Hill, New Jersey.
10/2-5	National Fall Conference, American Society of Non-Destructive Testing (Prof. Das), Denver, Colorado.
10/17-18	ARO/NSF Workshop on The Mechanics of Composite Materials (Profs. Hoff, Krempl, Sternstein), Duke University, Durham, North Carolina.
10/21-23	International Conference on Interactive Techniques in Computer Aided Design (Prof. Wozny), Bologna, Italy.
10/30-31	Grumman/University Technology Forum (Prof. Hagerup), Bethpage, New York.
10/31-11-2	Mechanics of Composites Review (Prof. Loewy), Dayton, Ohio.
11/13-17	Third International Meeting on Metallic Composite Materials (Prof. Diefendorf), Surolenice, Czechoslovakia.
11/13-18	4th Conference on Fibrous Composites in Structural Design (Prof. Hoff), San Diego, California.
11/14-15	QCSEE Engine Review (Prof. Loewy), Lewis Research Center, Cleveland, Ohio.
12/4-7	5th Structural Composites Manufacturing Applications Conference - SME (Profs. Helwig, LeMaistre), St. Petersburg, Florida.
12/8-16	ASME Annual Meeting (Prof. Hoff), San Francisco, California.

1979

1/9-10	NASA/Langley Composites Group Meeting (Prof. Sternstein), Langley Research Center, Norfolk, Virginia.

TABLE II continued.

1979

1/22-25	3rd Annual American Ceramics Society Conference on Composites and Advanced Materials (Prof. LeMaistre), Merritt Island, Florida.
1/22-26	Gordon Research Conference on Deformation and Failure Mechanisms in Polymers and Composites, (Prof. Diefendorf), Santa Barbara, California.
3/20-22	Special Review of NASA's ACEE Composites Programs (Prof. Helwig), Pasadena, California.
3/28-31	3rd International Symposium on The Science and Technology of Low Speed and Motorless Flight (Prof. Helwig), Langley Research Center, Norfolk, Virginia.

TABLE III

COMPOSITES RELATED MEETINGS/TALKS HELD AT RPI

(October '78 - April '79)

Topic	Date	Speaker(s)
Heat Propagation in Layered Composites; A Singular Perturbation Problem	Sep. 20, '78	Gabriel Horvay, Professor, Dept. of C.E., University of Massachusetts
Random Vibration Analysis of Structures and Identification of Structural Systems	Oct. 25, '78	Chung-Bang Yun, Polytechnic Institute of New York
Finite Element Analysis with Buckling Mode Superposition	Nov. 7, '78	Dennis A. Nagy, Princeton University
Gas Turbines - The State of the Art & What Lies Ahead	Nov. 14, '78	Justin Neuhoff, Consultant-Engineering Operations, Gas Turbine Div., G. E. Co.
Mechanical Invention: An Act of Inspiration or a Branch of Applied Mechanics?	Dec. 7, '78	Ferdinand Freudenstein, Prof., Dept. of M.E., Columbia Univ.
Reliability of Structural Systems	Jan. 23, '79	Mark P. Gorman, Case Western Reserve University
Analysis of Hartford Civic Center Roof Collapse	Jan. 26, '79	Howard Epstein, Professor, University of Connecticut
Advanced Prop Fan Development Program	Jan. 29, '79	George E. Clute, Mgr, Product Marketing; and Arthur Jackson, Mgr, Aero Systems, Hamilton Standard, Div of UTI
Light-Weight Fabrication Techniques for Wing Structures	Feb. 1, '79	Robert Baucom, NASA Langley
Reliability Evaluation of Existing Structures	Feb. 9, '79	S. J. H. Chen, Purdue University
Development of QCSEE Turbofan Composite Structures	Feb. 19, '79	Robert Stabrylla, Mgr, Composite Blade Design, G. E. Co.
Space Truss Design: The Polyhedral Chain Group	Feb. 27, '79	Martin F. Rooney, Professor, Carnegie-Mellon University
Design For The Prevention of Progressive Collapse Using Interactive Computer Graphics	Mar. 6, '79	John L. Gross, Cornell University

TABLE IV

COMPOSITE-RELATED VISITS TO RELEVANT ORGANIZATIONS

by RPI Faculity/Staff/Students

Visited	Date	By Prof(s).	Purpose
Cornell University: Profs. J. Abel L. Phoenix	10/30/78	R. G. Loewy	To review computer graphics, statistical approach to composites strength.
NASA/Langley: Mr. R. Baucom	12/20/78	N. Hoff	To discuss composite spoiler design for the 737.
U. of Deleware: Profs. B. Pipes A. Metzner	12/28/78	R. G. Loewy	To discuss program of the Delaware Composite Center
NASA/Lewis: Mr. J. Freche	1/8/79	P. Das H. Tiersten J. McDonald	To discuss NDE techniques.
MacD.D.A.C.: Mr. P. Fleetwood	1/10/79	P. Das H. Tiersten J. McDonald	To discuss NDE techniques.
NASA/Langley: Mr. B. Stein	1/10/79	E. Krempl N. Stoloff S. Sternstein	To discuss fatigue and fracture mechanism composites.
NASA/Langley: Mr. P. Hanson	1/11/79	E. Brunelle	To review developments in composite aeroelasticity.
Boeing Com. A.C.: Mr. S. Harvey	1/11/79	P. Das H. Tiersten J. McDonald	To discuss NDE techniques.

PART I

'APCOMP (Composite Aircraft Program Component)

CAPCOMP (Composite Aircraft Program Component)

(N. Hoff, Y. Hirano, K. Kenmochi)

CAPCOMP is a program to design flight critical structures to take the maximum advantage of composite materials. By combining the efforts of experienced faculty with bright and well trained but inexperienced graduate students in an environment relatively free of traditional design and manufacturing processes, we hope to devise new and hopefully useful design concepts.

There is sufficient information available today to prove that many structural elements can be built lighter of advanced composites than of metals. But if such elements have to be joined by any other method than adhesive bonding, difficulties and uncertainties arise which can be eliminated only through conservative designs with their attendant penalties in weight or by extensive and expensive programs of "cut and try". This stands as one important impediment to full adoption of composites by the aerospace industry.

On the basis of these considerations Rensselaer Polytechnic Institute began, as the first task aimed at new structural concepts, the design using composites of a joint used in an airplane elevator. To make the design realistic, an existing metal airframe component was chosen for redesign in composites. The existing design chosen was that of the Boeing 727 elevator actuator attachment. We conceive of

this work as carrying forward a Structures Demonstration Program using the joint of the 727 elevator, in parallel with NASA and its aerospace engineering contractor, the Boeing Commercial Airplane Company. Our design, fabrication and test effort will emphasize design ideas specifically suited to advanced composite construction for the purpose of minimizing the weight of the structure, but on a scale consistent with the university context and funding level. The staff of RPI is very grateful to the Boeing Aircraft Corporation and its engineers for their wholehearted support of the work at RPI.

During the reporting period, two different designs suitable for replacing the largely metal attachment produced by Boeing were begun. The first and more conservative made use of quasi-isotropic graphite-epoxy laminates; it was developed by R. W. Berg, a graduate student. A second graduate student, Christoph Muser, developed a second design in which a conscious attempt was made to use uniaxial graphite-epoxy tape to as great extent as possible. Both men carried out their designs, analyzed them, built parts of them, and tested representative sub-structures.

A third graduate student, Wonsub Kim, with the help of Research Associate, Kiyoshi Kenmochi, built tensile test specimens with empty or loaded circular holes to determine the most efficient arrangement of the fibers around the hole. The two men have been using photoelastic equipment

to find strain concentration factors. This work is largely in support of the design effort of Berg and Muser.

The entire work here described has been directed by Dr. Nicholas J. Hoff, Clark-Crossan Professor of Engineering.

1. The Elevator and Its Attachment

The conventional aluminum alloy elevator of the Boeing 727 is shown in the upper half of Figure 1. The lower half of the figure is the new version of the elevator redesigned by Boeing in graphite epoxy; it is evident from the pictures that the latter is composed of fewer parts than the former. However, the actuator fitting of the new design is still manufactured of aluminum alloy. This fitting is shown in Figure 2. The fitting is attached to outboard and inboard portions of a new graphite-epoxy spar and to a graphite-epoxy nomex-honeycomb rib as indicated in Figure 3.

The attachment was designed by Boeing to carry loads up to 19,000 lbs. The direction of the load varies as the elevator rotates over an angle of 28 degrees from the full-down to the full-up position.

2. Berg's Design

Berg's design is shown in Figures 4, 5 and 6. The first of these figures compares the Boeing composite design with Berg's design; both are shown. Figure 5 is an axonometric view of Berg's original design; it shows the

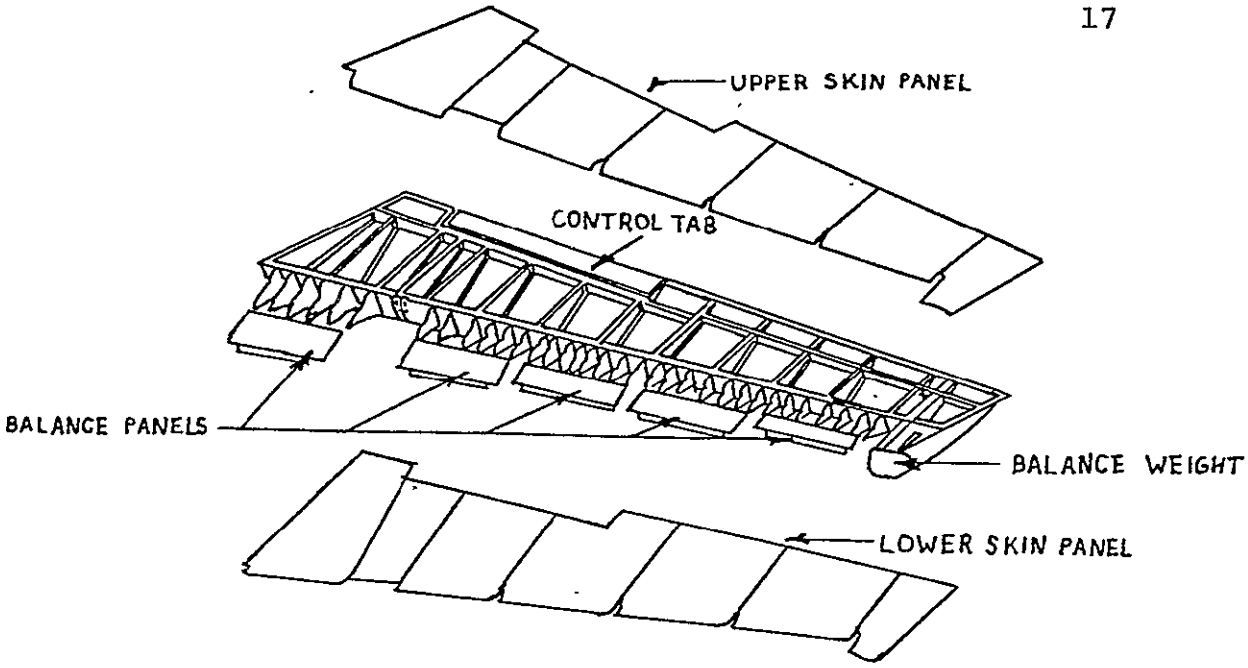

Conventional Aluminum Elevator

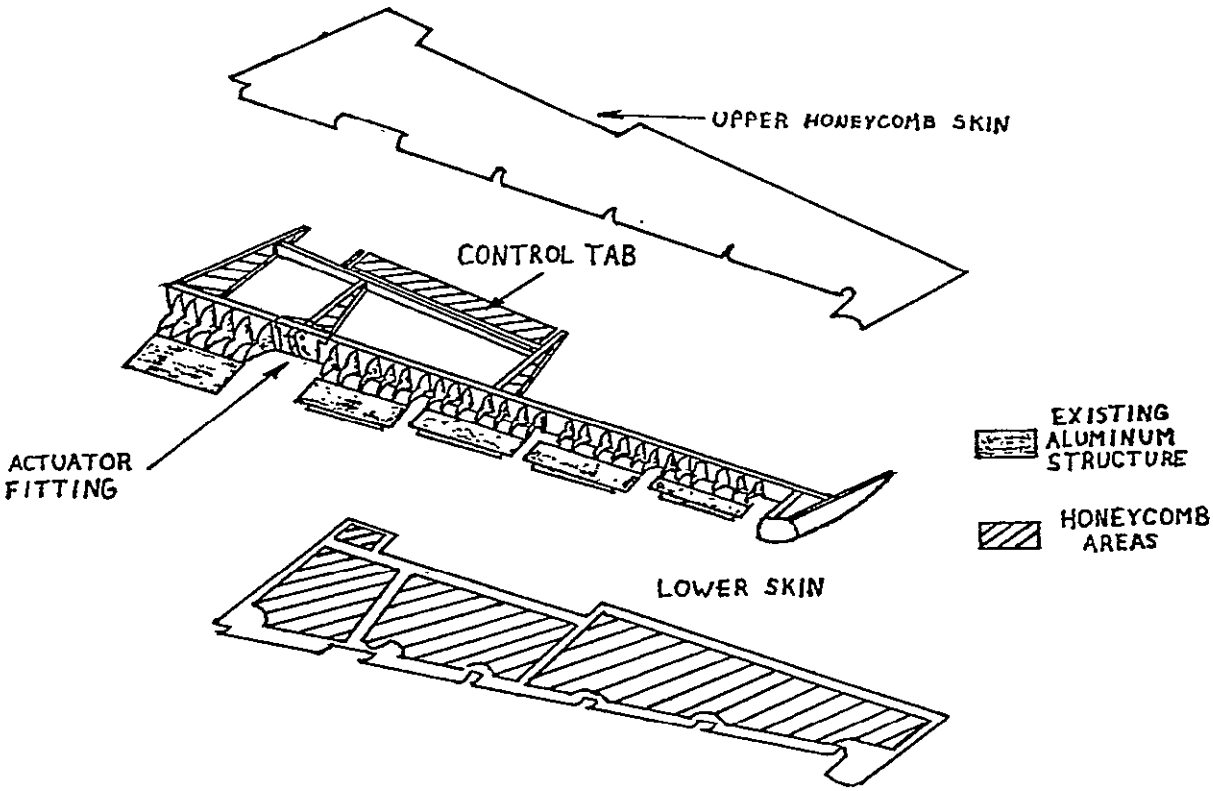

Advanced Composite Elevator

BOEING ELEVATOR ASSEMBLY

Fig. 1

ALUMINUM ACTUATOR FITTING (Boeing Design)

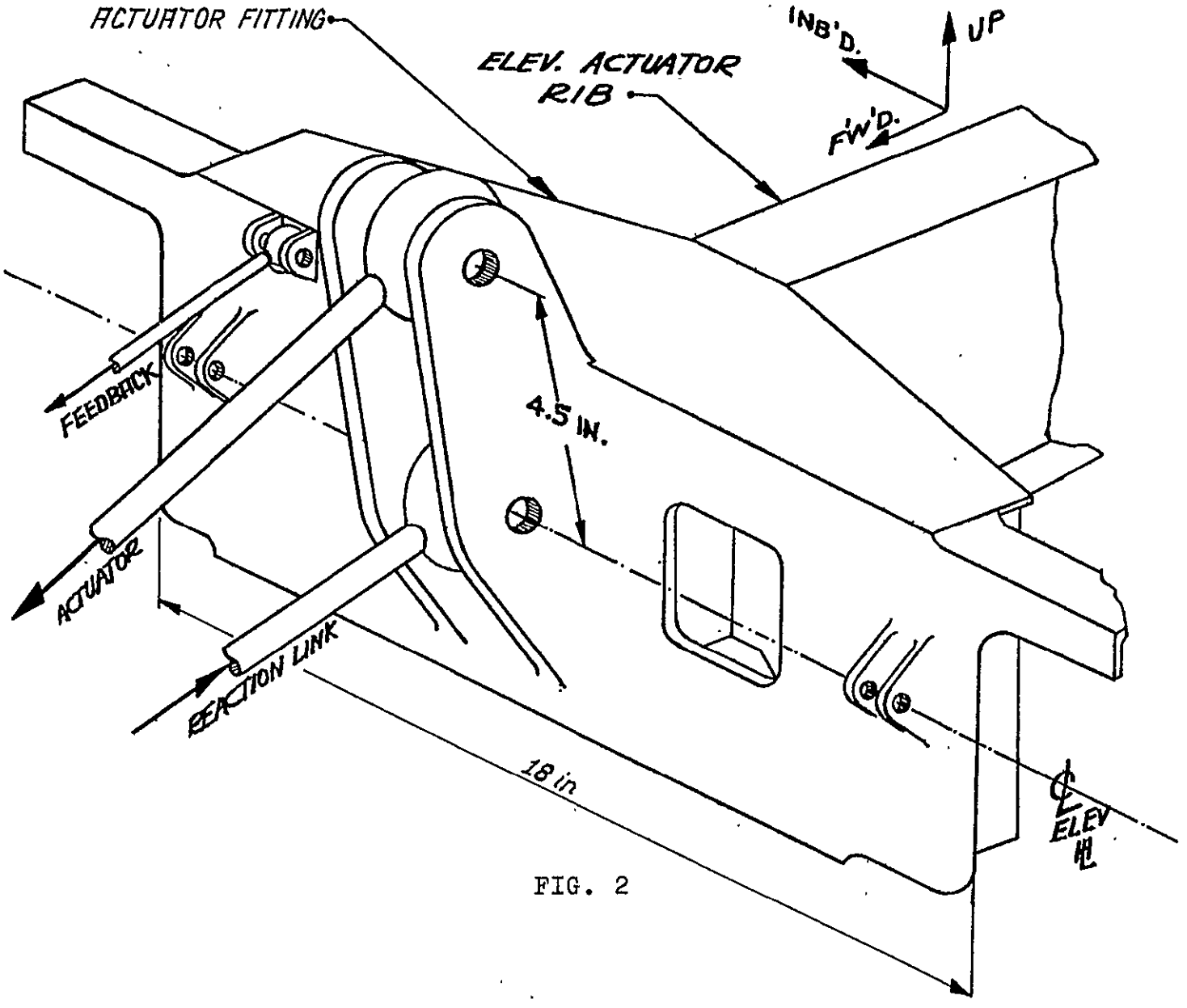

FIG. 2

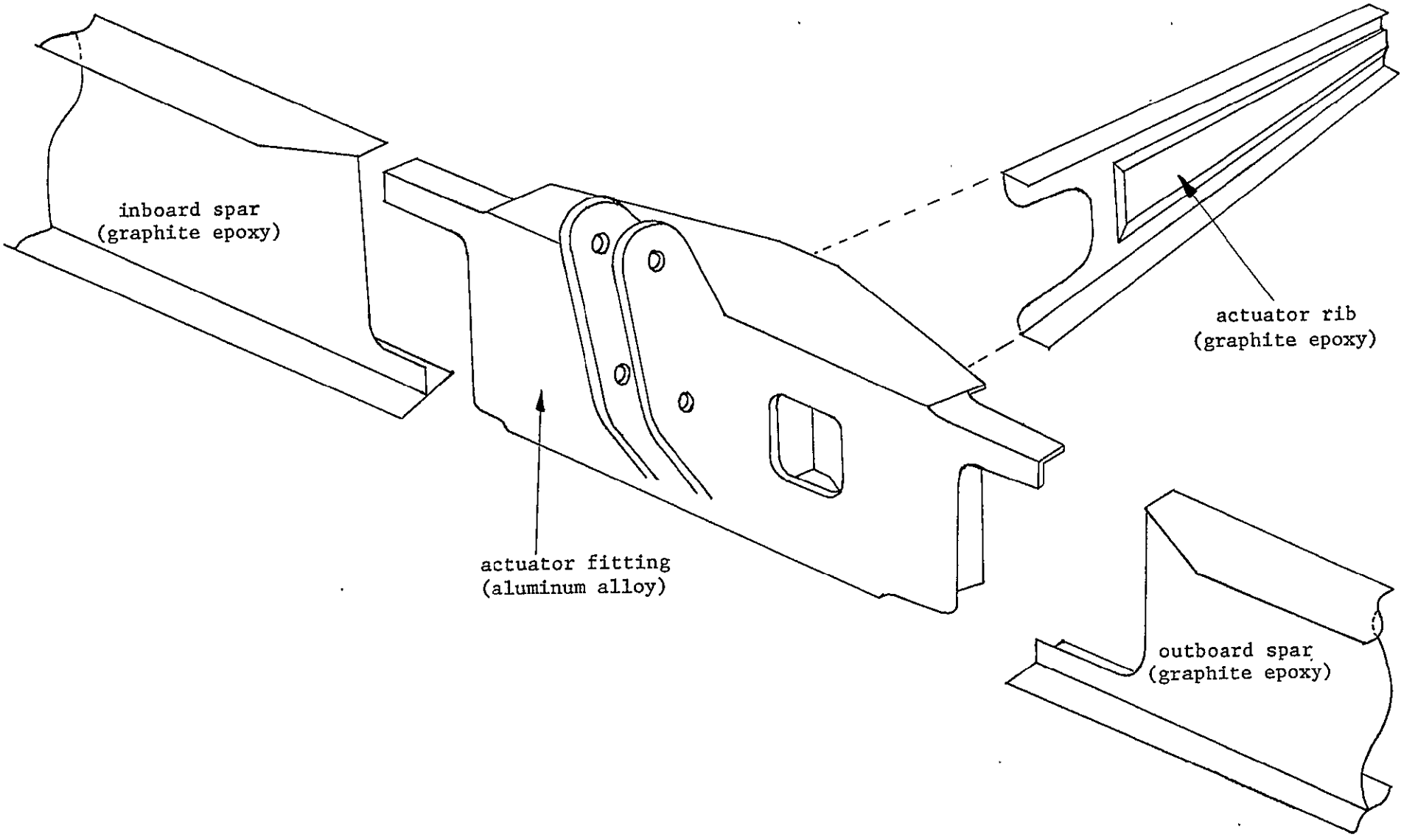

COMPOSITE ELEVATOR ACTUATOR ASSEMBLY (Boeing Design)

Fig. 3

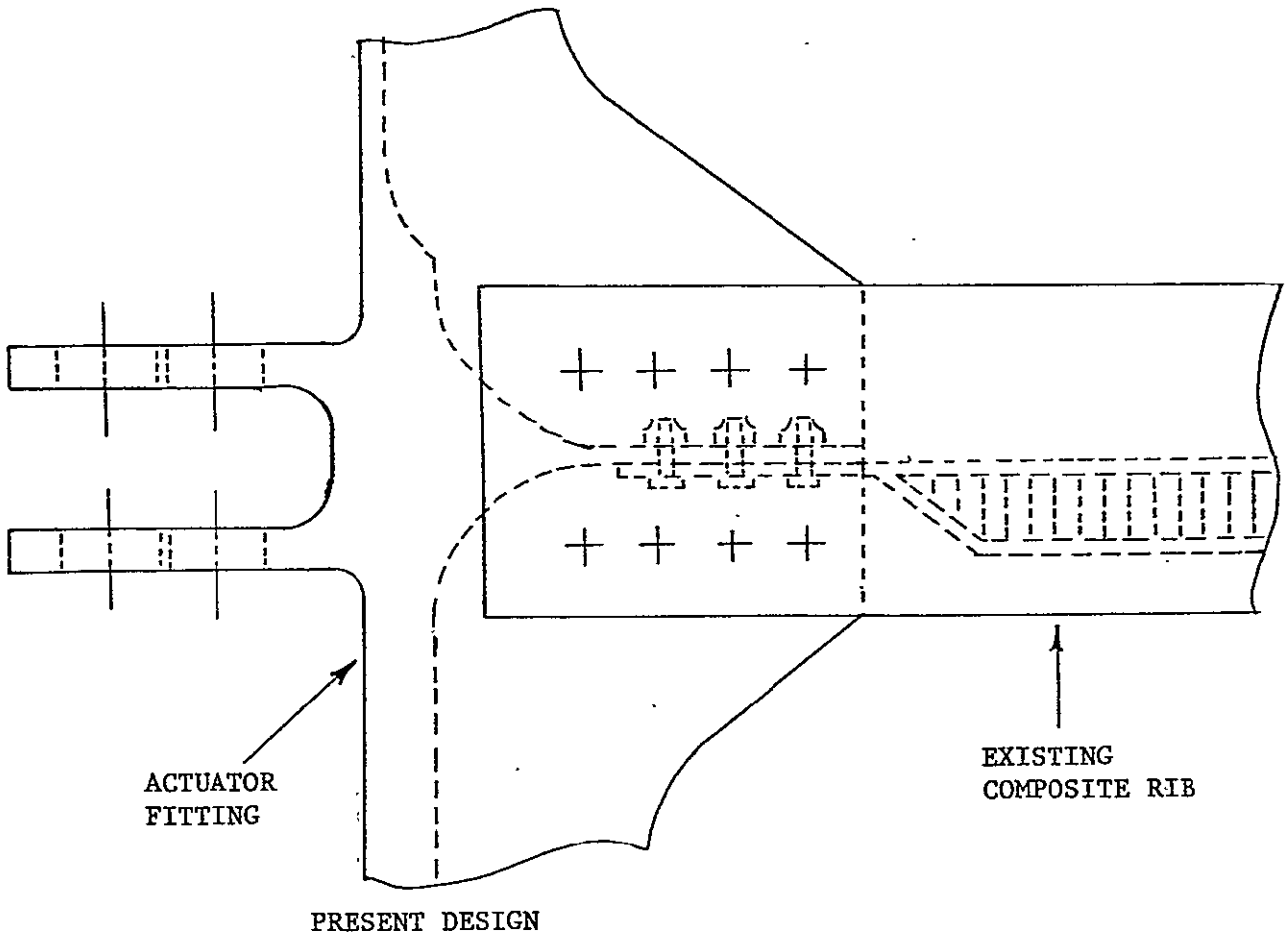

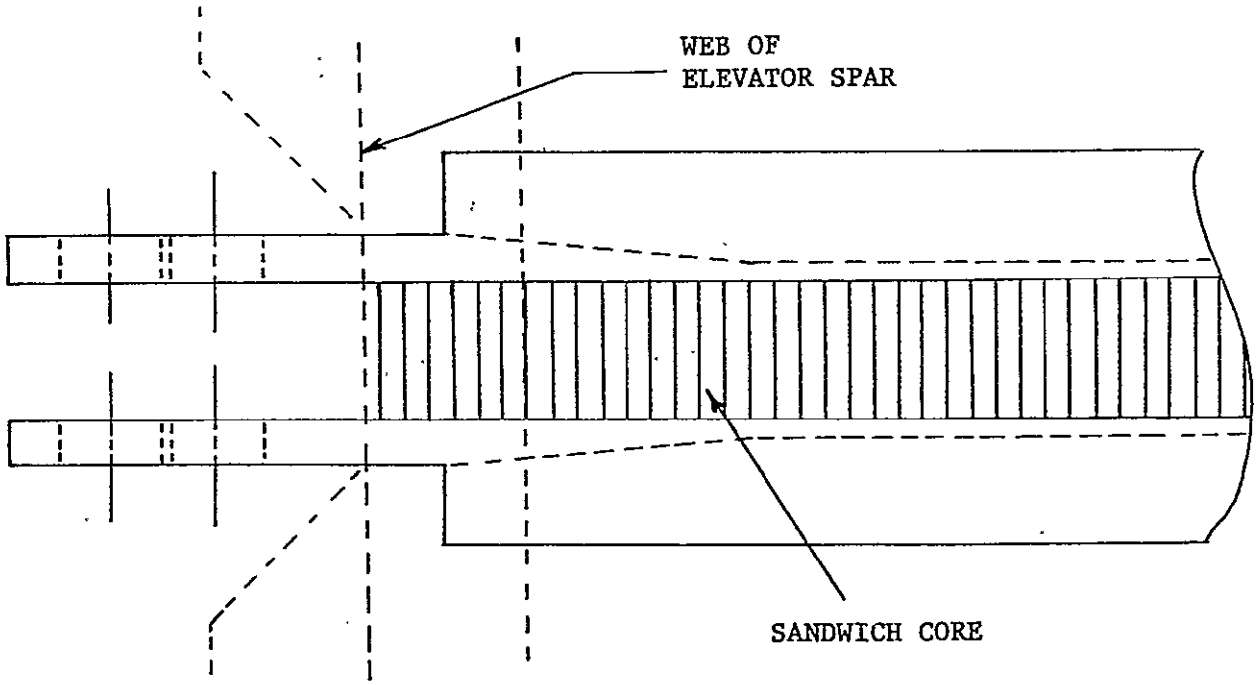

ACTUATOR LUG TO RIB TRANSITION - TOP VIEW

FIG. 4

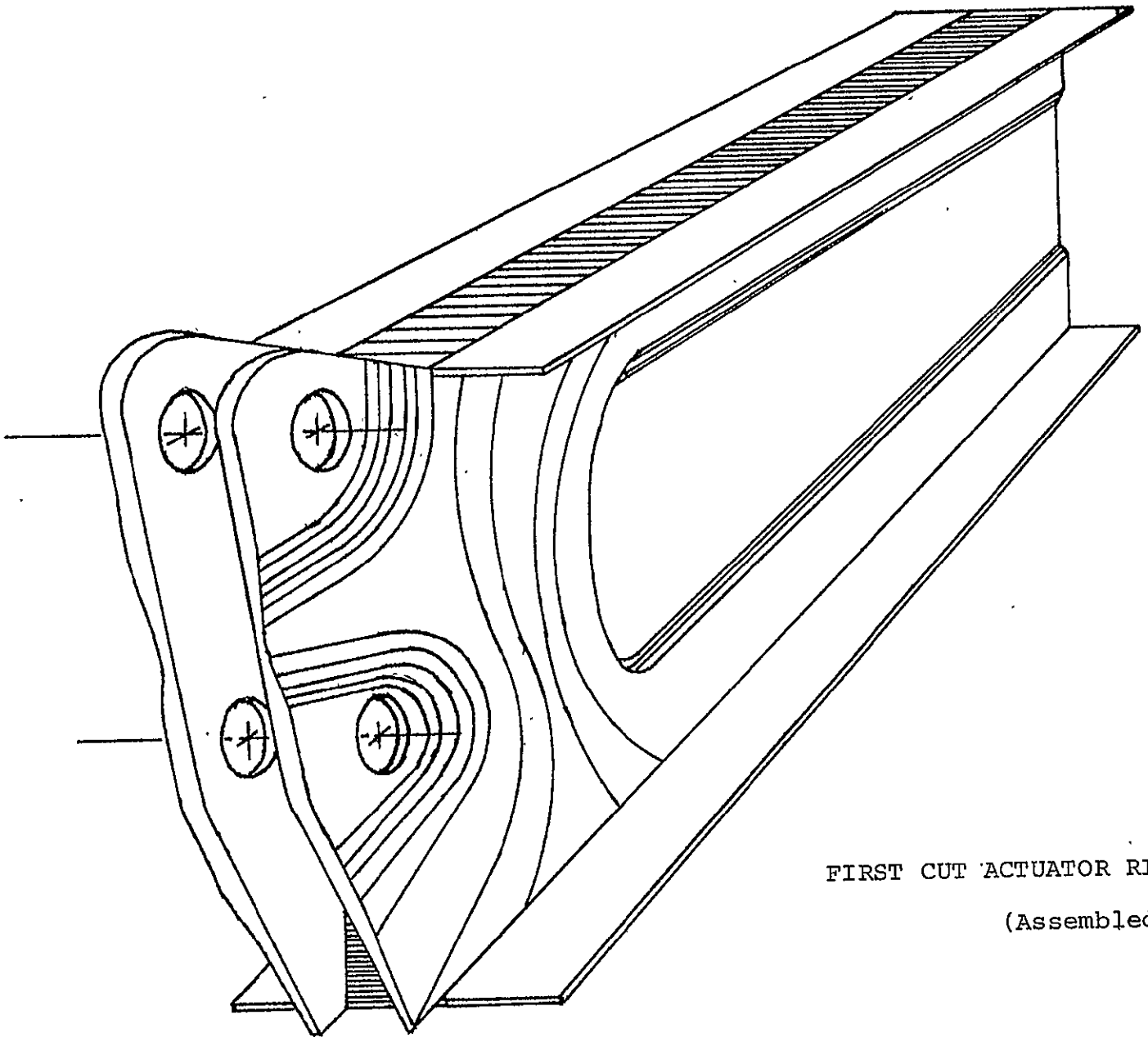

FIRST CUT ACTUATOR RIB (Berg Design)

(Assembled Rib)

FIG. 5

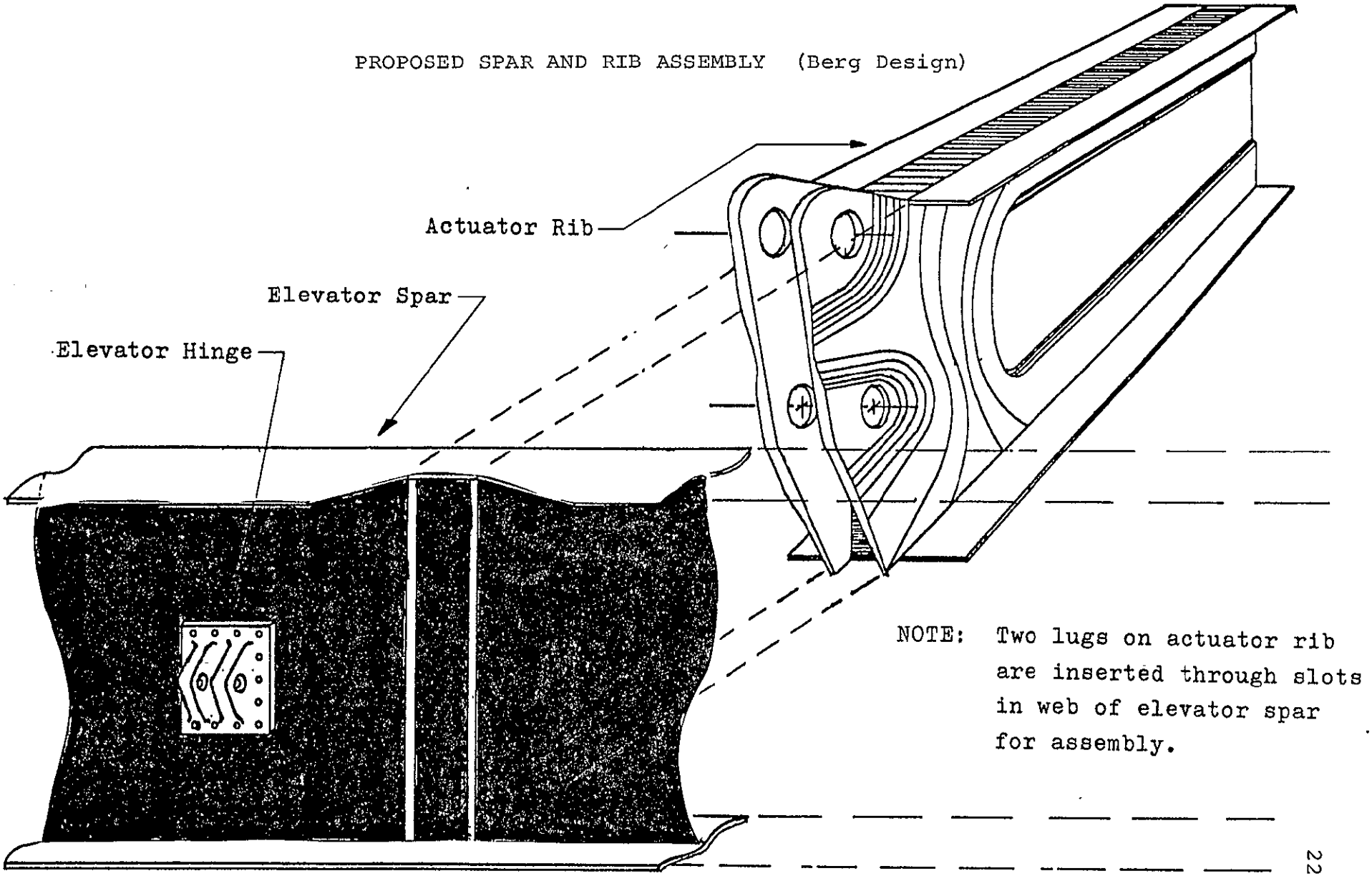
PROPOSED SPAR AND RIB ASSEMBLY (Berg Design)
Actuator Rib
Elevator Spar
Elevator Hinge
NOTE: Two lugs on actuator rib are inserted through slots in web of elevator spar for assembly.

FIG. 6

substantial build-up of thickness in the lug areas to provide the required bearing strength. The number of graphite-epoxy layers decreases with distance from the bolt holes. Figure 6 shows how the spar and new acturator rib would be assembled. It will be noted that the edges of some of the layers are bent 90 degrees to form flanges to which the upper and lower coverplates of the elevator can be attached. Attachment would be by means of titanium Hi-Loc fasteners. The right-hand and left-hand graphite-epoxy webs are stabilized by a layer of nomex-honeycomb between them.

After an approximate preliminary analysis, a computer program for a more accurate finite-element analysis of the actuator rib web (including the areas of the lugs with the bolt holes) was developed. The main objective of the analysis was to examine the stress distribution in the area of the holes and the way these stresses transfer loads to the flanges of the actuator rib. Thus, in the first computation the wall thickness of the actuator rib web was taken as constant. Forces were introduced as they would be through the actuator and reaction links (see Figure 2), simulating bolt loads. The reacting torque, as would result from aerodynamic forces on the elevator, was represented by distributed shear flow along the upper and lower edges of the actuator rib. The finite-element model contained 482 nodes and a total of 800 quadrilateral and triangular elements;

its length is 60% of the full length of the rib, the same length as the Boeing test specimen.

The results of the finite-element computations are the stress levels shown in Figure 7. As expected, there are high stress levels around both bolt holes, but unexpectedly lower levels between the holes. The stresses continue from the upper hole rearward on the upper rib flange at higher levels than first predicted. On the basis of these results, the thickness distribution of the web of the actuator rib was modified as shown in Figure 8.

A concurrent series of experiments were performed to obtain data on the strength of the composites to be used. Four simple test specimens, 7" long, 2" wide and 0.22" thick, were manufactured of 0°, ±45°, 90° graphite-epoxy tape. They were loaded through two holes, 1/2" in diameter, using an Instron testing machine. Among the more interesting test results is the fact that the maximum circumferential strain around the hole was found to be three times the average strain; this is in good agreement with predictions from the theory of isotropic plates. The quality of the specimens improved as experience was gained in their fabrication. The three best specimens failed in bearing. Even among these, however, failure loads varied from 2800 lbs. for the first, to 8800 lbs. for the last of these. The difference is attributed to quality of the holes; the first two of these three specimens were drilled with a high-speed

STRESS LEVELS PREDICTED FROM FINITE ELEMENT ANALYSIS

COMPOSITE ACTUATOR LUG (Rib Design)

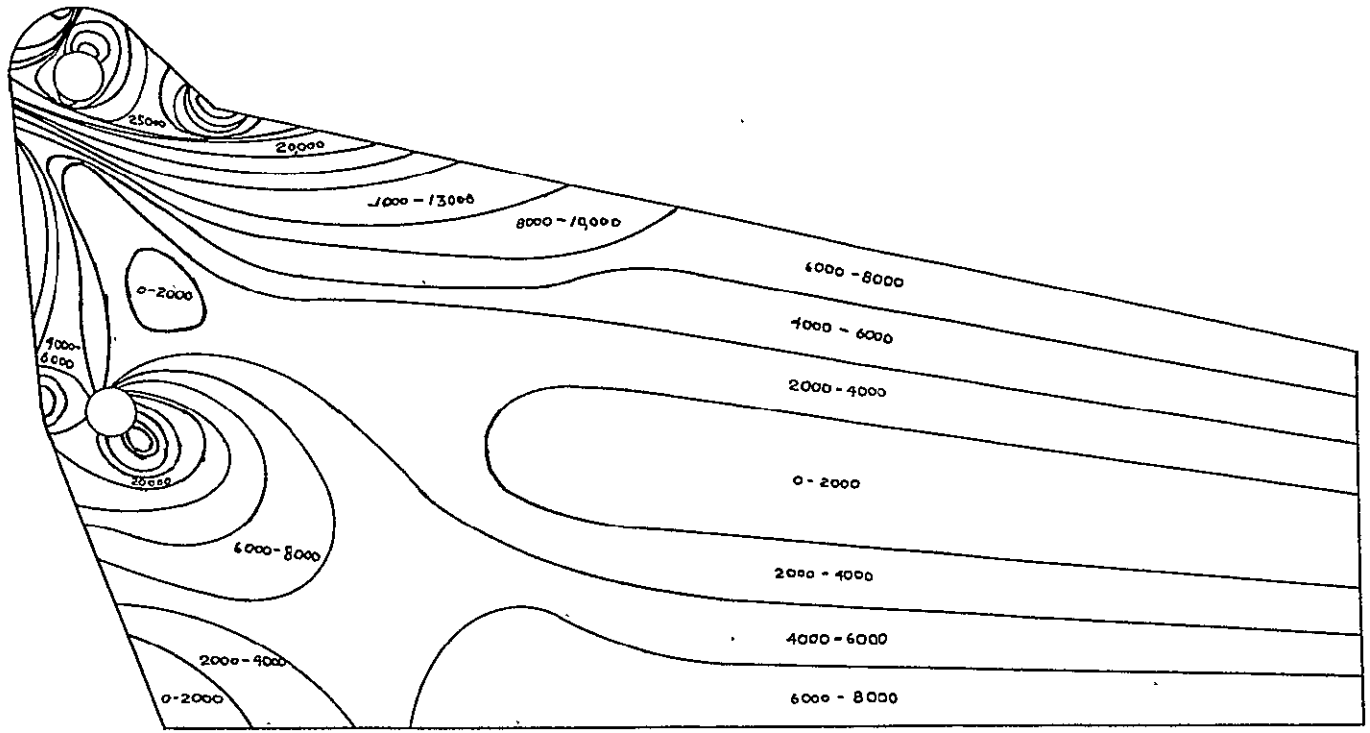

FIG. 7

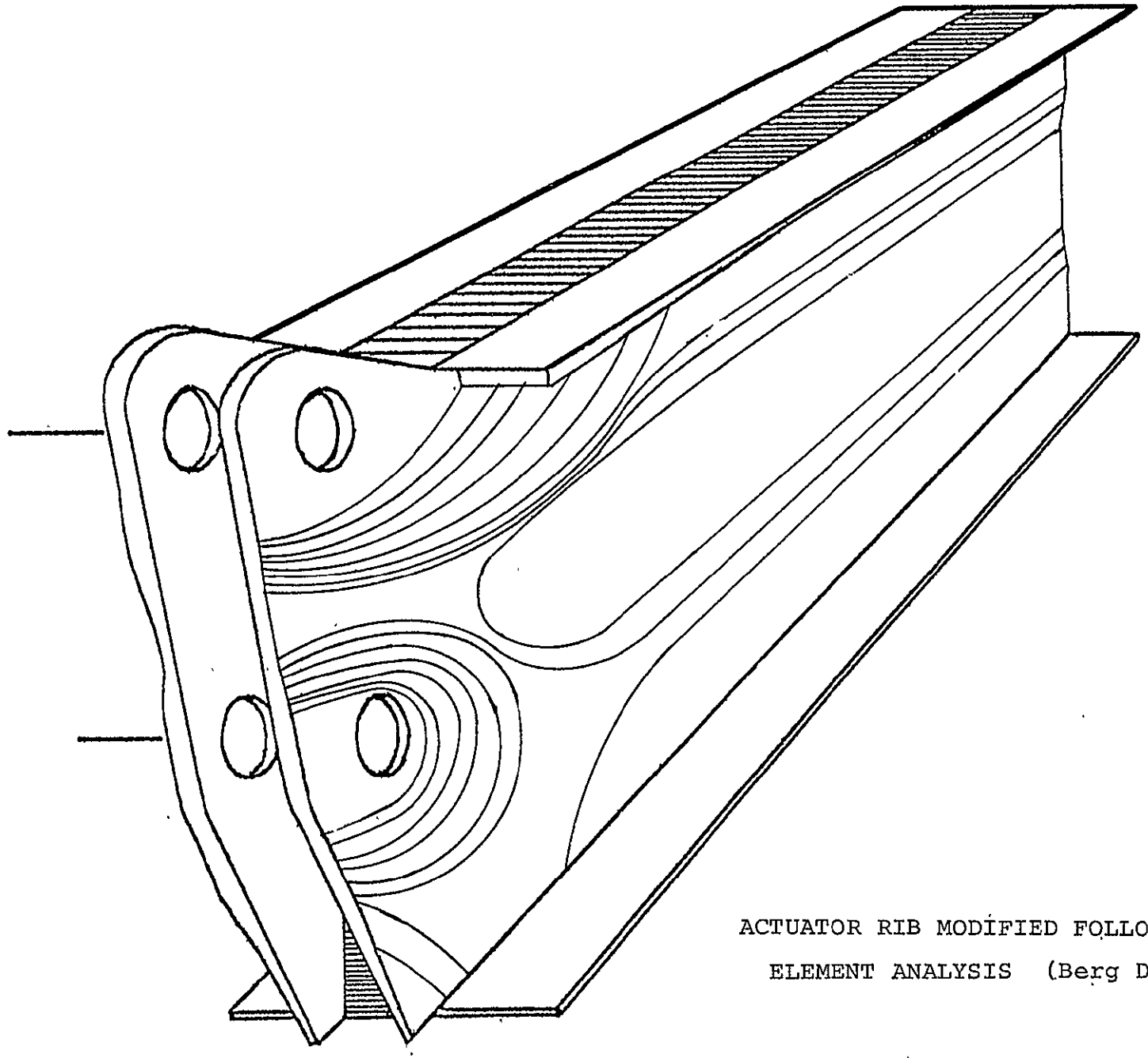

ACTUATOR RIB MODIFIED FOLLOWING FINITE ELEMENT ANALYSIS (Berg Design)

FIG. 8

steel bit which caused delamination between layers of the composite around the hole. The last specimen was drilled with a carbide-tipped drill bit, which resulted in much less delamination. The difficulties in eliminating delamination completely from drilled holes can be appreciated from our Table V; this is reproduced from Reference 1.

As each actuator rib contains two webs with two lugs and holes, the ultimate load the rib could carry is 2 x 8800 = 17,600 lb., which amounts to 93 percent of the required failure load.

Details of the test set-up are shown in Figure 9. Figure 10 is an enlarged photograph of the bearing failure of Specimen 3.

3. Muser's Design

Muser based his design approach on the fact that the great strength of graphite fibers is available only in the direction of the fibers. He attempted, therefore, to lay the fibers in the direction in which the load is transmitted, whenever possible, rather than to dilute this strength by arranging the fibers in several directions in order to arrive at a quasi-isotropic structural element.

His redesign of the Boeing 727 elevator actuator hinge rib is shown in Figures 11 to 14. The main load-carrying element of the attachment is the tension loop (Part 4); this consists mostly of uniaxial graphite tape laid around the steel bushing (Part 7) of the bolt and transmitting the

MATERIAL	THICKNESS IN.	DRILL TYPE	SPEED rpm	FEED ipr	TRACER RADIOGRAPHY	PENETRANT	COMMENTS
GRAPHITE/ EPOXY	0.300	1/8 DIA ROTA-KOTE	6000	0.001	0 020" – 0 085" DELAMINATION ON ALL HOLES	SMALL HOLES DIFFICULT TO TEST. MANY INDICATION DRILL MARKS GIVE FALSE POSITIVES	ALL HOLES FAIRLY SMOOTH, ALL HAVE BREAKOUTS PROGRESSIVELY WORSTENING TO LAST HOLE
GRAPHITE/ EPOXY	0.300	3/16 DIA ROTA-KOTE CARBIDE	6000	0 001	0 – 0 200" DELAMINATION ON ALL HOLES WORSE TOWARD LAST		FIRST HOLES FAIRLY SMOOTH BUT BECOME ROUGHER ALL HOLES HAVE BREAKOUT WITH CONDITION WORSTENING AT LAST 50 HOLES
GRAPHITE/ EPOXY	0.275	15/16 DIA DIAMOND-TIPPED (80-100 GRIT)	6000	0.001	ALL HOLE DELAM-INATED 0.100" – 0.125"		HOLES FAIRLY SMOOTH, LITTLE BREAKOUT
GRAPHITE/ EPOXY	0.275	1/4 DIA DIAMOND-TIPPED (220 GRIT)	6000	0.001	ALL HOLES DELAM-INATED 0.055" – 0.125"		HOLES CLEAN; MINOR BREAKOUT ON LASY PLYS
GRAPHITE/ EPOXY	0.275	1/4 DIA DIAMOND-TIPPED (100 –120 GRIT)	6000	0 001	ALL HOLES DELAMINATED 0.50" – 0 130"	BREAKOUT AND DELAMINATION CAN BE SEEN AT BOTTOM OF HOLE MANY FALSE POSITIVES	MINOR FIBER PULLOUT IN LAST THREE HOLES, MINOR BREAKOUT
GRAPHITE/ EPOXY	0 275	1/4 DIA CARBIDE-TIPPED	6000	0 001	ALL HOLES DELAMINATED 0.010" 0.075" NO RELATIONSHIP TO NUMBER OF HOLES DRILLED		FIBER PULLOUT IN ALL HOLES; BREAKOUT INCREASES AS NO. OF HOLES INCREASE, SOME DELAMINATION ON ENTRANCE SIDE
GRAPHITE/ EPOXY	0.300	1/4 DIA MICROGRAINED CARBIDE	6000	0 001	ALL HOLES DELAMINATED 0 – 0.125" DELAMINATION WORSTENING FROM HOLE 1 to 60		FIBER PULLOUT BECOMES PROGRESSIVELY WORSE WITH INCREASED HOLE NUMBER NO SIGNIFICANT BREAKOUT FOR FIRST 20 HOLES THEN BREAKOUT INCREASES TO LAST HOLE
GRAPHITE/ EPOXY	0.275	1/4 DIA FISH TAIL POINT, CARBIDE-TIPPED	6000	0.001	ALL HOLES DELAMINATED 0.055" – 0 130"		FIBER PULLOUT IN ALL HOLES, MINOR BREAKOUT FROM ALL HOLES
GRAPHITE/ EPOXY	0.300	1/8 DIA ROTA-KOTE HSS	6000	0 001	DELAMINATION AND BREAKOUT ON ALL HOLES TO 0.125" MAX.	MANY INDICATORS HOLES SMALL TO TEST ACCURATELY	SOME FIBER PULLOUT, BAD BREAKOUT ON ALL HOLES
GRAPHITE/ EPOXY	0.275	0 190 DIA ROTA-KOTE HSS	6000	0 001	ALL HOLES DE-LAMINATED 0.110" – 0.140"	SOME FALSE INDICATIONS	HOLES FAIRLY SMOOTH SOME FIBER PULLOUT BREAKOUT ON ALL HOLES,
GRAPHITE/ EPOXY	0.270	0.250 DIA TWIST HSS	3000	0.003	DELAMINATION OF HOLE 1 OF 0.120" PROGRESSING TO 0.150" AT LAST HOLE	MATERIAL IN HOLE HOLDS PENETRANT, FALSE INDICATIONS	HOLE SMOOTH AT FIRST PROGRESSIVELY GETTING ROUGHER TO HOLE 14. BAD BREAKOUT ON ALL HOLES
GRAPHITE/ EPOXY	0.270	0.250 DIA TWIST HSS	6000	0.003	DELAMINATION IN ALL HOLES 0.120" – 0.150"		ALL HOLES FAIRLY SMOOTH OF SOME QUALITY THROUGH ALL SIX SOME FIBER PULLOUT, BAD BREAKOUT ON ALL HOLES
GRAPHITE/ EPOXY	0.270	0.250 DIA CARBIDE TIPPED	6000	0.001	ALL HOLES DELAMINATED 0 120" – 0.150"		HOLE QUALITY ESSENTIALLY THE SAME THROUGH OUT ALL 60 HOLES, BREAKOUT ON ALL HOLES, SOME GOUGING BY DRILL.
GRAPHITE/ EPOXY	00.270	0.190 DIA CARBIDE DRILL/C'SINK Z114104 0.2055 DIA	6000	0 001	HOLES DELAMINATED 0.080"		HOLE QUALITY SIMILAR FOR ALL 140 HOLES ALL HOLES DELAMINATED WITH BREAKOUT.
GRAPHITE/ EPOXY	0.270	MEGADIAMOND TIPPED	2500 4500	0.001	DELAMINATION AT HOLE 1 of 0.120" PROGRESSING TO 0.150" AT HOLE #60		HOLE QUALITY THE SAME FOR ALL 60 HOLES SOME FIBER PULLOUT, ALL HOLES HAVE BREAKOUT
GRAPHITE/ EPOXY	0.275	0.250 DIA TWIST, CARBIDE TIPPED	21,600	0.001	DELAMINATION AT HOLE # 1 OF 0.005" PROGRESSING TO 0.125" AT HOLE # 120	PENETRANT GIVES MANY FALSE POSITIVES	FAIR SURFACE FINISH IN ALL 120 HOLES. ALL HOLES HAVE BREAKOUT
GRAPHITE/ EPOXY	0.275	0 190 DIA CARBIDE Z114104	21,000	0.001	DELAMINATION AT HOLE # 1 OF 0.050 PROGRESSING TO 0.130" AT LAST HOLE # 250		FAIR SURFACE FINISH IN ALL 250 HOLES ALL HOLES HAVE BREAKOUT

TABLE V Summary of Non-Destructive Evaluation of Drilled Holes

(Reproduced from Manufacturing Methods for Cutting, Machining and Drilling Composites, Volume II - Tests and Results, AFML-TR-78-103 Vol. II, August 1978.)

SPECIMEN IN TESTING MACHINE

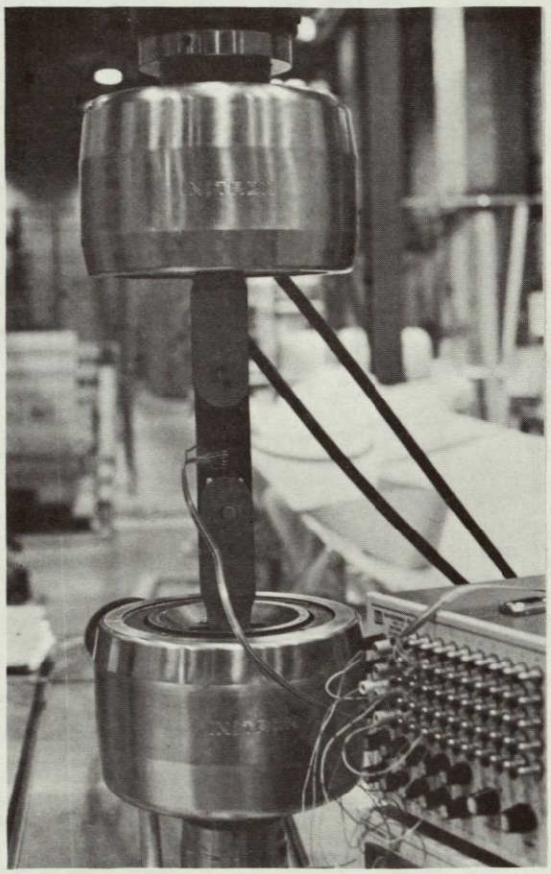

FIG. 9

BEARING FAILURE OF SPECIMEN 3

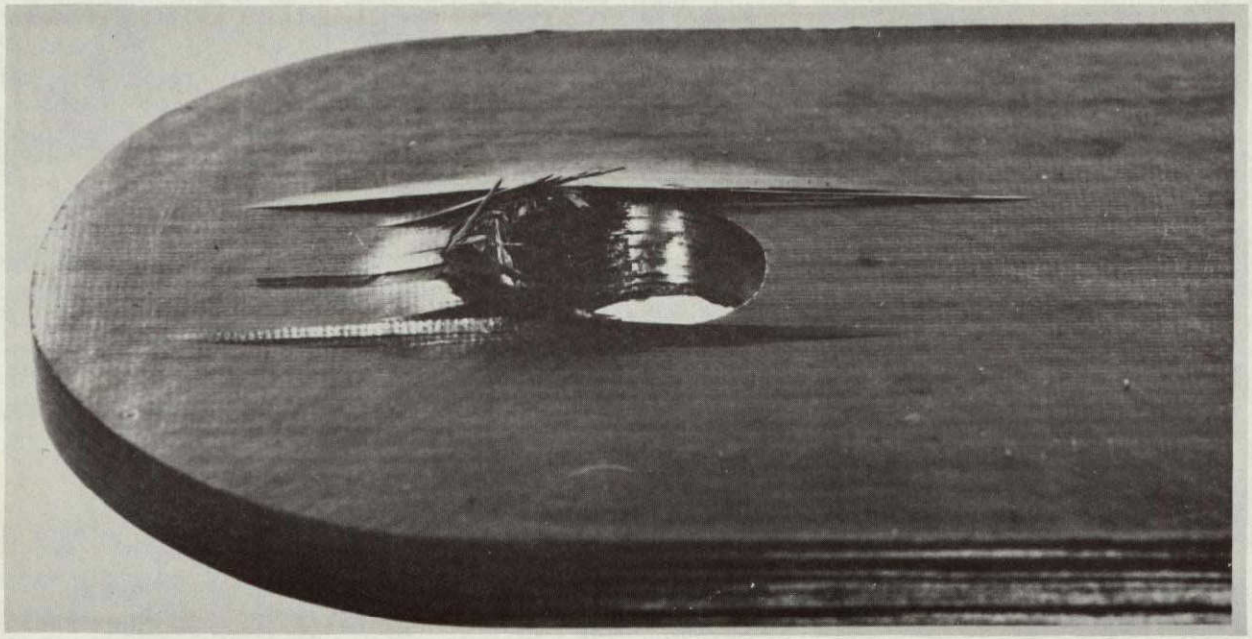

FIG. 10

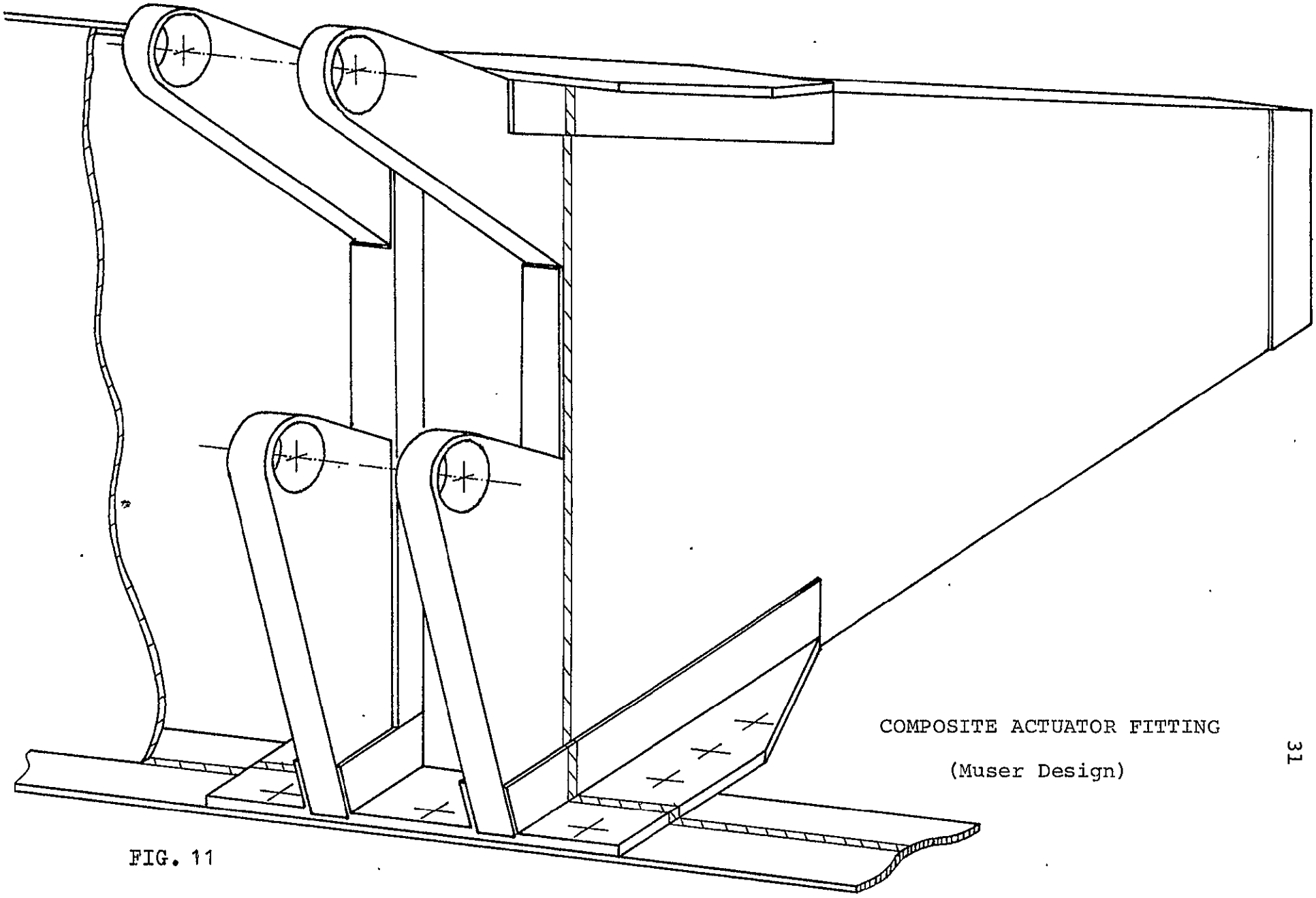

COMPOSITE ACTUATOR FITTING

(Muser Design)

FIG. 11

EXPLODED VIEW

(Muser Design)

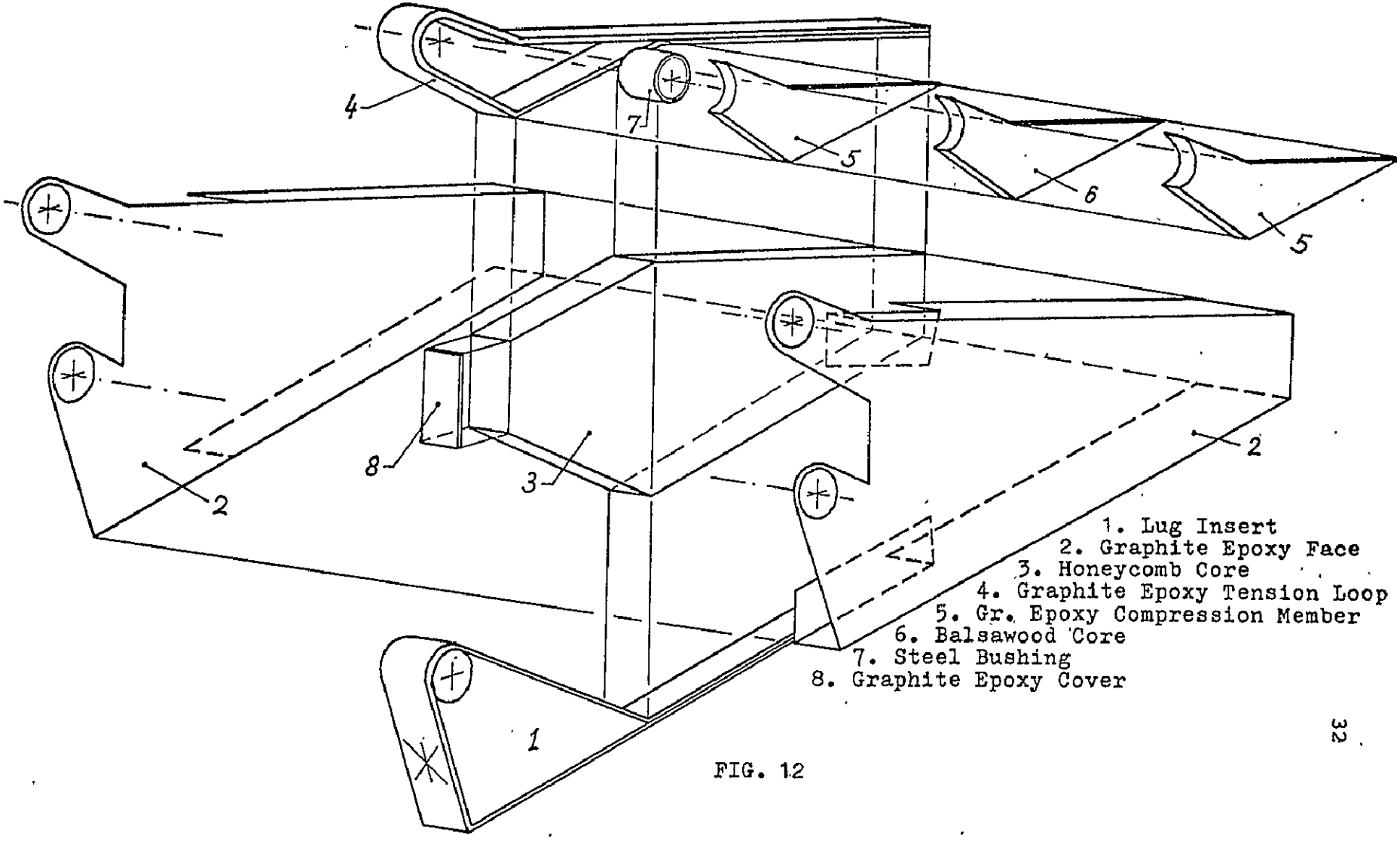

1. Lug Insert
2. Graphite Epoxy Face
3. Honeycomb Core
4. Graphite Epoxy Tension Loop
5. Gr. Epoxy Compression Member
6. Balsawood Core
7. Steel Bushing
8. Graphite Epoxy Cover

FIG. 12

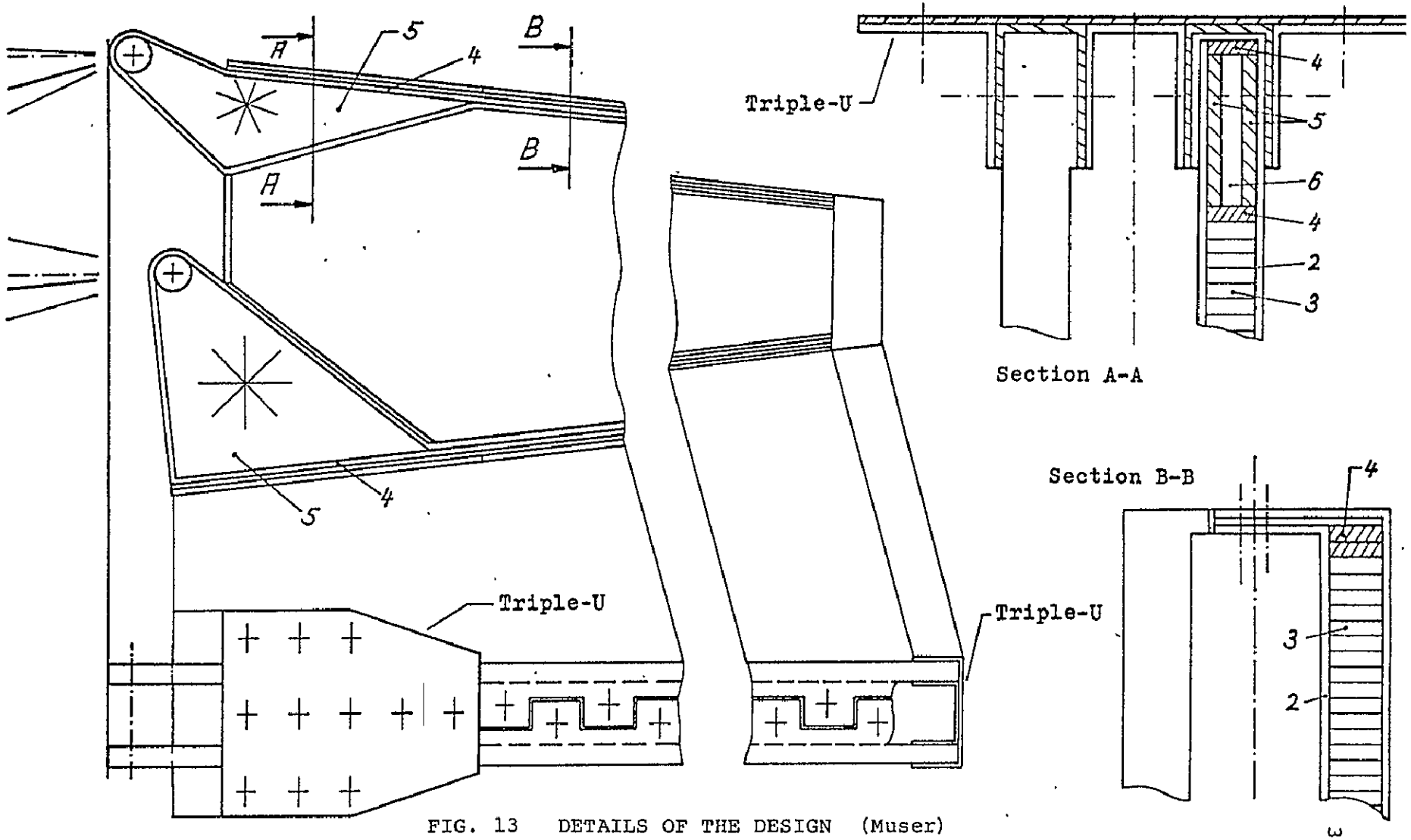

FIG. 13 DETAILS OF THE DESIGN (Muser)

THREE-VIEW DRAWING (Muser Design)

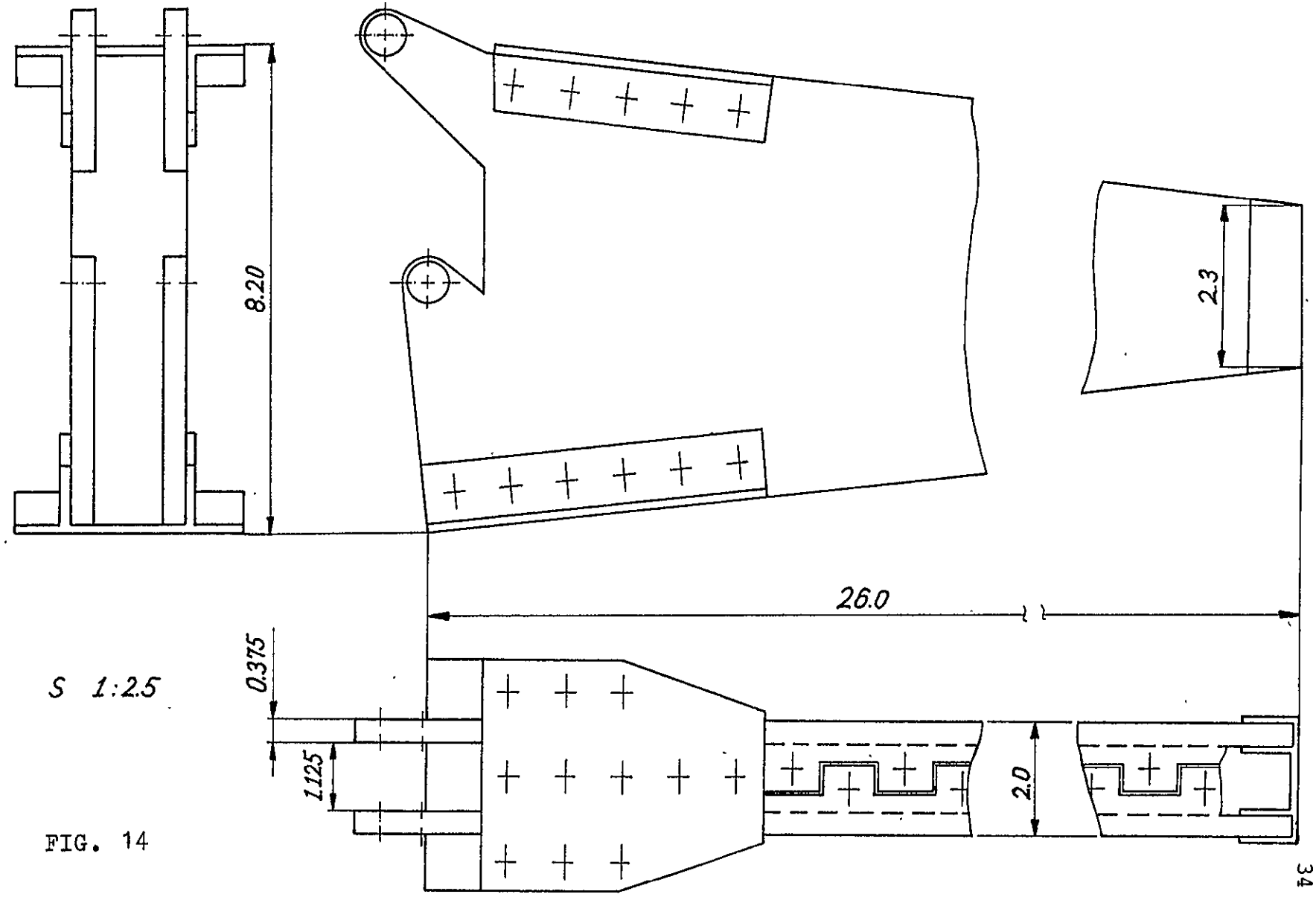

S 1:2.5

FIG. 14

actuator load to the upper and lower flanges of the actuator rib. From these flanges the load is transmitted to the upper and lower cover plates of the elevator by means of titanium Hi-Loc connectors. The distance between branches of the loop is maintained by graphite-epoxy compression members (Part 5) and a balsawood core (Part 6) sandwiched between them. A few layers of ±45° graphite-epoxy tape placed between the 0° layers of the tension loop stabilize this structural element and prevent the cracking of the matrix and the separation of the fibers under both tensile and compressive loads, but particularly the latter.

Since there are two upper and two lower lugs in the actuator attachment, there are four tension loops in all. One upper and one lower loop form the main load-carrying elements of each of the right-hand side and the left-hand side of the (double) actuator rib visible in Figure 11 and in Section A-A of Figure 13. Each side is covered with graphite-epoxy faces (Part 2) and the faces are stabilized by a honeycomb core (Part 3). The right-hand and left-hand sides of the actuator rib are attached to each other by the Triple-U; this is the prefabricated combination of graphite-epoxy U and channel sections visible in Section A-A of Figure 13.

To check the feasibility of the design, a simplified model of the tension loop was designed, built and tested. The specimen is shown in the drawing of Figure 15. The reference numbers in the figure have the same meaning as in Figure 12.

TEST SPECIMEN 1

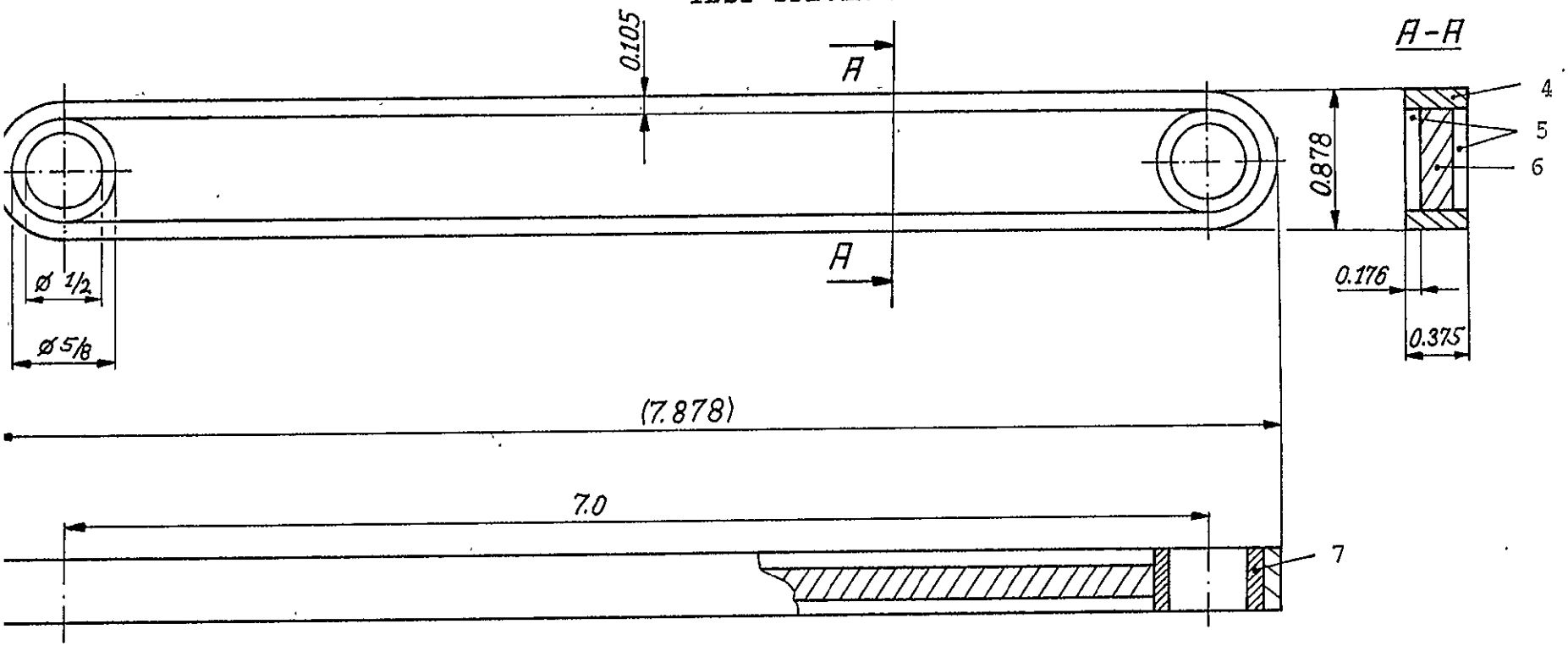

lay-up tensile loop: $23 \times 0°$

compression member: $2\{\pm 45°/4 \times 0°/\mp 45°/5 \times 0°/\mp 45°/\text{core}\}$

FIG. 15

The tension loop was made of 23 layers of Fiberite Hy-E1048AE prepreg. The layup differed from that described earlier as all fibers ran in the 0° direction and ±45° fibers were not included. The prepreg carbon tape in our stores was quite wide, and frugality dictated that, rather than taking one long thin strip, a series of shorter strips be used requiring overlapping of layers. Some of these occurred near the steel bushings. It is possible that these irregularities in geometry contributed to the relatively low value of the failure load, as described in the following paragraphs.

During the manufacturing process the two steel bushings of the specimen were fixed to a flat steel plate. This was the tool for the layup and for the curing process. A dam of silicone rubber was built around the graphite piece and the assembly was covered with a vacuum bag. The specimen was cured in an autoclave at a maximum curing temperature of 250°F and an applied pressure of 85 psi.

The shape of the final specimen was not satisfactory. The core was crushed along a line and the hoop layers translated laterally because of the weakness of the dam. As a consequence the piece did not have the exact rectangular cross section shown in the drawings. This can be seen from the photographs (Figures 16 and 17). The specimen was tested, nevertheless, partly to find its strength and partly to gain experience in testing.

UNDAMAGED END OF SPECIMEN

(one quadrant removed)

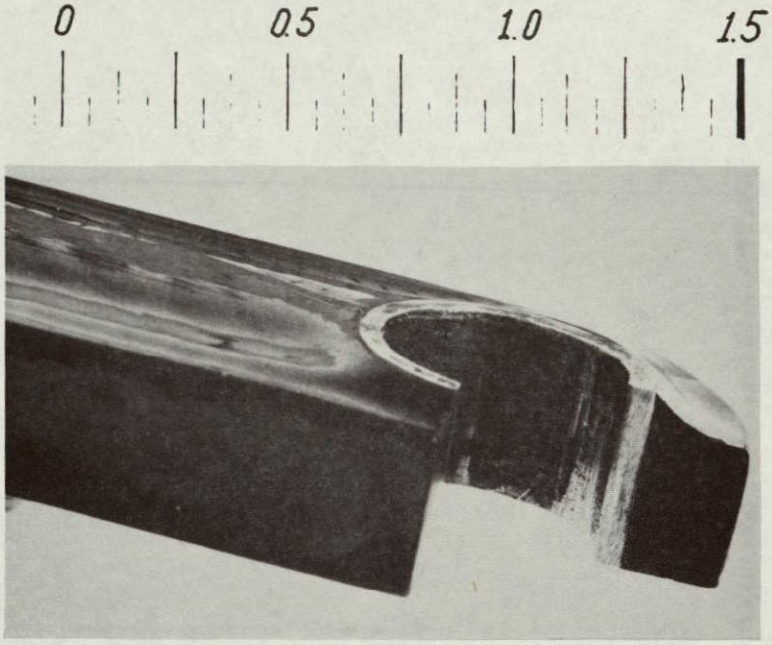

FIG. 16

CROSS SECTION OF SPECIMEN

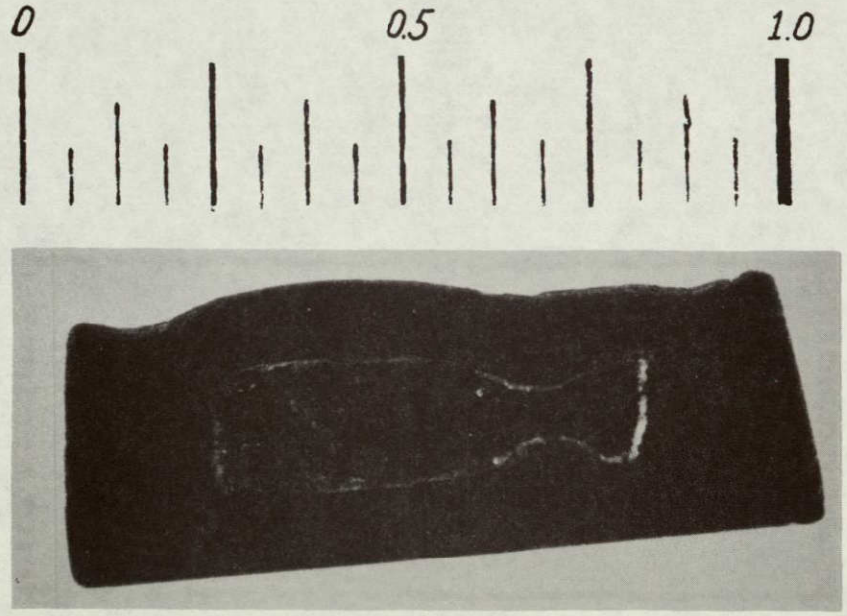

FIG. 17

Figure 16 shows the undamaged end of the specimen out of which one quadrant was cut. Figure 17 is a cross section of the middle of the specimen which was sawed in two after the completion of testing. Figure 18 shows the tension failure at one side of one of the holes.

The test specimen was subjected to tension in an Instron testing machine, Model 1333. Weak crackling noises were heard at a very early stage of the loading (around 2500 lb.) and then again near the maximum load. The specimen broke suddenly with a big bang after it had withstood a load of 8755 lb. for two or three seconds. One side of the specimen opened up into the shape of a hook, but it snapped back when the load was removed. The failure was clearly of the tensile type, without any deformations due to bearing stresses.

As the design ultimate load of one lug was 9500 lb., the specimen withstood 92% of the design ultimate load. The addition of two or three layers of 0° tape would bring up the strength of the design to the desired ultimate strength. However, if the efficiency of the design is defined as the average stress (load divided by cross-sectional area) divided by the ultimate tensile stress σ_{TU} of the material, the design is not very efficient. The area of the cross section that failed in tension was 2 x 0.126 x 0.375 inches = 0.0945 inches squared. For the ultimate load of 8755 lbs., this gives an average failure stress of 92,857 psi. Since the ultimate tensile stress of the material (uniaxial filament

TENSION FAILURE

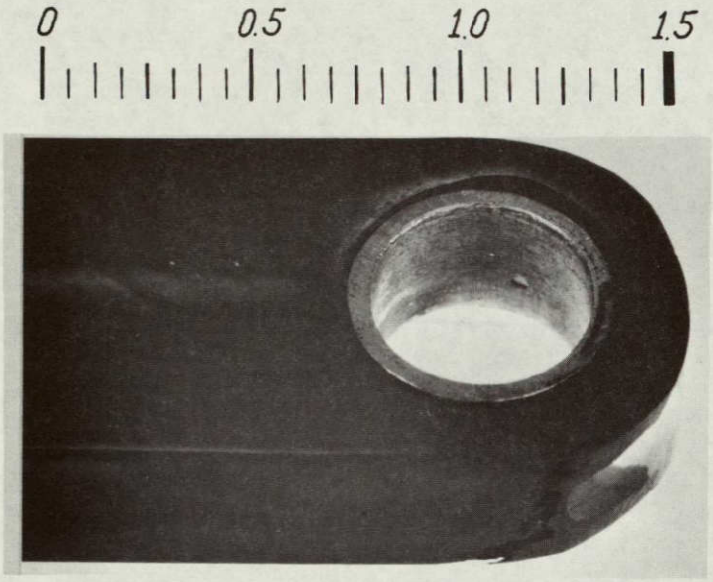

FIG. 18

SPECIMEN 2 AND MANUFACTURING TOOL

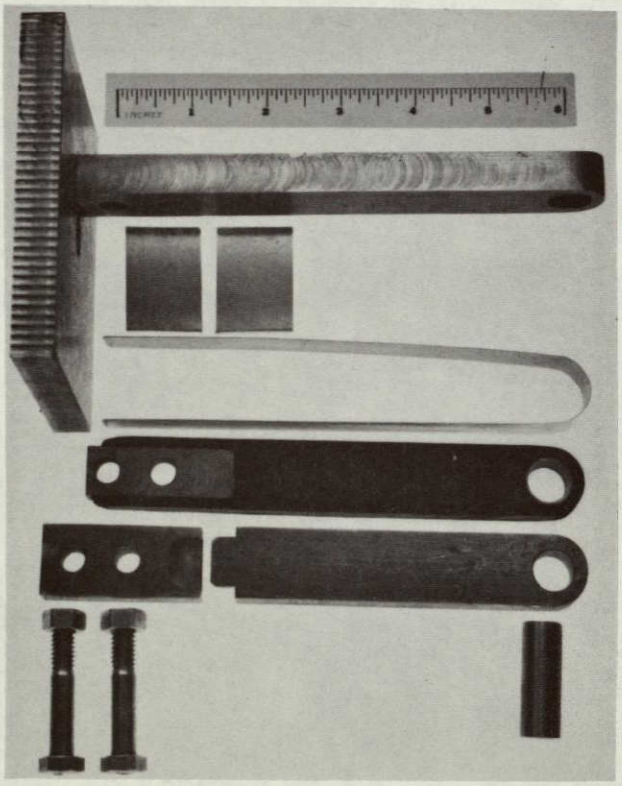

FIG. 19

tape) is listed as 160,000 psi, the efficiency of the design is $\eta = 0.58$.

Some increase over the average stress corresponding to a uniform distribution over the cross section was expected for the stress near the bolt hole. The efficiency value of 0.58 corresponds to a stress-concentration factor of 1.72. An effort was made to reproduce this value theoretically, but without success. Calculations based on the theories of curved bars and circular rings all yielded much higher stress-concentration factors, probably due to the fact that the distribution of loads as applied in these calculations are unsatisfactory representations of the conditions prevailing in the test. This theoretical effort continues.

Concurrent with the theoretical analyses, a second specimen was designed and constructed. In this design the closed tensile loop concept was dropped in favor of an open loop. A straighter tape layup was thereby achieved through the application of tension in forming the loop. The tool has the exact measurements the specimen should have after curing. It has a movable top which attains its proper final position when pressure is applied. A thin aluminum alloy strip presses the layers of the loop against the tool and against the compression members. Photographs of the tool and the specimen are shown in Figure 19.

Unfortunately, the vacuum bag broke in the autoclave during the curing process, and this specimen was not cured

properly. It was decided not to test this specimen. However, the proper shape was obtained, as can be seen from Figure 19, which shows both the specimen and its manufacturing tool. The experimental work will continue using the revised fabrication concept.

4. Supporting Development of Mechanical Joints

The supporting effort made by Research Associate, Kiyoshi Kenmochi and Graduate Student, Wonsub Kim had as its purpose the development of equipment and methods to determine the stress distribution and the stress concentration factors in, and the failure modes and failure loads of, simple structural joints made of advanced composites.

At first, experience was gained in manufacturing flat graphite-epoxy sheets of Hy-E1048AE prepreg tape with various combinations of fiber direction in a press with a heated platen. The tension test specimens were cut from these sheets on a band saw with carbide dust saw blade. The edges were finished with sandpaper.

Great difficulties were encountered in drilling holes in these specimens because it was impossible to avoid delamination and some broken fibers at the edge of the hole when HSS (high-speed-steel) twist drill bits were used. Moreover, the average life of the drill bit was two holes. The drill was driven at speeds varying from 120 to 5500 rpm.

The appearance of the surface of the hole improved greatly when spade-type carbide drill bits were introduced. These were manufactured by Pen Associates, Inc., who recommended a speed of 25,000 rpm for drilling a 1/4" hole. Unfortunately, the highest speed which we could use satisfactorily on campus was 5500 rpm. Another machine which has a maximum speed of 8000 rpm exists at RPI, but it vibrated severely when run at more than about 4000 rpm. Tool life was satisfactory.

Even better results were obtained with carbide-tipped drill bits having straight cutting edges (parallel to the axis of the drill). Those used were manufactured by Greenfield Tap & Die Division of TRW, Inc. With graphite-epoxy plates as back-up plates and speeds between 300 and 5500 rpm, high-quality holes were obtained when the hole diameter was 1/4". In the case of 1/2" holes, severe vibrations occurred above 2500 rpm. Again, tool life was found to be satisfactory.

A fixture for testing specimens in tension was built and is shown in Figure 20. It succeeded in applying rather uniform tensile stress in the plates, except in the vicinity of a hole. Along the edge of the hole, the stress varied greatly. The fixture was mounted in an MTS universal testing machine of 20,000 lbs. capacity.

Five specimens, symmetrical about their mid-plane, were tested with the following fiber orientations: Case A: 0°, 90°; Case B: 0°, ±45°; Case C: 90°, ±45°; Case D: 0°, ±45°, 90° and

FIXTURES FOR TESTING SPECIMENS IN TENSION

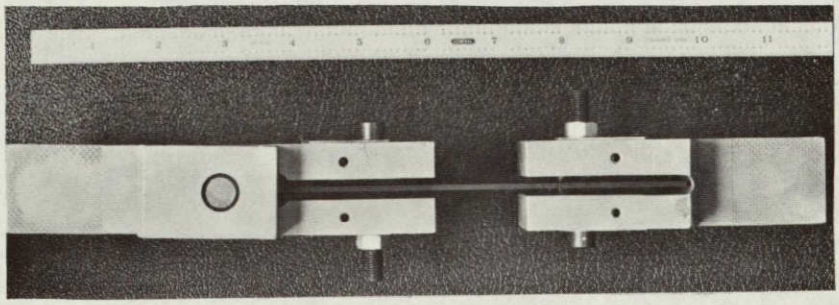

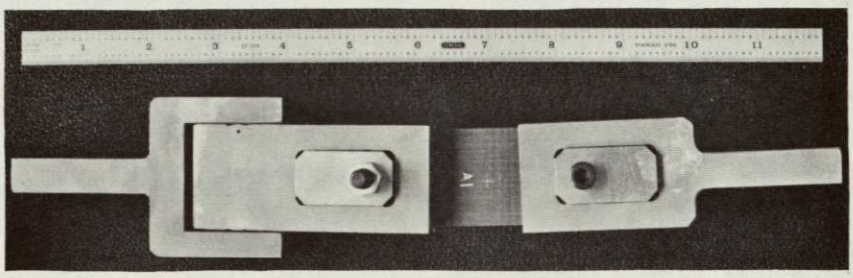

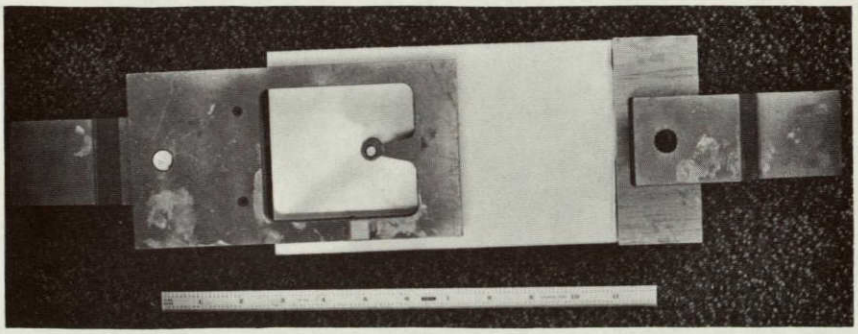

(for photoelastic test)

FIG. 20

Case E: 0°, ±22.5°, ±45°, ±67.5°, 90°. The number of layers was either 18 or 20. The thickness of the specimen varied from 0.083 inches to 0.095 inches.

The specimens were designed so as to fail in bearing. They are shown after failure in Figure 21. The large deformations of Specimen E2 occurred because loading was continued for one minute after the maximum load had been reached. The almost complete absence of visible deformations of Specimen C2 in the photograph is due to the fact that all load was removed immediately after the maximum load had been reached. The maximum load values varied between 1310 lbs. and 1725 lbs. and the maximum average stress values between 62,000 psi and 74,900 psi.

As the purpose of the effort described in the present report is the discovery of the most efficient fiber arrangement around holes and the analysis of the stresses and strains in the vicinity of the holes, it is advantageous to have available means by which the variation in strain can be determined accurately in experiments. For this purpose a fixture was developed which is capable of introducing a load into a plate specimen through a pin and allows "fringes" in a photoelastic plate bonded to the specimen to be photographed at the same time.

The assembled fixture for photoelastic tests is shown in Figure 22. The fixture for bearing failure tests is depicted in Figure 23, again in the form of an axonometric

FIVE SPECIMENS AFTER FAILURE

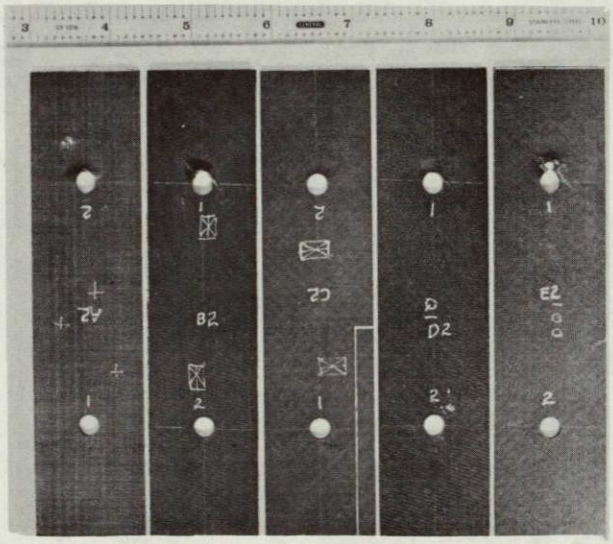

FIG. 21

ASSEMBLY OF FIXTURE FOR PHOTOELASTIC TESTS

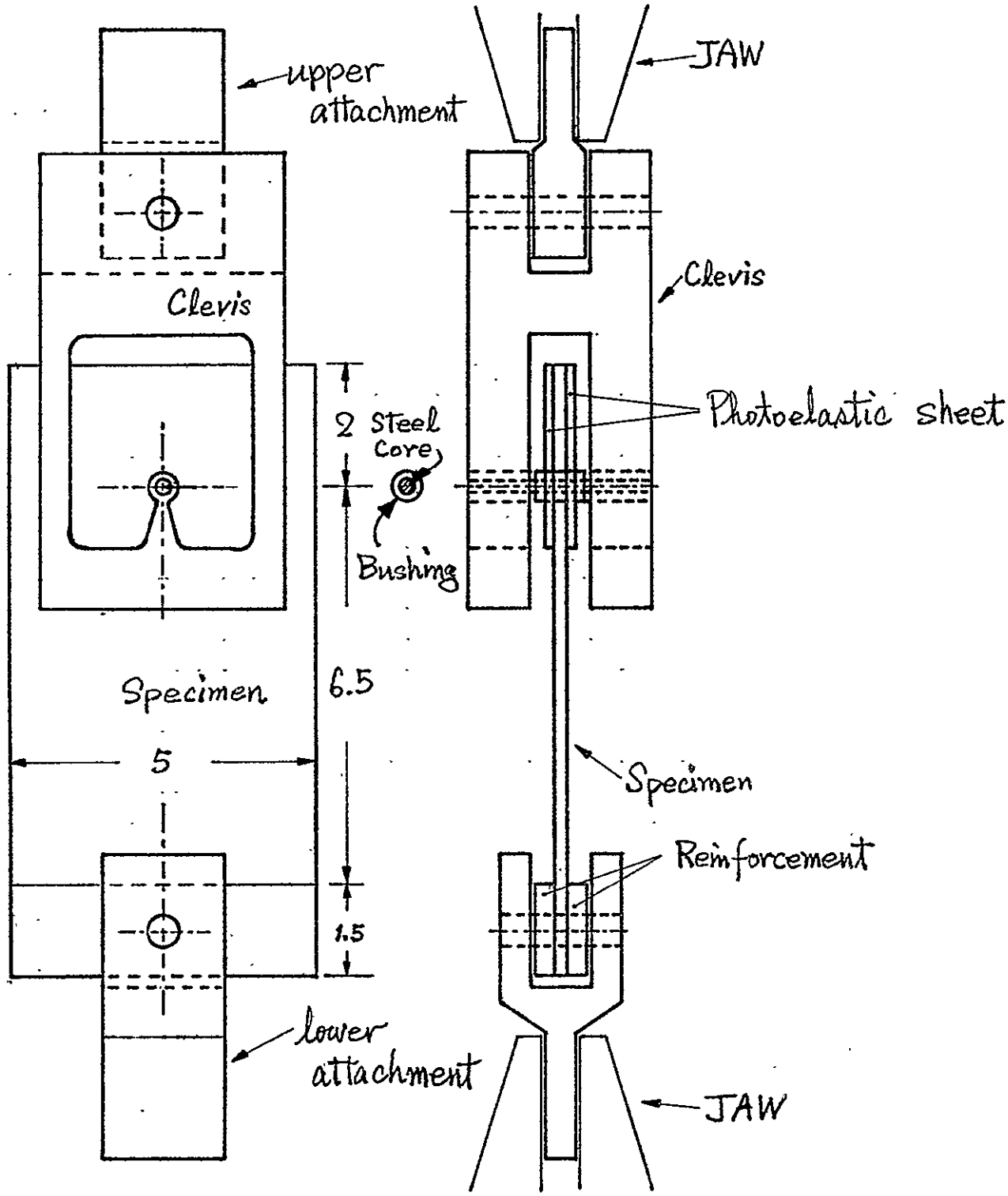

FIG. 22

AXONOMETRIG DRAWING OF FIXTURE

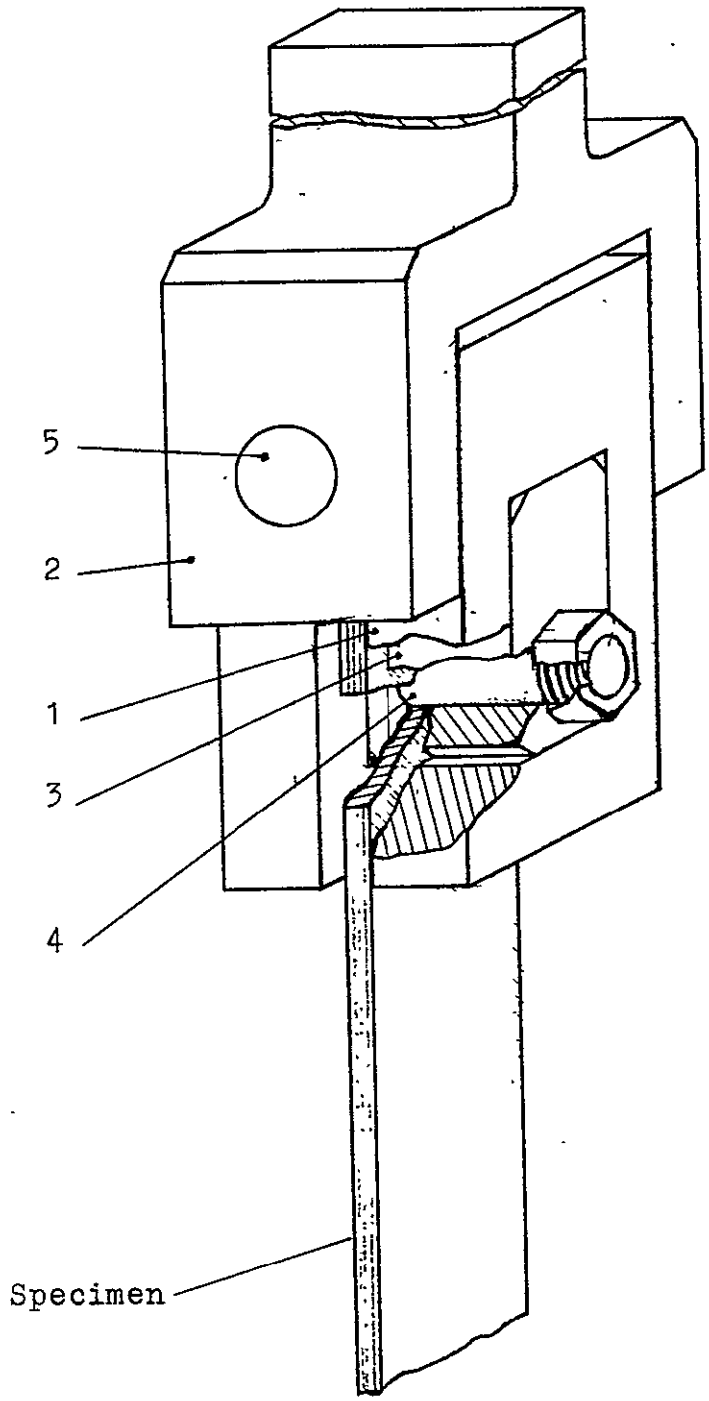

FIG. 23

drawing. The numbers in Figure 23 refer to the parts whose workshop drawings are presented in Figures 24 to 27.

The photoelastic test jig is shown on the workshop drawing in Figure 28, and Figure 29 is a photograph of a photoelastic test in progress. Figure 30 shows in detail the test specimen and the fringes in the photoelastic plate bonded to the specimen. Figure 31 is a close-up of the specimen with its fringe pattern; this picture was taken with an isotropic test specimen.

Difficulties, not yet overcome, have arisen in drilling holes in the plate with photoelastic sheets on it. The selection of the material of the photoelastic plate and of its thickness is important because the number of fringes depends on it. Good drilling procedures are equally important. Without them, prefringes develop in consequence of residual stresses or delamination of photoelastic sheets from the specimen. Uneven spots on the surface of the hole and delamination of the test specimen itself can disturb the fringe pattern caused by the load.

The photoelastic equipment used in the tests consisted of a polariscope (Model 031, Photolastic Inc.), a specially prepared test fixture (Figure 23) and a camera (Nikon FM). A photoelastic sheet calibrator (Model 010-B, Photolastic Inc.) and a compensator (Model 232-RE) were used for preparing the tests. For analysis purposes, a strain direction analyzer was specially designed and fabricated.

SHOP DRAWING OF PART 1.

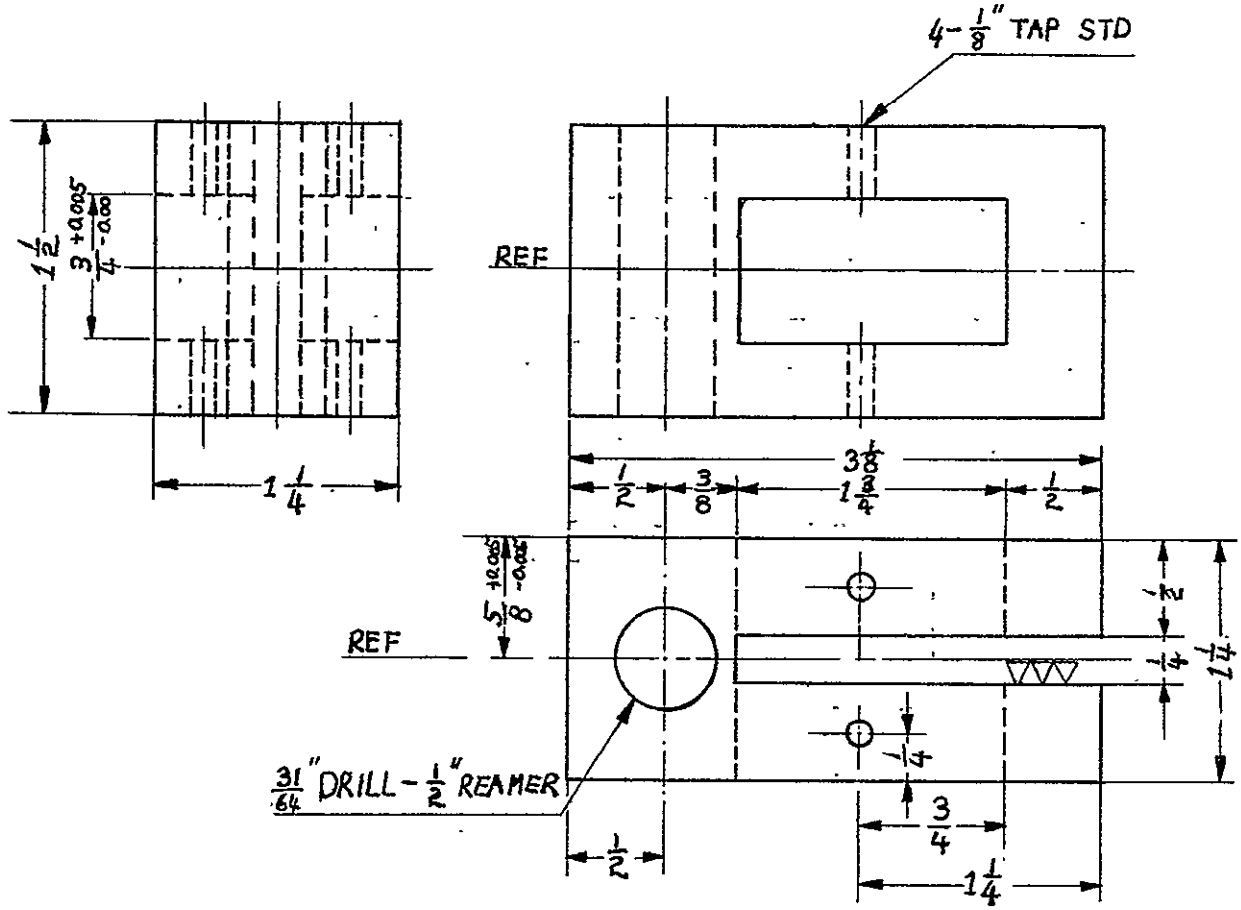

COMMON: 1. Tolerances: ± 0.001 for all inner surfaces
± 0.005 for all outer surfaces to ref. line

2. ⊥ 0.001 for all surfaces to ref. line

3. ▽▽▽ all inner surfaces
▽▽ all outer surfaces

Material: Steel, Hardness > R_C 34

Chamfer: All outside corners chamfered by 1/16"

FIG. 24

SHOP DRAWING OF PART 2

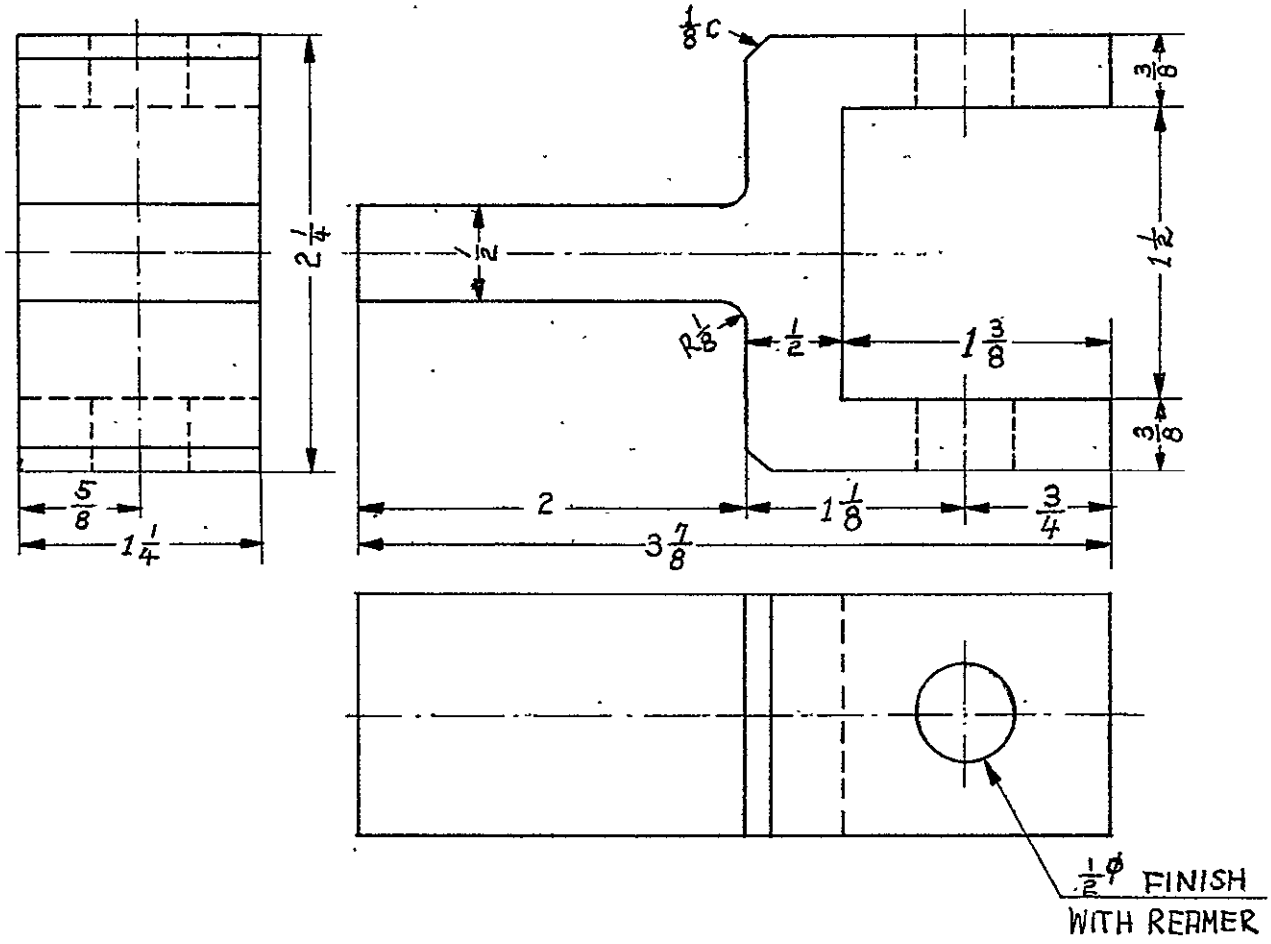

COMMON: 1. Tolerances $\pm$ 0.005

2. $\perp$ 0.005 for all inner surfaces to ref. line

Material: Steel, Hardness $>$ R_c34

FIG. 25

SHOP DRAWING OF PARTS 3 TO 5

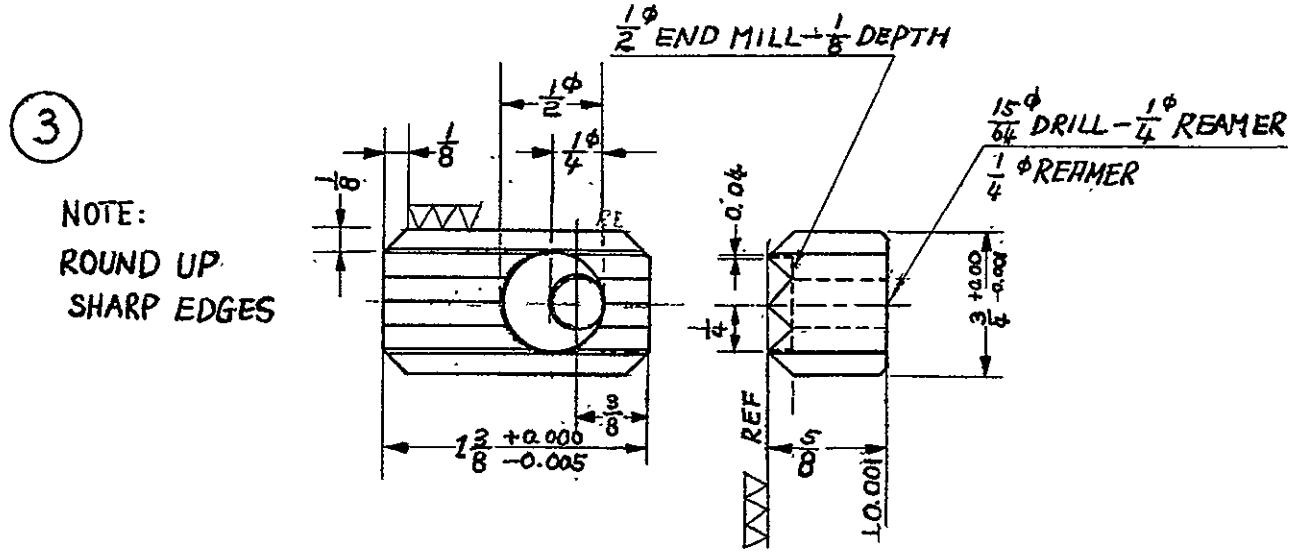

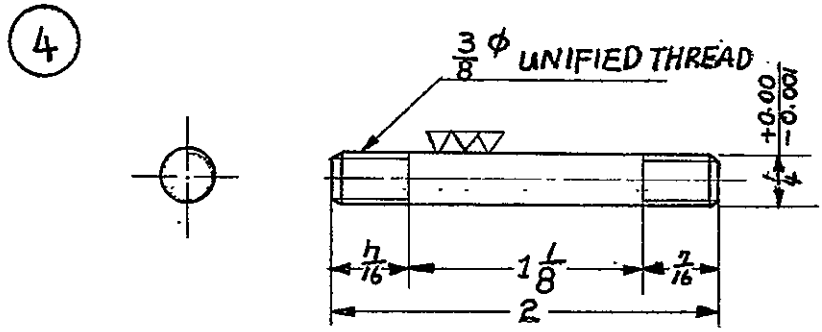

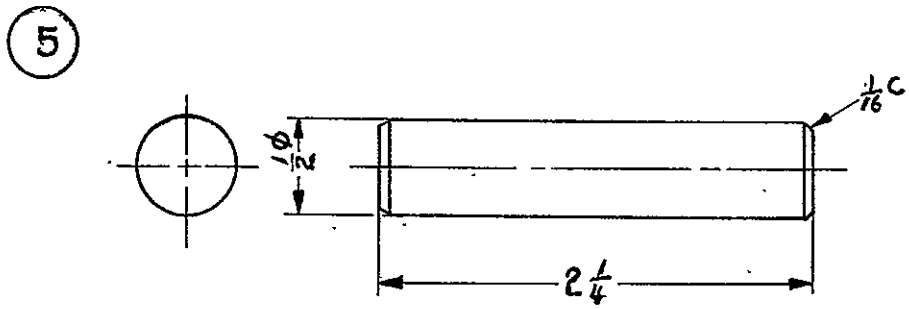

5	PIN CONNECT	1	SAE4130
4	SHEAR PIN	2	SAE4130
3	FACING BLOCK	4	SAE4130
NO	PART NAME	EA	MATERIAL

FIG. 26

SHOP DRAWING OF PART 6

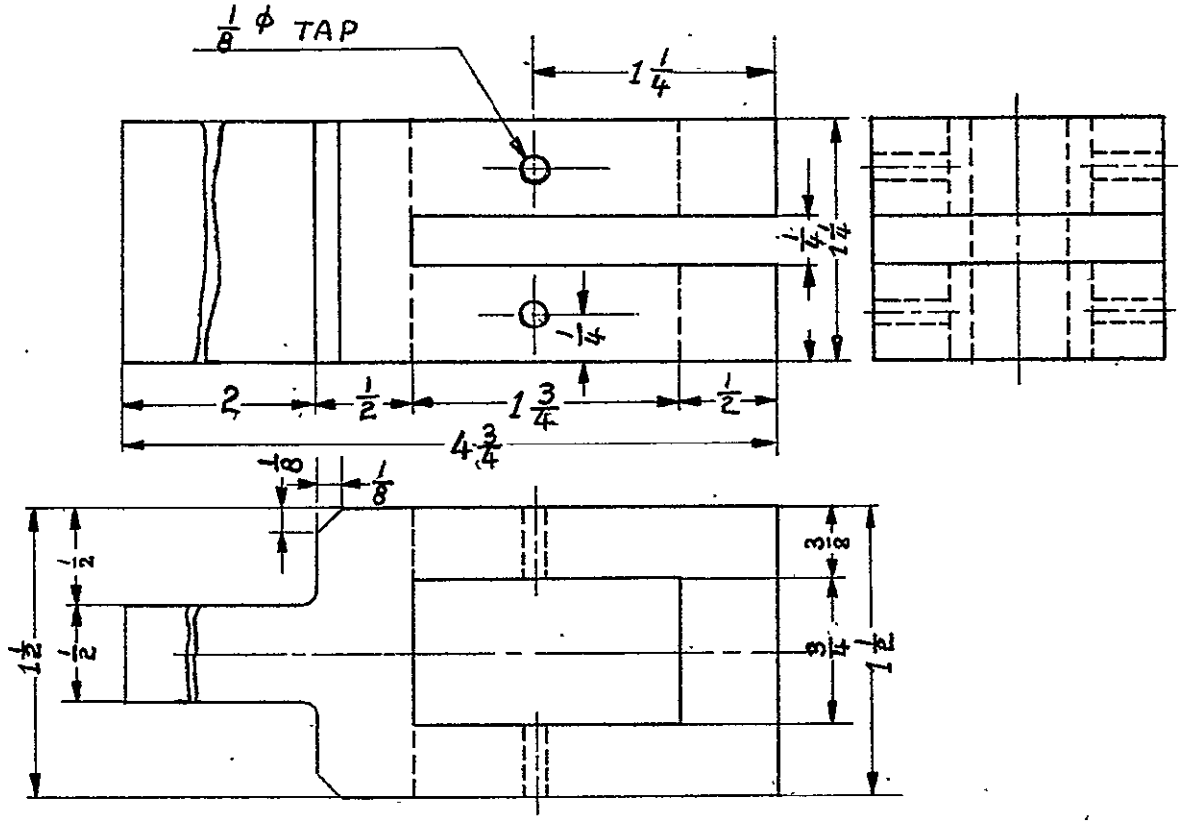

* NOTE : SEE PART No. 1

FIG. 27

SHOP DRAWING OF PHOTOELASTIC TEST JIG

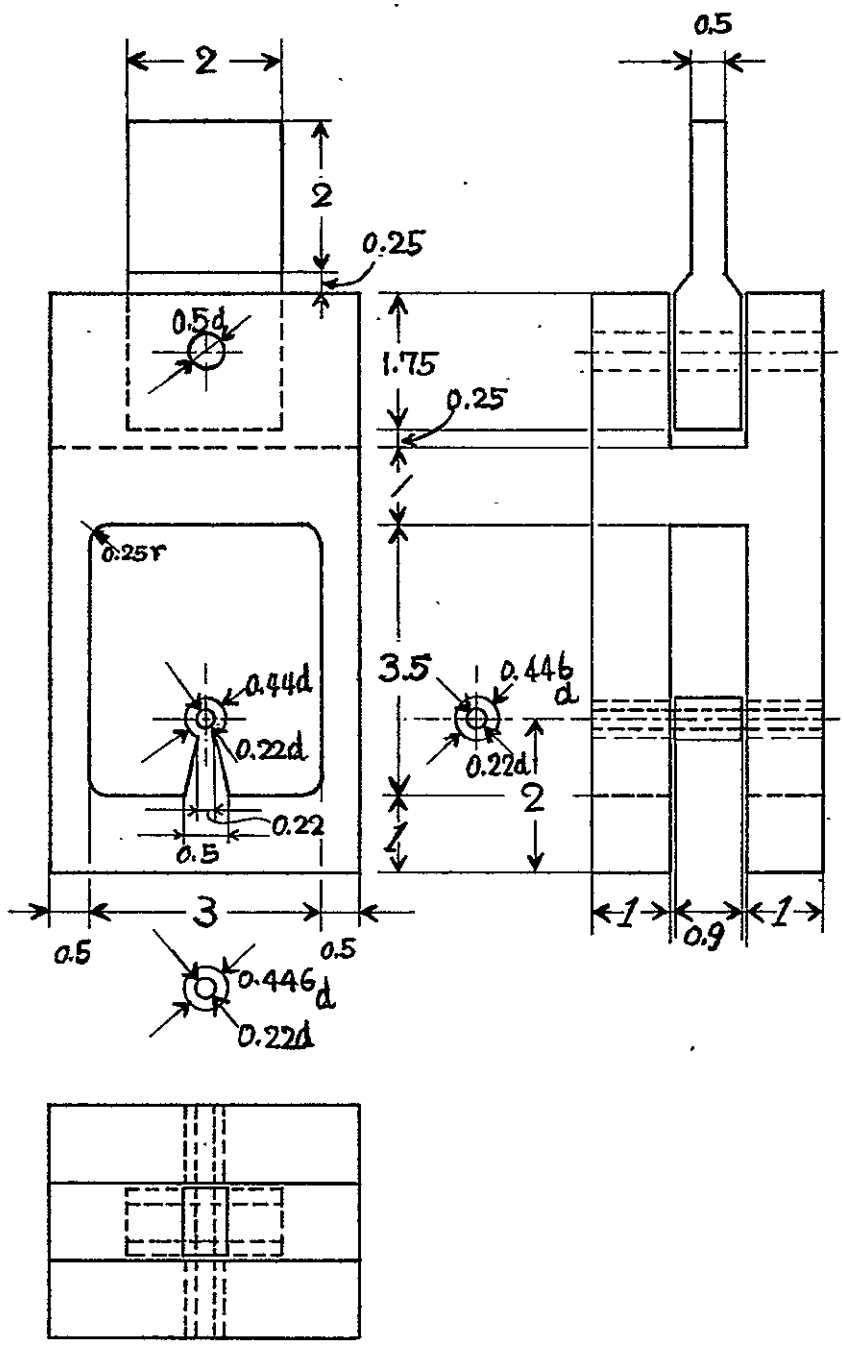

FIG. 28

PHOTOELASTIC TEST IN PROGRESS

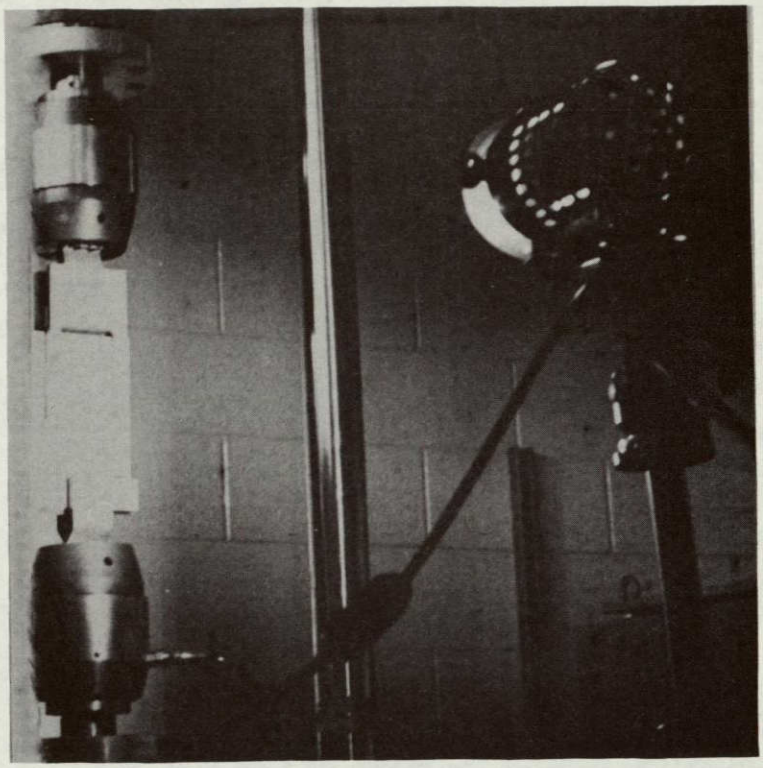

FIG. 29

SPECIMEN PHOTOGRAPHED UNDER LOAD

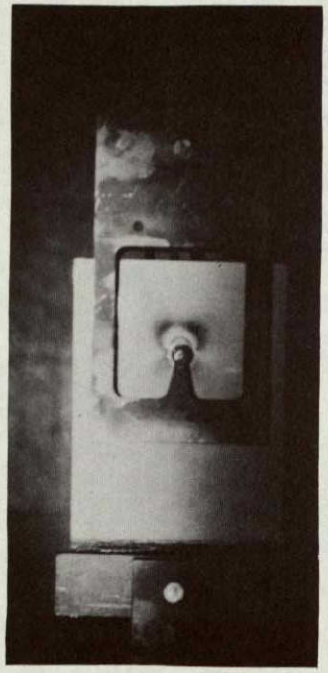

FIG. 30

FRINGE PATTERN IN ISOTROPIC SPECIMEN

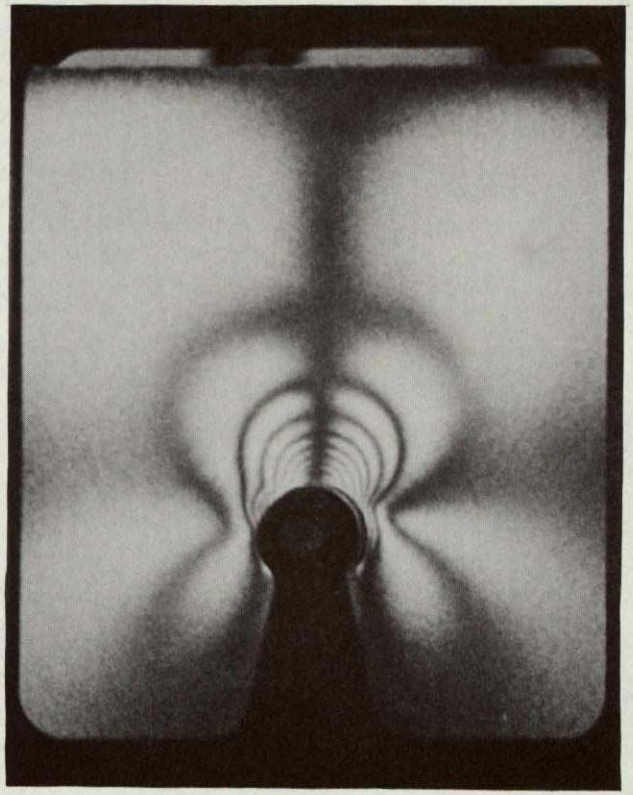

FIG. 31

Plans for future testing of the kind described here to determine composite laminate bearing stress include correlation of failure stresses with delamination patterns around the holes caused by drilling, as sensed and recorded by ultrasonic N.D.E. Here again, Table V from Reference 1* suggests the unlikelihood of completely eliminating delamination around drilled holes, so that correlation efforts of this type seem well advised.

*Manufacturing Methods for Cutting, Machining and Drilling Composites, Volume II - Tests and Results, AFML-TR-78-103 Vol. II, August 1978.

PART II

CAPGLIDE (Composite Aircraft Program Glider)

CAPGLIDE (Composite Aircraft Program Glider)

(E. J. Brunelle, R. J. Diefendorf, H. J. Hagerup, G. Helwig, N. J. Hoff and C. LeMaistre)

CAPGLIDE is an undergraduate program to design, build and test advanced composite structures. Students will obtain direct "hands-on" experience in advanced composite structures which can serve as a springboard for the more sophisticated CAPCOMP projects. In dealing with the design of a complete vehicle, the effect of any given change on other aspects must be dealt with. In this way the project also requires students majoring in aeronautical, mechanical and materials engineering to interact in much the same way as they do in industry.

An ultra-light sailplane was selected as the first demonstration project because a full scale flight vehicle would maximize student interest and would be of relative simplicity and low cost to build. A conventional layout monoplane with three-axis control resulted in the following estimated performance:

1) Stall speed, 15 knots,
2) Best glide ration, 17 and
3) Minimum sink rate, 2.0 feet per second.

While the glide ratio of the ultra-light sailplane is similar to that of post World War II utility gliders, the more important sink rate is in the range of standard class sailplanes.

Although comparative theoretical analyses continue in some areas, the ultra-light sailplane project has moved from detail design to a primarily fabrication phase. Student activity during the present contract period has concentrated on "hands-on" experience with composite material layups, adhesive bonding and co-curing of structural parts, with structural proof-tests of subassemblies and with coupon tests for process-control and property determination.

In the light of our rapidly accumulating fabrication experience and test results, some detail design features are still being modified. However, the important design decisions have now been made, and the prototype aircraft is being built. Construction of the aircraft is on schedule. We expect that the main airframe components will be finished by mid-summer, connections and control systems by the end of summer and that the prototype aircraft will have been proof-tested and ready for operations in early fall.

During the design phase (extensively reported in earlier semi-annual reports), the student working teams were organized according to disciplines. For the production phase, the teams have been realigned to focus on the individual major parts of the aircraft. The progress of each working team is summarized in the following pages.

1. Wing Group - 12 students

Female wing-molds, incorporating the external contour of the top and bottom surfaces of the airfoil, have been assembled from Formica sheet bonded to a framework of plywood and composition board. The Formica surface has been carefully filled and sanded to the contour of the Wortmann FX 63-137 airfoil and spray-painted with primer and acrylic paint. Sections of the molds were used to secure experience with release agents. Problems were encountered with respect to interaction between acrylic paint, release agent and the epoxy resin of the layup. These problems were overcome by laying-up the skins in two stages. The outside layer of the skin sandwich is laid-up and cured on a flat polyethylene sheet, for which there is no need for a release agent. Then, after the cure is nearly complete, this still pliable half-sandwich is transferred to the wing mold with the laminate side facing the mold. The inside layer is now added as a wet layup and vacuum-bagged to complete the sandwich. The sandwich cures rigid, in the shape of an airfoil contour. Production of the first full-span wing panels is expected to begin in late May.

Torsion tests were conducted on three separate three-foot span sections of the wing, primarily for the purpose of determining the rib spacing required to prevent panel buckling.

Carbon flanges for the prototype wing spar were produced in the RPI designed 22 foot, temperature-controlled pressure vessel. The final flange design for the spar is of graduated thickness, starting with 34 plies at the root end and terminating with 2 plies at the tip.

The prototype wing spar has been assembled. A graduated kevlar/foam sandwich web and the carbon flanges, described above, were used, bonded together by a mixture of Cabosil and epoxy resin. A narrow strip of kevlar/foam sandwich was bonded to the outside of the flanges to simulate the presence of wing skins. This kevlar/foam sandwich prevents splitting of the unidirectional flanges. A photograph of the semi-span prototype wing spar is shown as Figure 32. Pending fabrication of the final design center-joint and the load-application rig, the prototype wing spar will be ready in late May for load-deflection tests. The expected wing-spar failure mode is web buckling at the root, the flange itself having been designed for stiffness.

The wing center-section joint has been redesigned for a third time. The present version consists of a male-female box joint secured by a single bolt. This simplified center-joint design was achieved by redesigning the wing for zero degrees dihedral, with roll stability now secured through a 25 degree uptilt of the wing tips. A photograph of a model of the glider is given in Figure 33.

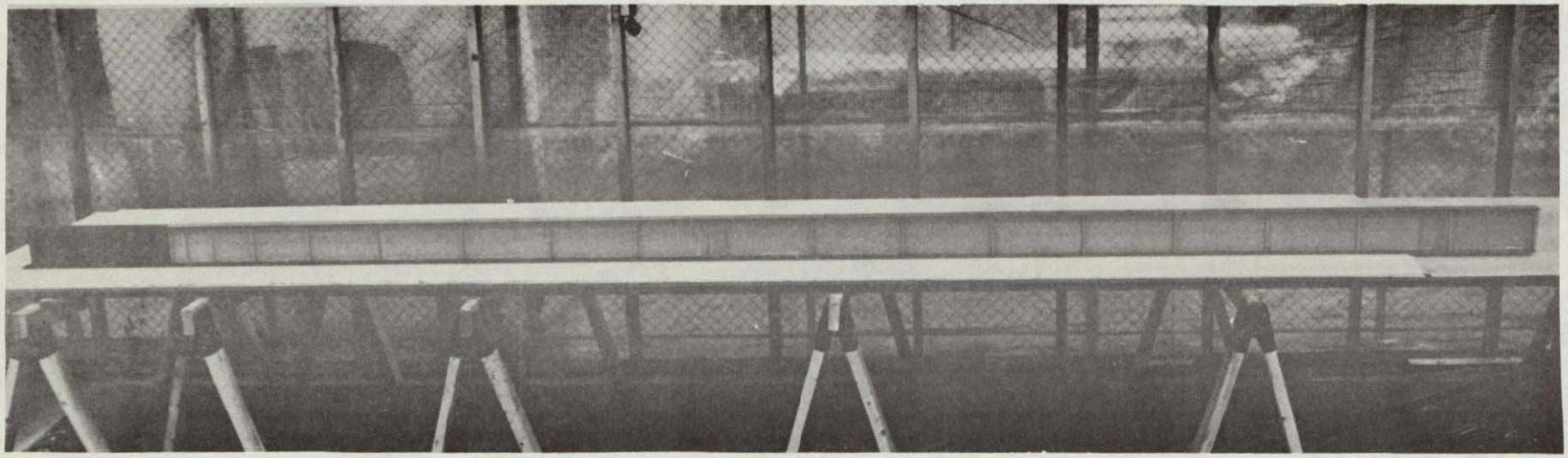

Fig. 32 WING SPAR TEST SPECIMEN (Semi Span)

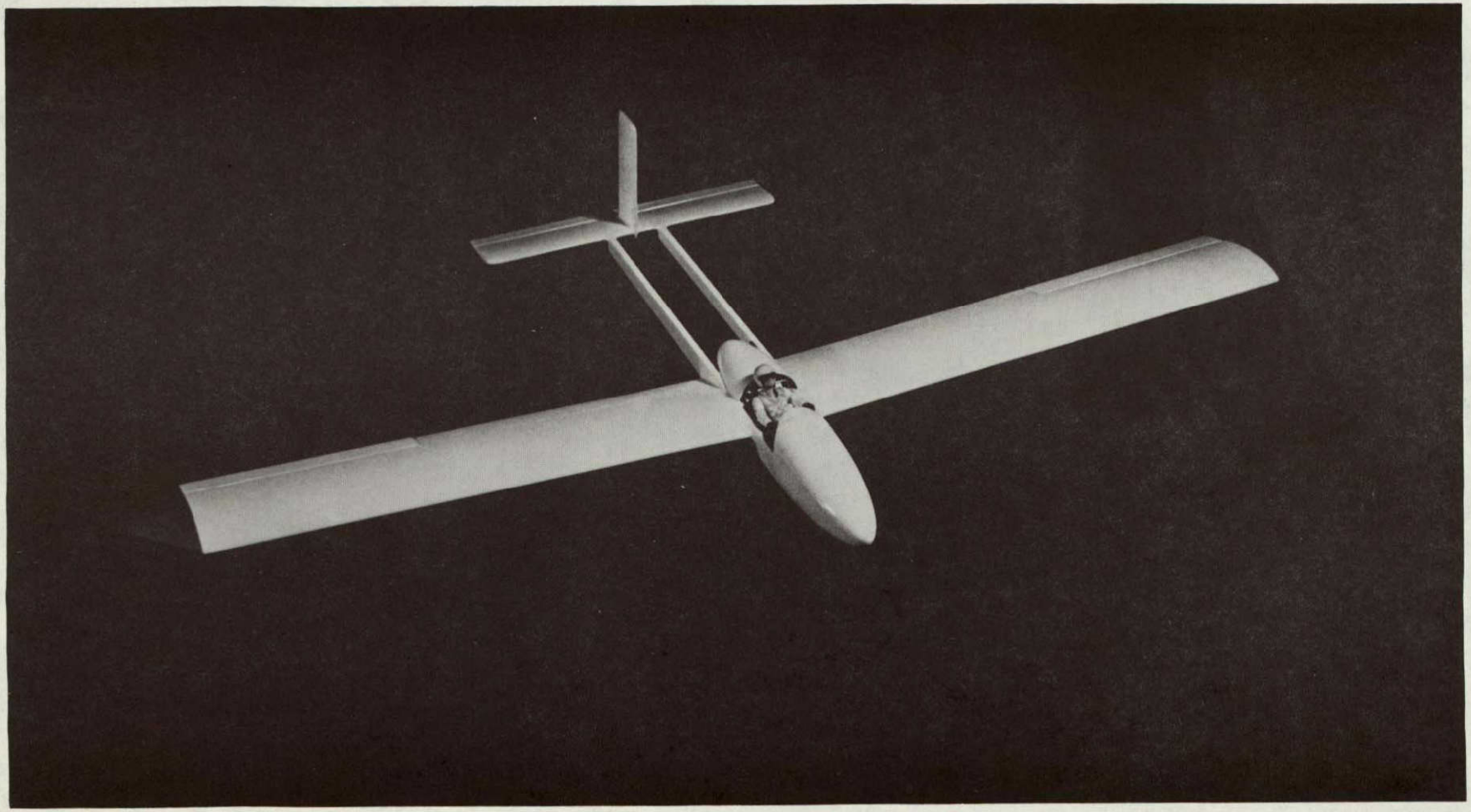

Fig. 33 MODEL OF THE ALL COMPOSITED ULTRALIGHT GLIDER

2. Fuselage Group - 6 students

A mock-up of the tail-boom and forward fuselage shell has been fabricated in plywood and fiber glass, with the final accommodation and structural protection for the reclining pilot presently being assessed.

The fuselage shell fabrication technique has been worked out, the female mold has been constructed and two kevlar/fiber glass half-shells have been fabricated. Figure 34 is a photograph of the mock-up and forward fuselage shell.

3. Tail Group - 6 students

The prototype tail module for both the vertical and horizontal tail surfaces has been fabricated, employing a new technique of panel-on-ribs construction. In this process, a single side, kevlar-stabilized foam sheet is laid up on a flat surface. When the foam sheet is partially cured, it is molded to the airfoil contour imposed by the foamed plastic sheet ribs. A tail module rib assembly is shown in Figure 35 and a completed surface in Figure 36. The skins are kevlar, the leading edge is balsa.

This new technique produces an extremely lightweight and true-to-tolerance airfoil shape, when the flight loads are in the proper range, without the need for time-consuming preparation of female molds. For the wing, the twisting moment associated with the Wortmann FX 63-137 airfoil is too

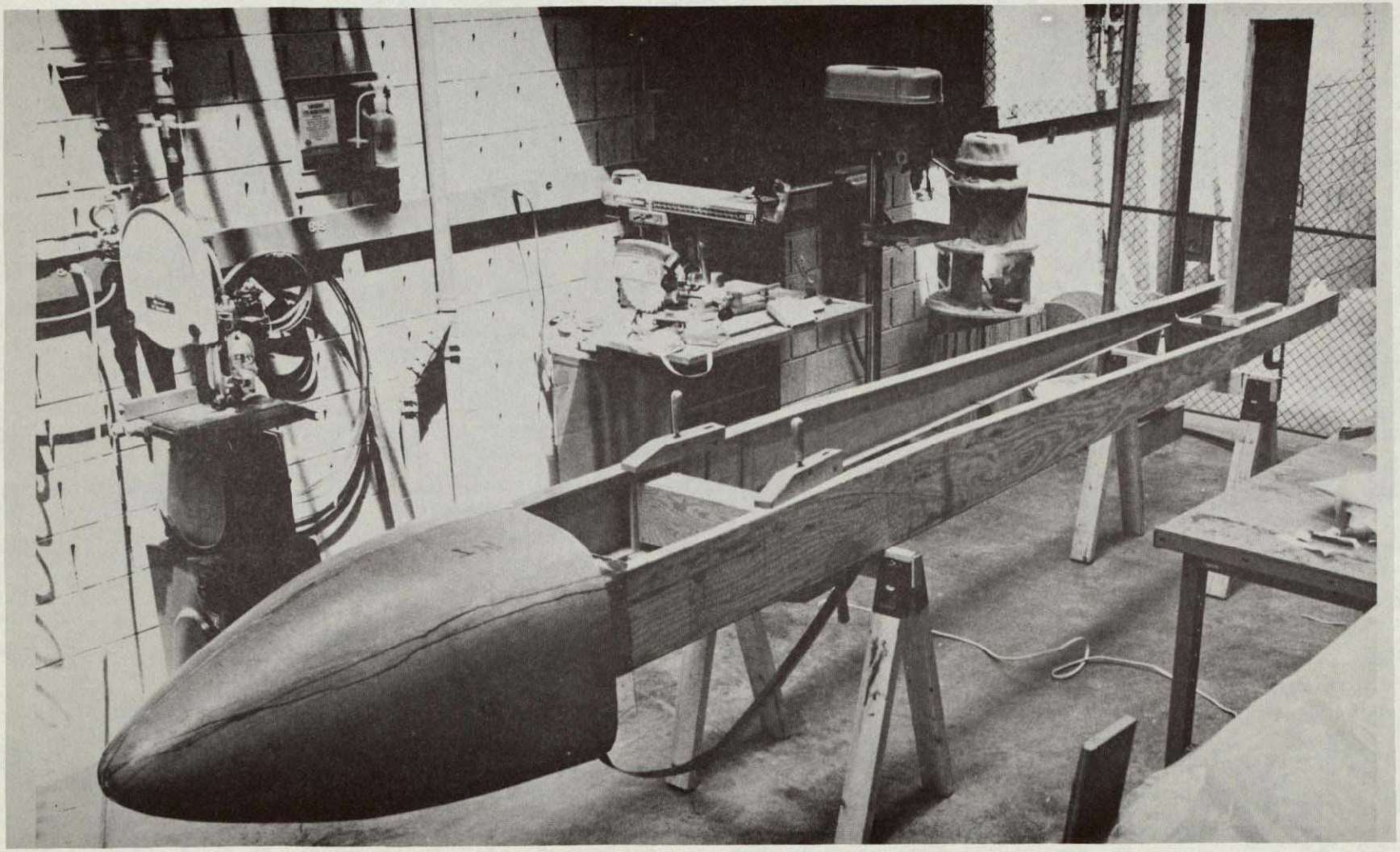

Fig. 34 TAIL BOOM MOCK-UP AND FIBERGLASS FORWARD FUSELAGE

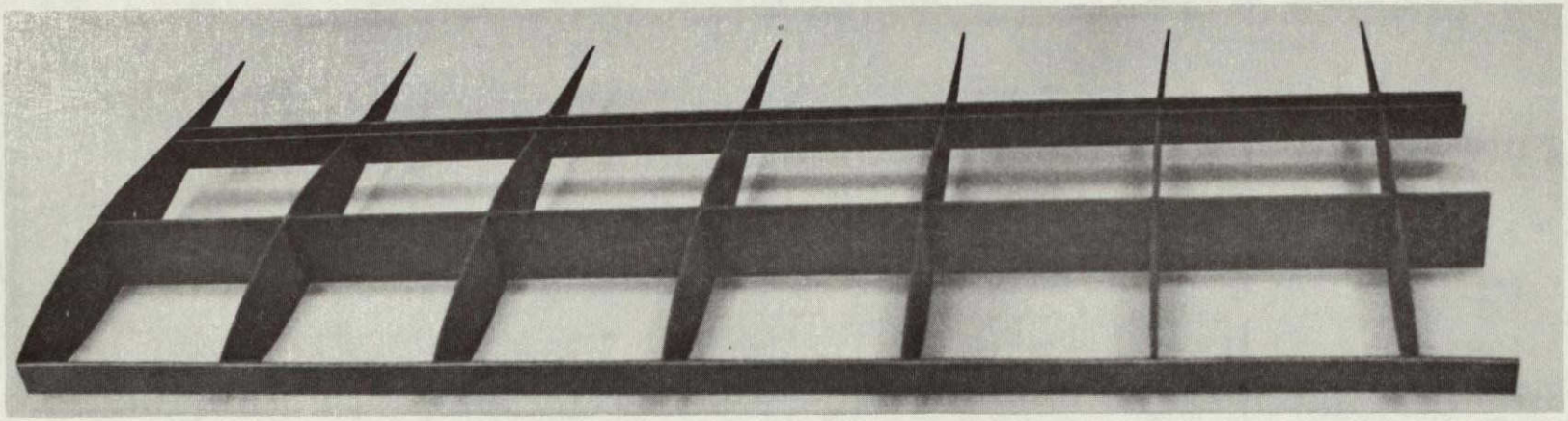

Fig. 35 TAIL MODULE RIB ASSEMBLY

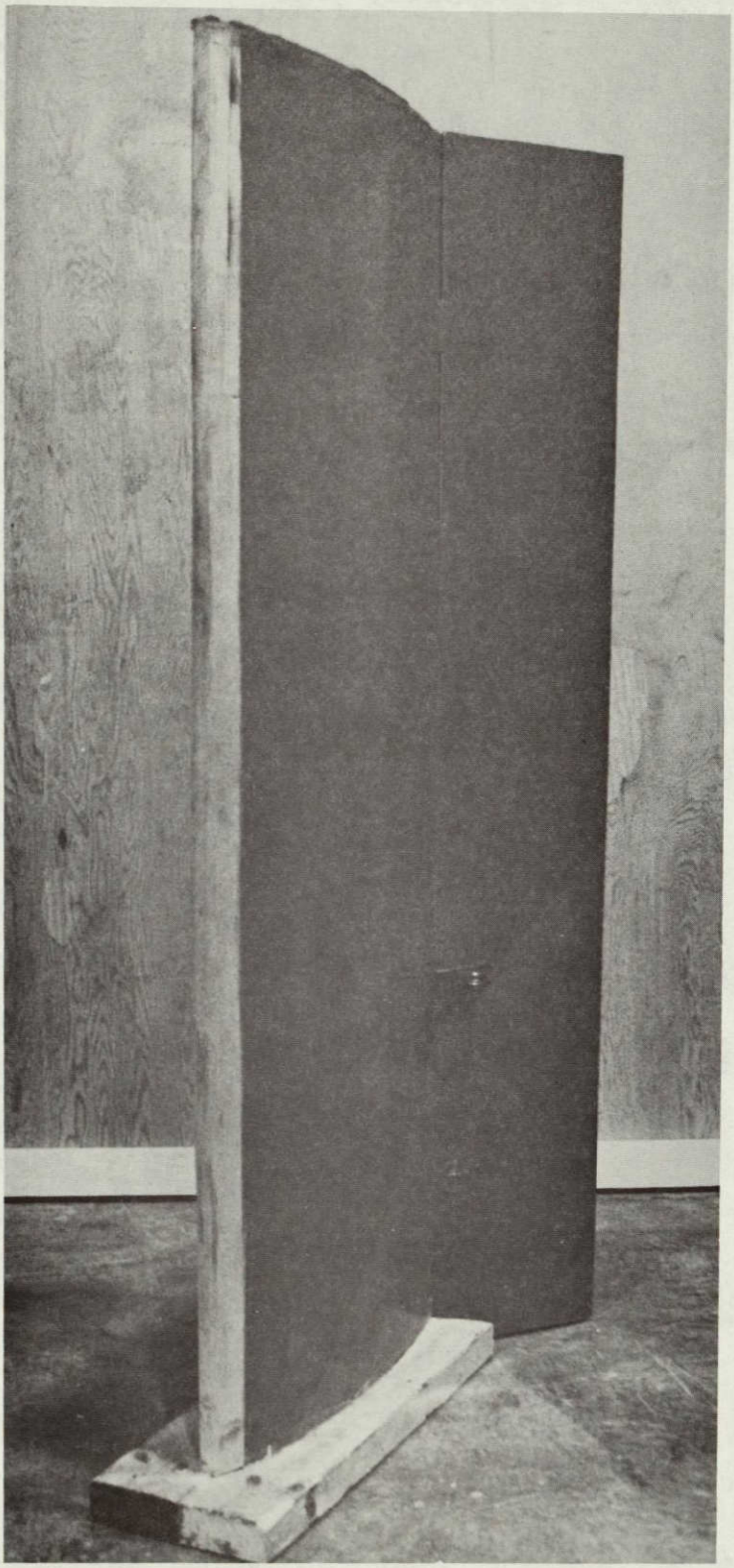

Fig. 36 COMPLETED TAIL SURFACE

high for us to use this simplified construction method, but the final method used on the wing is also an outgrowth of the new technique described here. For future development of ultra-light sailplanes, if low pitching moment wing sections are selected, the new technique can be used throughout and represents an important breakthrough. Composite high-performance ultra-lights with air frame weights between 60 and 70 lbs. appear easily achievable by this construction technique.

4. Controls Group - 6 students

Sample bell cranks and control horns have been produced from symmetric carbon layups and have passed proof tests under control forces according to FAA compliance suggestions. Rudder and elevator hinge design alternatives have been explored and fabricated. Their proof tests remain to be conducted. Control fixtures have been redesigned for the reclined and/or upright pilot. These fixtures permit separate elevator control but interconnected ailerons and rudder. Sample control pushrods have been fabricated in the form of 3-foot length, 1-inch diameter carbon tubes. Attempts to produce smaller diameter and greater length pushrods have not yet been successful. In view of the fabrication schedule, however, standard general aviation control hardware suitable for the prototype ultra-light sailplane has been identified and ordered to provide a satisfactory though slightly heavier back-up system.

5. Engine Group - 2 students

An air-cooled engine nominally rated at 9 hp was secured to achieve the self-launch capability proposed as the second demonstration project making use of a modification of the current version of the aircraft. This engine is presently undergoing tests, and the pusher propeller, drive train and deployment mechanism are under study.

6. Aeroelastic Studies

An extensive set of calculations has been completed for the new wing design which is currently being built. These analyses verify that the static aeroelastic wing characteristics are satisfactory. For completeness (as well as the student's edification), the distributions of lift, angle of attack, elastic angle, torque, shear and bending moment were calculated, assuming (in turn) a rigid wing, a semi-rigid wing and a completely elastic wing. These calculations were performed for the 30.5 m/s penetration condition.

The planform and the cross-sectional properties (of interest) of the new wing are constant with span except for a small tapered wing tip section. (See Figure 37 for both planform and cross-sectional items of interest.) Therefore, it was more convenient to deal analytically with the planform as a straight wing with a rigid weightless wing tip of tapered planform. This method of formulation leads to an

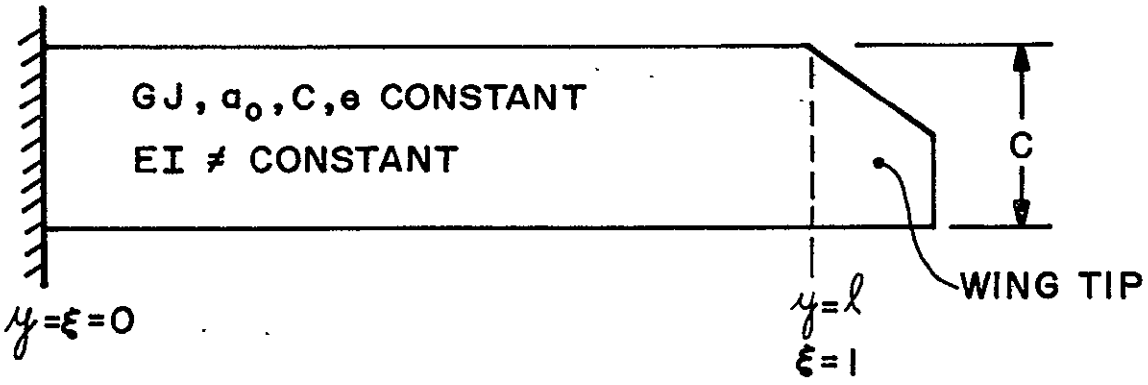

WING PLAN FORM

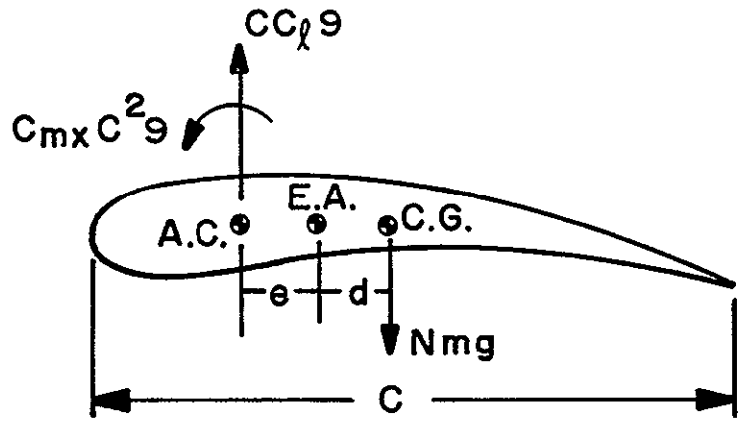

"CONSTANT" WING CROSS-SECTION

Fig. 37 Schematic wing plan form and cross-section

unusual aeroelastic boundary value problem which is described in the sequel in detail.

For conventional unswept subsonic wings, the offset distance "e" between the aerodynamic center and the elastic axis usually contributes much more of a twisting moment at any generic wing section than does the couple customarily called the aerofoil pitching moment. However, this is not true for our glider wing since its pitching moment is an order of magnitude larger than that of airfoil sections used on conventional aircraft. Thus we will witness the unusual phenomenon of aeroelastic effects unloading the outboard portions of a straignt wing and moving the center of pressure inboard. This in turn modifies the usual shapes of all the above-mentioned distribution calculations.

A. The Basic Boundary Value Problem in Terms of the Elastic Wing

The basic problem is to determine, for a given load factor N, the root angle of attack $\alpha^r(0)$ and the elastic twist angle distribution $\theta(\xi)$ where ξ measures the nondimensional length along the constant planform semi-span. Here $0 \leq \xi \leq 1$ and $\xi = 1$ is the interface between the constant planform semi-span and the root of the wing tip.

Given the rigid wing tip contributions to torque, moment and lift per radian exerted on the boundary at $\xi = 1$ (T_1, M_1 and L_1, respectively), all distributions of interest may be found from the elastic twist relation and its two boundary

conditions, subject to the constraint that the lift equals the weight times the load factor (L = NW). These are given by

$$\frac{d^2\theta}{d\xi^2} + (\lambda\ell)^2\theta = K^* \qquad \text{(Twist Eq.)}$$

$$\left.\begin{aligned} &\theta(0) = 0 \\ &\frac{d\theta}{d\xi}(1) = \frac{T_1 \ell}{GJ}\left[\alpha^r(0) + \theta(1)\right] \end{aligned}\right\} \text{(Boundary Conditions)}$$

$$NW = 2qca_o\ell \int_o^1 [\alpha^r(0) + \theta(\xi)]d\xi + 2L_1[\alpha^r(0) + \theta(1)] \qquad \text{(L = NW Constraint Eq.)}$$

where, referring to Figure 37 and in terms of usual aeronautical notation,

$$\lambda^2 = \frac{qcea_o}{GJ}$$

$$a_o = \partial c_\ell/\partial\alpha$$

$$q = \tfrac{1}{2}\rho V^2$$

$$K^* = -\frac{\ell^2}{GJ}(qcea_o\alpha^r(0) + c_{mac}c^2 - mNgd)$$

The unusual feature of this problem is that the twist rate boundary condition at $\xi = 1$ $\left[\text{i.e. } \frac{d\theta}{d\xi}(1) = \ldots.\right]$ depends on the root angle $\alpha^r(0)$ which is unknown until the L = NW equation (which contains $\alpha^r(0)$ and $\theta(\xi)$ in integral form) is explicitly solved for. As an additional complication, K^* also depends on $\alpha^r(0)$ and N as shown above.

B. Elastic Wing Results

With much more labor than is characteristic of a usual static aeroelastic problem we find

$$\alpha^r(0) = \left[\left\{1 - F_2\left(\frac{W_{wing}}{W}\right)\frac{d}{e}\right\}\frac{NW}{2qca_o\ell} + F_2\frac{c_{mac}}{a_o}\frac{c}{e}\right]/(F_1 - F_2)$$

$$\theta(\xi) = A\sin\lambda\ell\xi + \frac{K^*}{(\lambda\ell)^2}(1 - \cos\lambda\ell\xi)$$

where

$$\frac{K^*}{(\lambda\ell)^2} = \frac{WN}{2qca_o\ell}\left(\frac{W_{wing}}{W}\right)\frac{d}{e} - \alpha^r(0) - \frac{c_{mac}}{a_o}\frac{c}{e}$$

$$A = \frac{\frac{K^*}{(\lambda\ell)^2}\left[(1 - \cos\lambda\ell)(T_1\ell/GJ) - \lambda\ell\sin\lambda\ell\right] + (T_1\ell/GJ)\alpha^r(0)}{[\lambda\ell\cos\lambda\ell - (T_1\ell/GJ)\sin\lambda\ell]}$$

$$F_1 = 1 + \frac{L_1}{qca_o\ell}\left(\frac{1 - \cos\lambda\ell}{\lambda\ell} + \frac{L_1\sin\lambda\ell}{qca_o\ell}\right)\left(\frac{(T_1\ell/GJ)}{\lambda\ell\cos\lambda\ell - (T_1\ell/GJ)\sin\lambda\ell}\right)$$

$$F_2 = 1 - \frac{\sin\lambda\ell}{\lambda\ell} + \frac{L_1}{qca_o\ell}(1 - \cos\lambda\ell)$$

$$+ \left(\frac{1 - \cos\lambda\ell}{\lambda\ell} + \frac{L_1}{qca_o\ell}\sin\lambda\ell\right)\left[\frac{-\lambda\ell\sin\lambda\ell + (1 - \cos\lambda\ell)(T_1\ell/GJ)}{\lambda\ell\cos\lambda\ell - (T_1\ell/GL)\sin\lambda\ell}\right]$$

With the $\theta(\xi)$ distribution and $\alpha^r(0)$ solved for a given N, we find the lift distribution to be

$$qcc_\ell(\xi) = qca_o[\alpha^r(0) + \theta(\xi)]$$

and we may write the torque, shear and moment distribution in primitive form as

$$T(\xi) = (GJ/\ell)\frac{d\theta}{d\xi}$$

$$S(\xi) = qca_o\ell \int_{\xi}^{1} [\alpha^r(0) + \theta(\eta)]d\eta - mg\ell N \int_{\xi}^{1} d\eta + L_1[\alpha^r(0) + \theta(1)]$$

$$M(\xi) = qca_o\ell^2 \int_{\xi}^{1} (\eta - \xi)[\alpha^r(0) + \theta(\eta)]d\eta - mg\ell^2 N \int_{\xi}^{1} (\eta - \xi)d\eta$$

$$+ [\alpha^r(0) + \theta(1)][M_1 + \ell L_1(1 - \xi)]$$

where η is a dummy variable of integration. Carrying out the integrations and simplifying we find

$$T(\xi) = \frac{GJ}{\ell}(\lambda\ell)\left[A\cos\lambda\ell\xi + \frac{K^*}{(\lambda\ell)^2}\sin\lambda\ell\xi\right]$$

$$S(\xi) = \left[qca_o\ell\left\{\alpha^r(0)\frac{K^*}{(\lambda\ell)^2}\right\} - mg\ell N\right](1 - \xi)$$

$$+ \frac{qca_o\ell}{\lambda\ell}\left[A(\cos\lambda\ell\xi - \cos\lambda\ell) + \frac{K^*}{(\lambda\ell)^2}(\sin\lambda\ell\xi - \sin\lambda\ell)\right]$$

$$+ L_1\left[\alpha^r(0) + A\sin\lambda\ell + \frac{K^*}{(\lambda\ell)^2}(1 - \cos\lambda\ell)\right]$$

$$M(\xi) = \tfrac{1}{2}\ell^2\left[qca_o\{\alpha^r(0) + \frac{K^*}{(\lambda\ell)^2}\} - mgN\right](1 - \xi)^2$$

$$+ qca_o\ell^2\left[\frac{A}{(\lambda\ell)^2}\{\sin\lambda\ell - \sin\lambda\ell\xi - (1 - \xi)\lambda\ell\cos\lambda\ell\}\right.$$

$$\left. - \frac{K^*}{(\lambda\ell)^4}\{\cos\lambda\ell - \cos\lambda\ell\xi + (1 - \xi)\lambda\ell\sin\lambda\ell\}\right]$$

$$+ [L_1\ell(1 - \xi) + M_1]\left[\alpha^r(0) + A\sin\lambda\ell - \frac{K^*}{(\lambda\ell)^2}(1 - \cos\lambda\ell)\right]$$

where $\alpha^r(0)$, $\frac{K^*}{(\lambda\ell)^2}$, and A have been previously given (for the elastic wing).

C. Semi-Rigid Wing Results

Neglecting the additional lift due to elastic deformation yields the semi-rigid wing basic formulation as follows

$$\frac{d^2\theta}{d\xi^2} = K^* \qquad \text{(Approx. Twist Eqn.)}$$

$$\left.\begin{aligned} \theta(0) &= 0 \\ \frac{d\theta}{d\xi}(1) &= \frac{T_1 \ell}{GJ}[\alpha^r(0) + \theta(1)] \end{aligned}\right\} \qquad \text{(Boundary Conditions)}$$

$$L = NW \qquad \text{(Constraint Eqn.)}$$

Solving the above equations yields[1]

$$\alpha^r_{S.R.}(0)\left\{\left[1 - \frac{f_2}{2}\left(\frac{W_{wing}}{W}\right)\left(\frac{d}{e}\right)(\lambda\ell)^2\right]\frac{WN}{2qca_o\ell} + \frac{f_2}{2}\left(\frac{c_{mac}}{a_o}\right)\left(\frac{c}{e}\right)(\lambda\ell)^2\right\}\Big/\left[f_1 - \frac{f_2}{2}(\lambda\ell)^2\right]$$

$$\theta_{S.R.}(\xi) = \frac{K^*}{2}\xi^2 + C_1\xi$$

where,

$$K^* = (\lambda\ell)^2\left[\frac{WN}{2qca_o\ell}\left(\frac{W_{wing}}{W}\right)\frac{d}{e} - \alpha^r(0) - \frac{c_{mac}}{a_o}\frac{c}{e}\right]$$

$$C_1 = \left[\left(\frac{T_1\ell}{GJ} - 2\right)\frac{K^*}{2} + \frac{T_1\ell}{GJ}\alpha^r(0)\right]\Big/\left[1 - \frac{T_1\ell}{GJ}\right]$$

$$f_1 = 1 + \frac{\dfrac{L_1}{qca_o\ell} + \tfrac{1}{2}\left(\dfrac{T_1\ell}{GJ}\right)}{\left[1 - \dfrac{T_1\ell}{GJ}\right]}$$

$$f_2 = \tfrac{1}{3} + \frac{\left[\tfrac{1}{2}\left(\dfrac{T_1\ell}{GJ}\right) - 1\right] - \dfrac{L_1}{qca_o\ell}}{\left[1 - \dfrac{T_1\ell}{GJ}\right]}$$

---

[1] The subscript S.R. means "semi-rigid" case.

and carrying out the torque, shear and moment distribution expressions yields

$$T(\xi) = \frac{GJ}{\ell}[K^*\xi + C_1]$$

$$S(\xi) = qca_o\ell\left[\alpha^r_{S.R.}(0)(1-\xi) + \frac{C_1}{2}(1-\xi^2) + \frac{K^*}{6}(1-\xi^3)\right]$$

$$- mg\ell N(1-\xi) + L_1\left[\alpha^r_{S.R.}(0) + C_1 + \frac{K^*}{2}\right]$$

$$M(\xi) = qca_o\ell^2\left[\frac{1}{4}(1-\xi^4)\frac{K^*}{2} + \frac{1}{3}(1-\xi^3)\left(C_1 - \frac{K^*}{2}\xi\right) - \tfrac{1}{2}(1-\xi^2)C_1\xi\right]$$

$$+ \tfrac{1}{2}\ell^2[qca_o\alpha^r_{S.R.}(0) - mgN](1-\xi)^2$$

$$+ \ell(1-\xi)L_1\left[\alpha^r_{S.R.}(0) + C_1 + \frac{K^*}{2}\right]$$

$$+ M_1\left[\alpha^r_{S.R.}(0) + C_1 + \frac{K^*}{2}\right]$$

where $\alpha^r_{S.R.}(0)$, K^* and C_1 have been previously defined in this section. Particularly note that the definition of K^* is different for the elastic case and the semi-rigid case.

D. Rigid Wing Results

By letting $GJ \to \infty$ we obtain the (almost) trivial results for the rigid wing. The rigid angle of attack $\alpha^r_{rigid}(0)$ is immediately given by

$$\alpha^r_R(0) = NW/(2a_oS_Tq)$$

where S_T is the total area of the left (or right) wing, and the torque, shear and moment distributions are given by

$$T(\xi) = [qca_o e\ell(1 - \xi) + T_1]\alpha_R^r(0) + [c_{mac} gc^2 \ell - Nmg\ell d](1 - \xi)$$

$$S(\xi) = [qca_o \ell(1 - \xi) + L_1]\alpha_R^r(0) - mg\ell N(1 - \xi)$$

$$M(\xi) = [qca_o \alpha_R^r(0) - mgN]\left(\frac{\ell^2}{2}\right)(1 - \xi)^2 + [L_1 \ell(1 - \xi) + M_1]\alpha_R^r(0) .$$

where $\alpha_R^r(0)$ has just been previously defined.

E. Numerical Results

Using the physical properties of the CAPGLIDE wing design and the results of the previous sections, twist, total angle, shear, bending increment and torque distribution with span have been plotted in Figures 38 - 51 for various load factors. Table VI presents the root angles of attack versus load factor for the cases of rigid, semi-rigid and elastic wings. Note that for N = 1, Table VI predicts that the elastic wing root angle is 2.480 times larger than the rigid root angle calculation; the semi-rigid to rigid root angle ratio for N = 1 is shown to be 2.362.

TABLE VI

ROOT ANGLES OF ATTACK FOR RIGID $[\alpha_R^r(0)]$, SEMI-RIGID $[\alpha_{S.R.}^r(0)]$ AND ELASTIC WINGS $[\alpha^r(0)]$ VERSUS LOAD FACTOR

N	$\alpha_R^r(0)$	$\alpha_{S.R.}^r(0)$	$\alpha^r(0)$
1	0.036096	0.08526	0.08952
2	0.072191	0.11703	0.12094
3	0.108288	0.14880	0.15236
4	0.144284	0.18057	0.18378
5	0.180480	0.21234	0.21520
6	0.216584	0.24411	0.24662

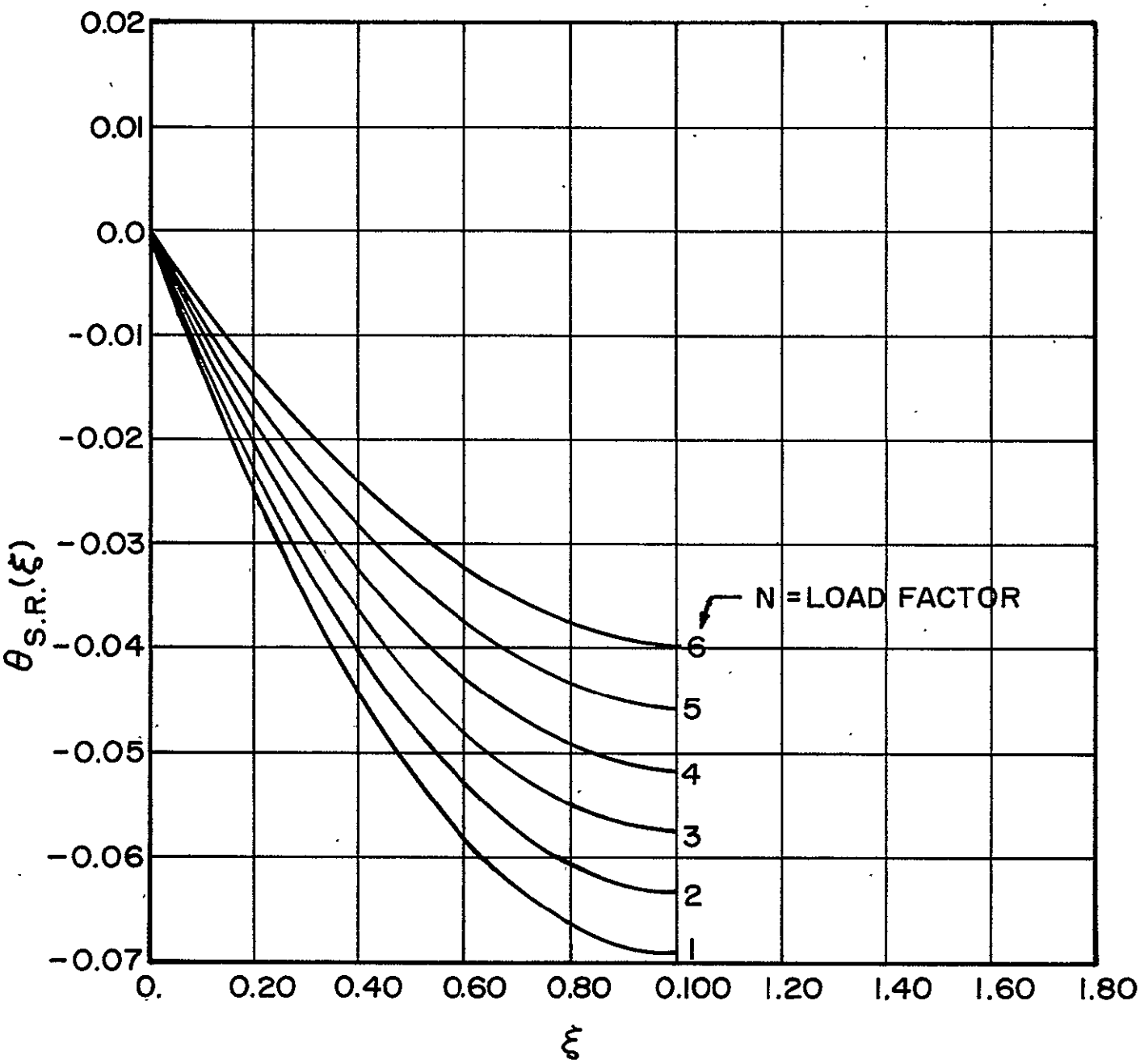

Fig. 38 Semi-rigid elastic twist angle vs ξ with load factor N as a parameter

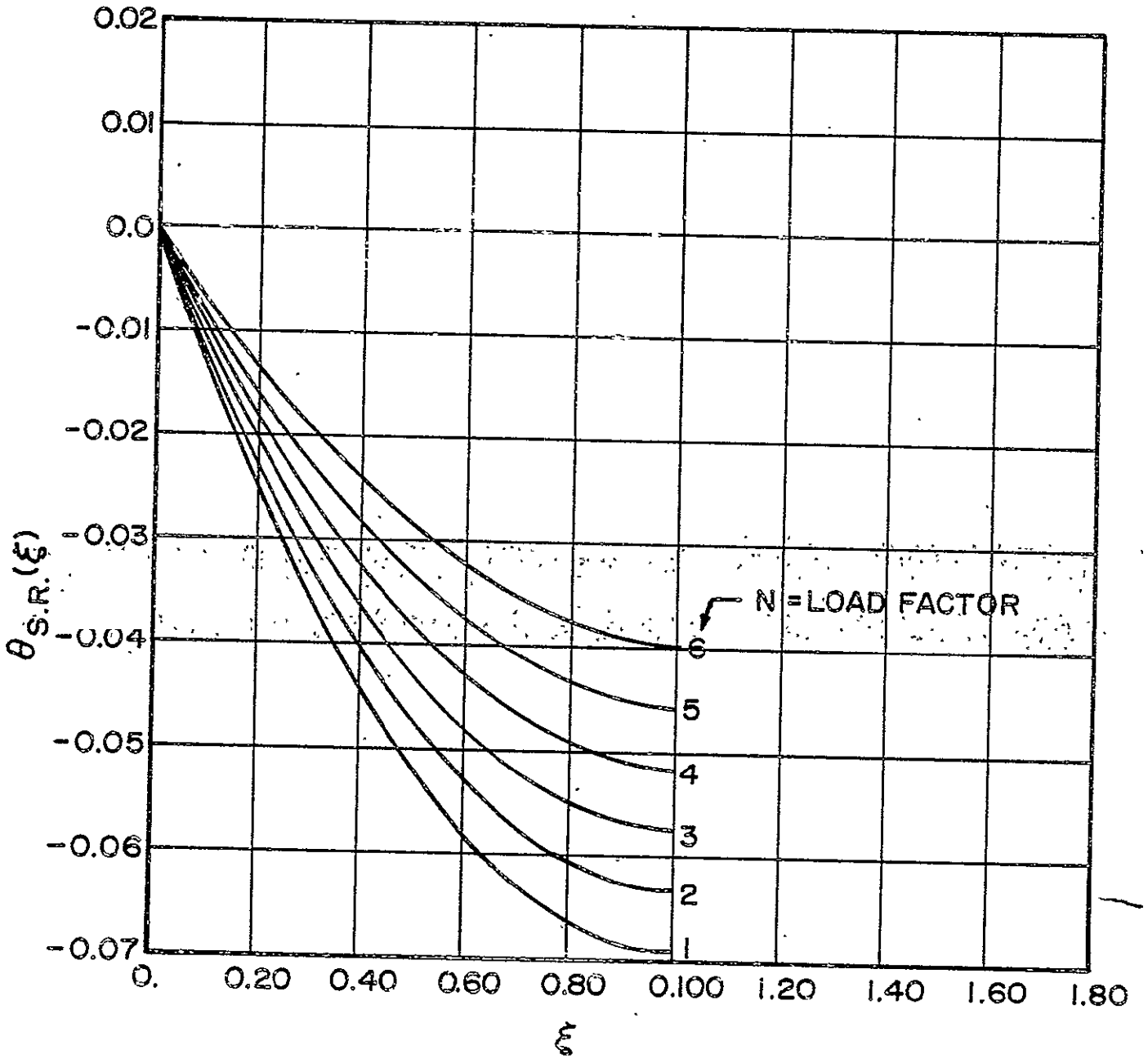

Fig. 38 Semi-rigid elastic twist angle vs ξ with load factor N as a parameter

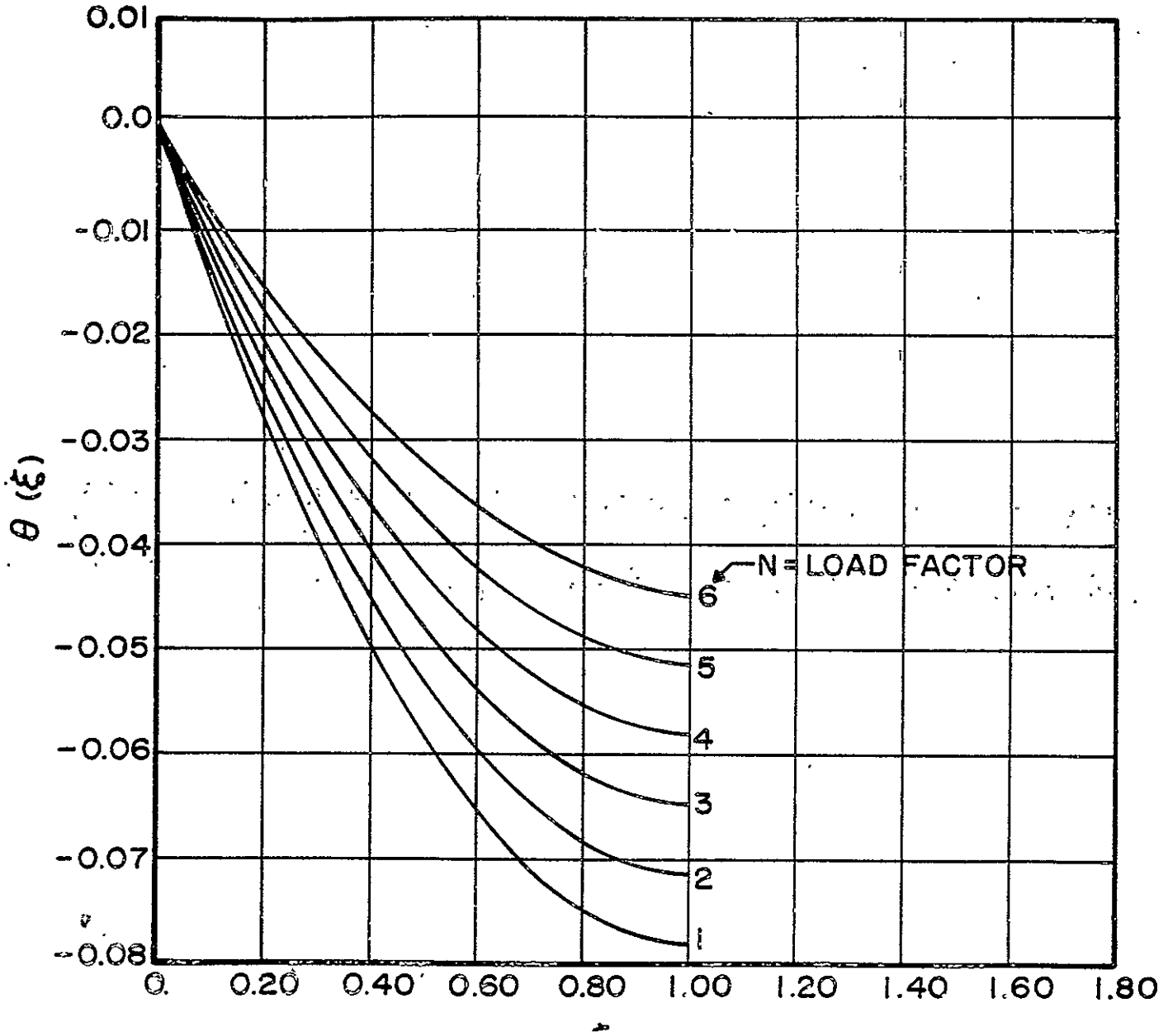

Fig. 39 Elastic twist angle vs. ξ with load factor N as a parameter

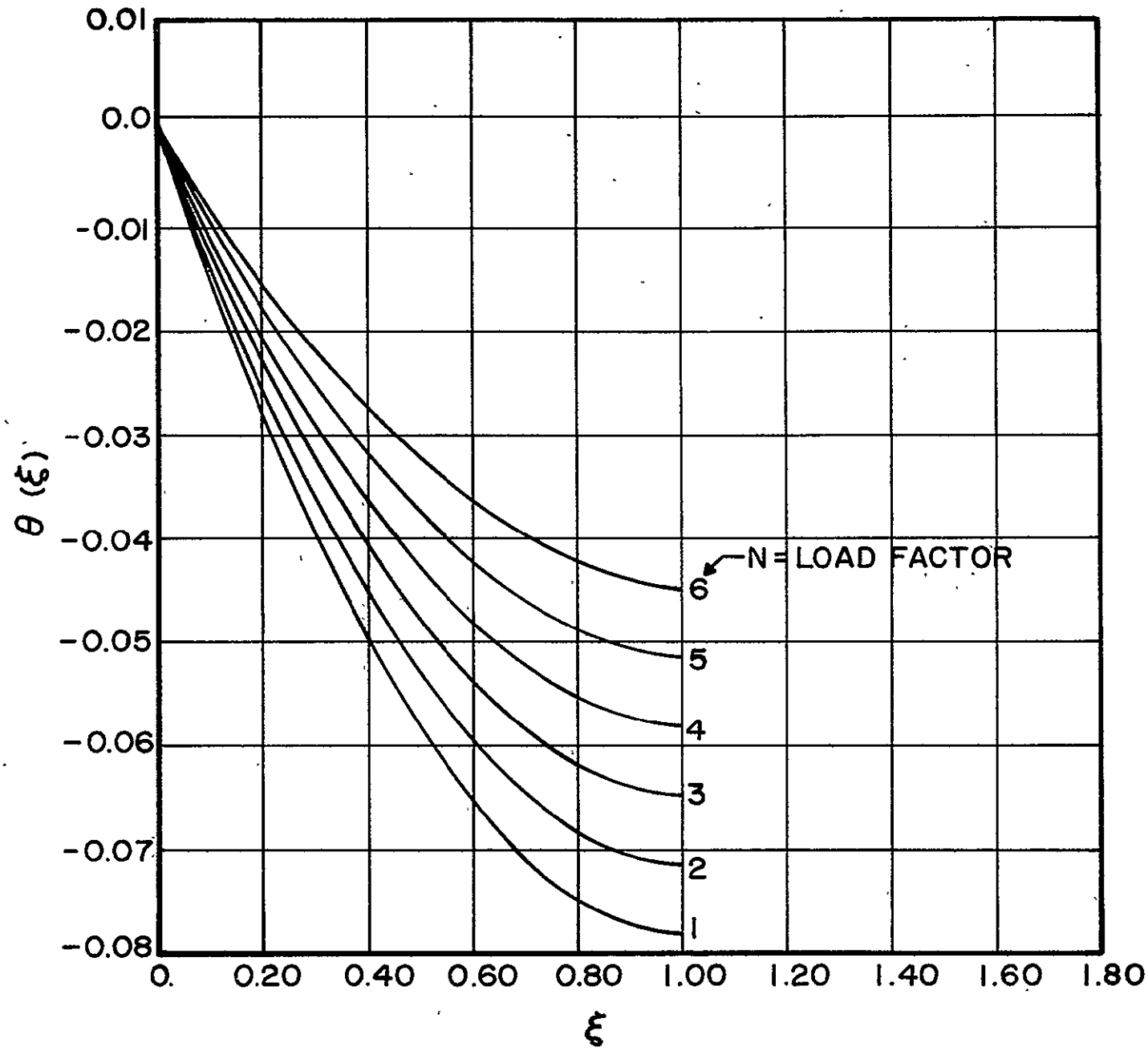

Fig. 39 Elastic twist angle vs. ξ with load factor N as a parameter

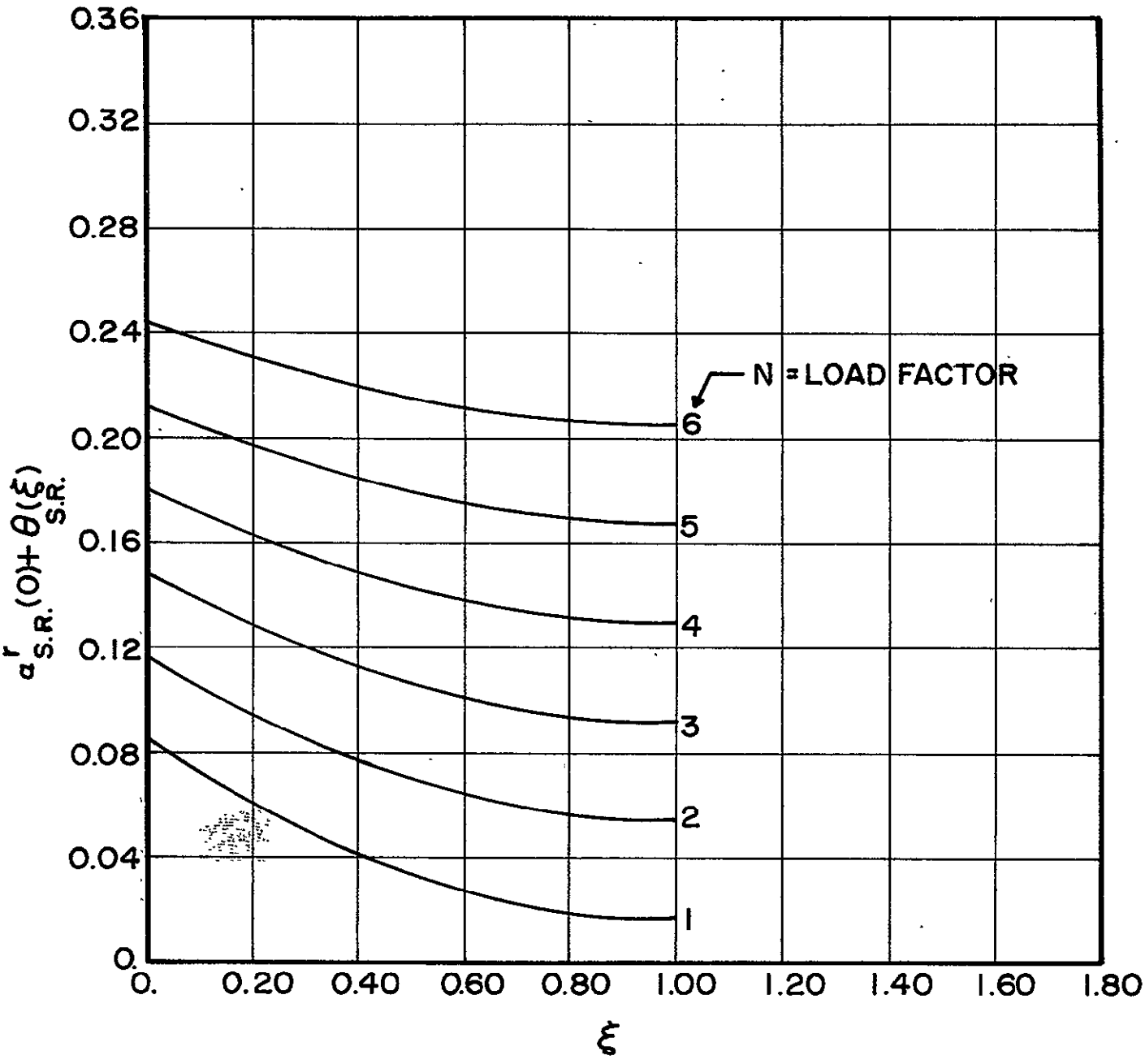

Fig. 40 Semi-rigid wind total angle vs.ξ with load factor as a parameter

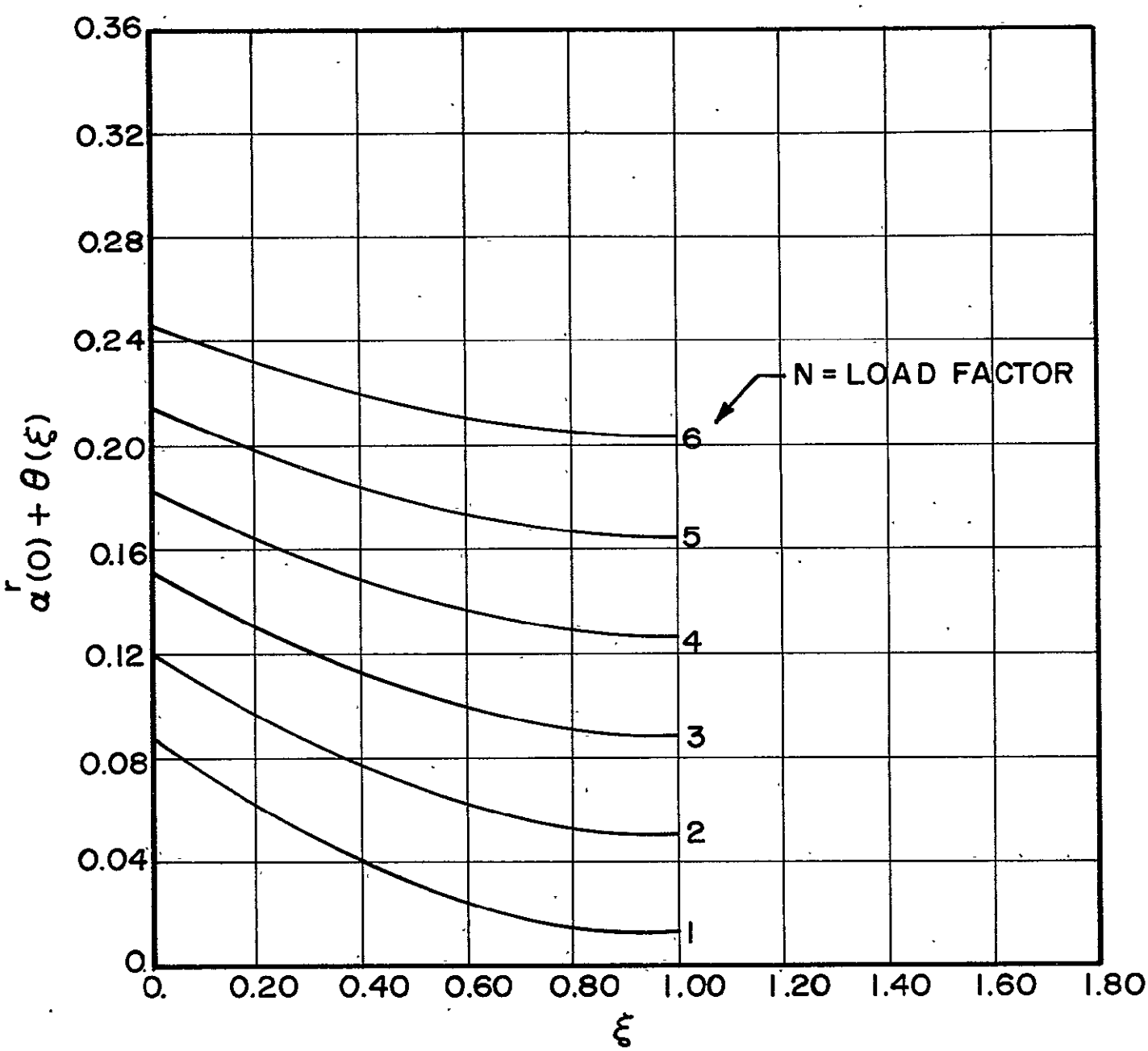

Fig. 41 Elastic wing total angle vs. ξ with load factor as a parameter

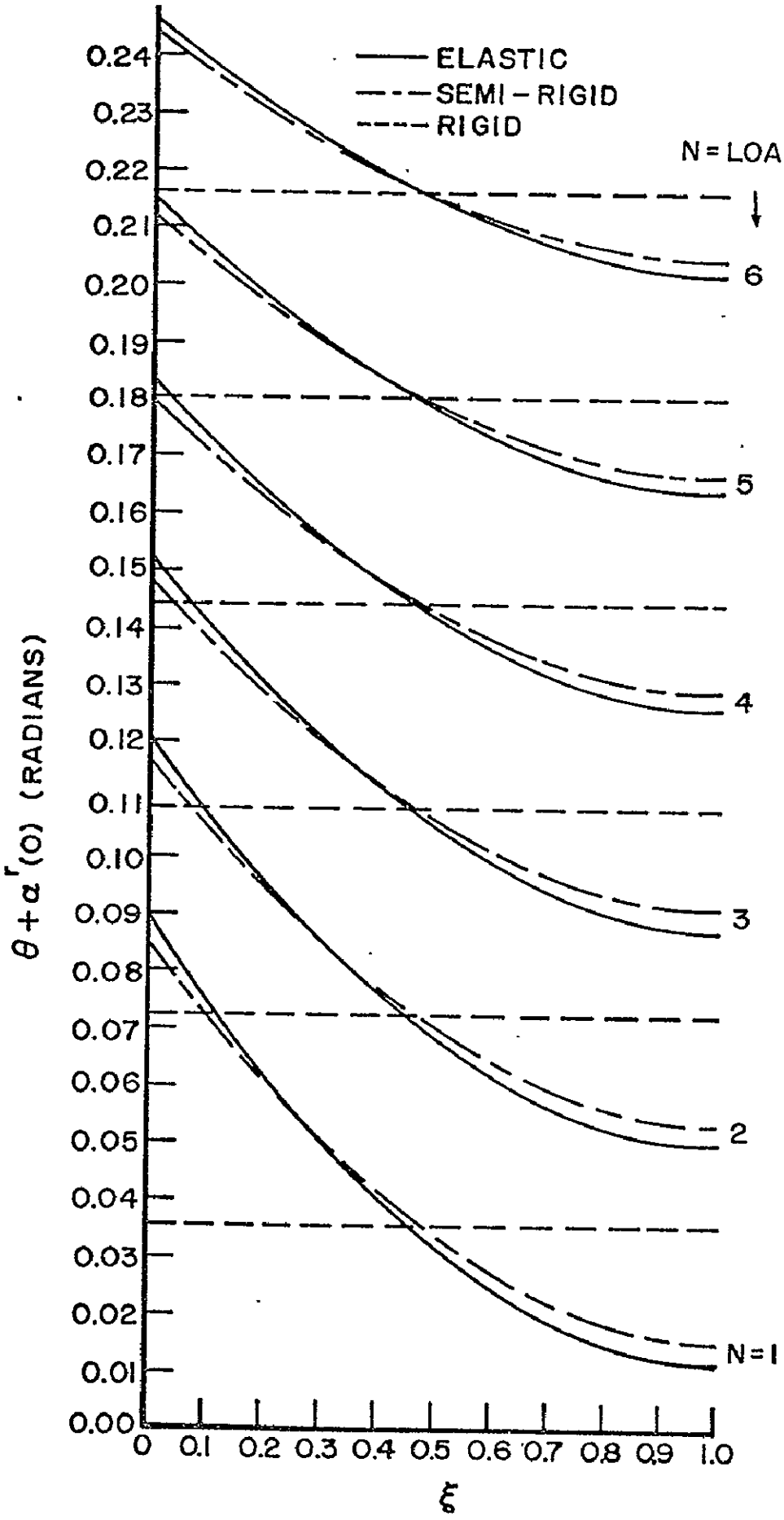

Fig. 42 Total wing angles vs. ξ with load factor as a parameter for the elastic wing, semi-rigid wing, and rigid wing

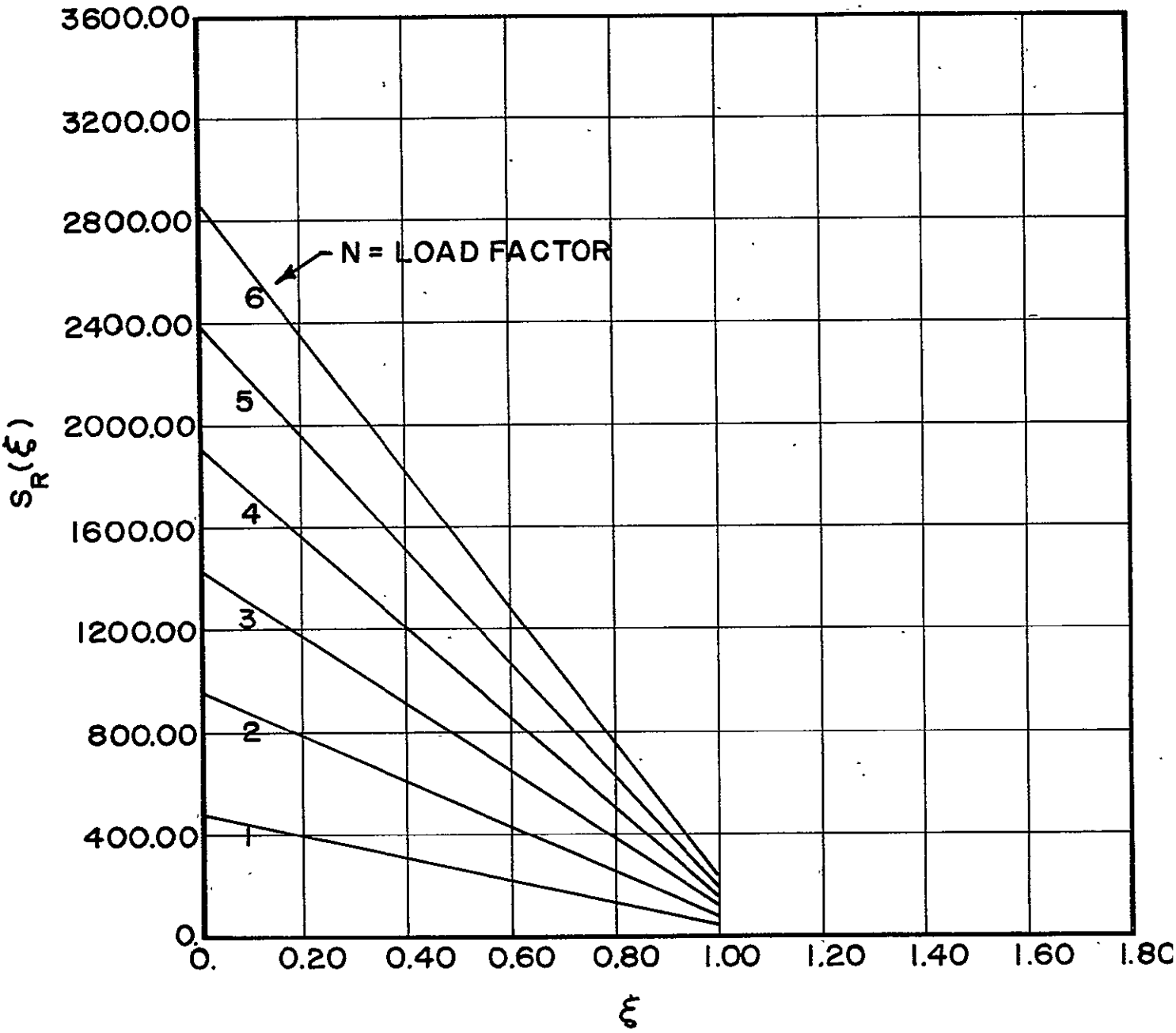

Fig. 43 Rigid wind shear vs. ξ with load factor N as a parameter

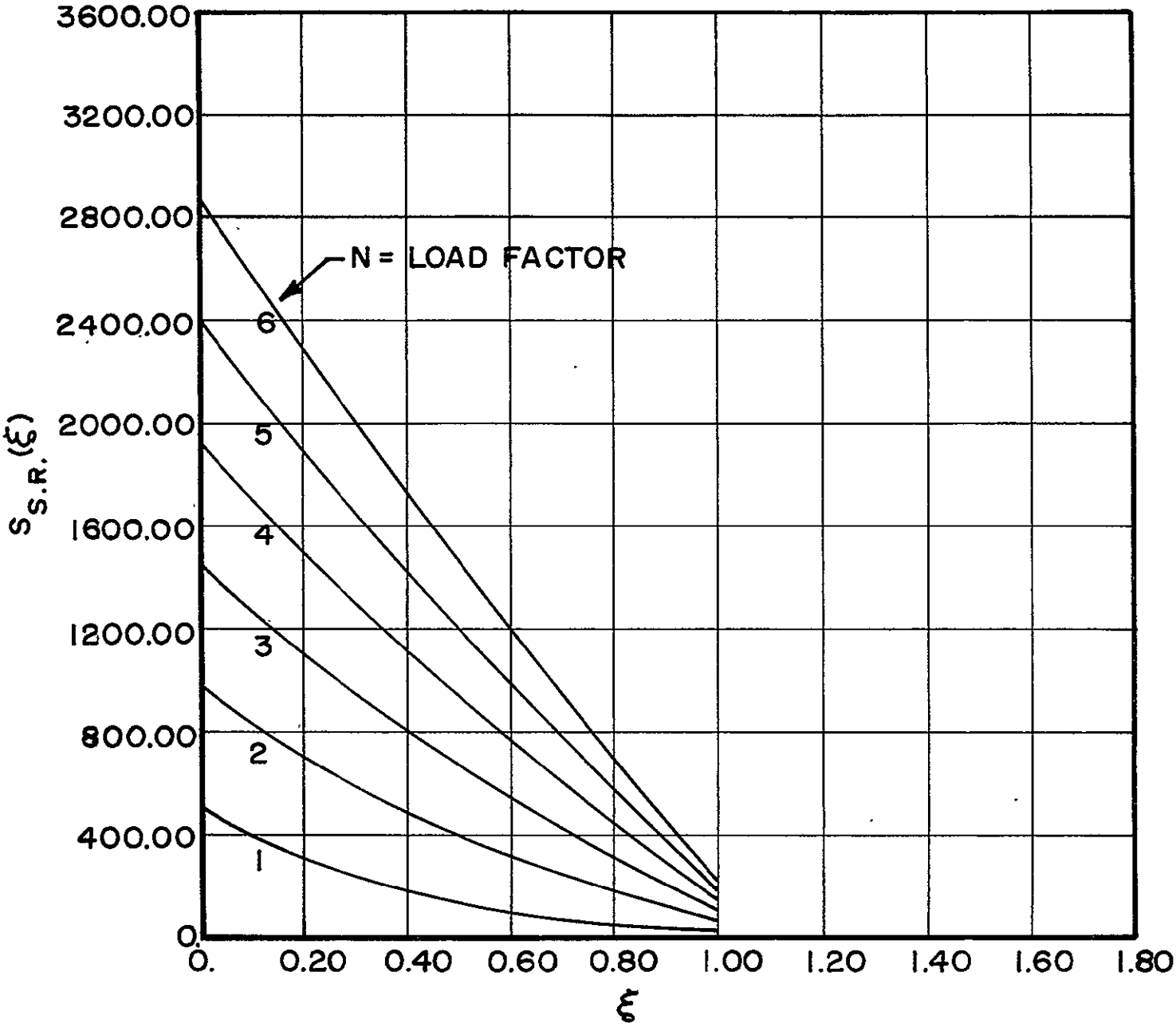

Fig. 44 Semi-rigid wind shear vs. ξ
with load factor N as a parameter

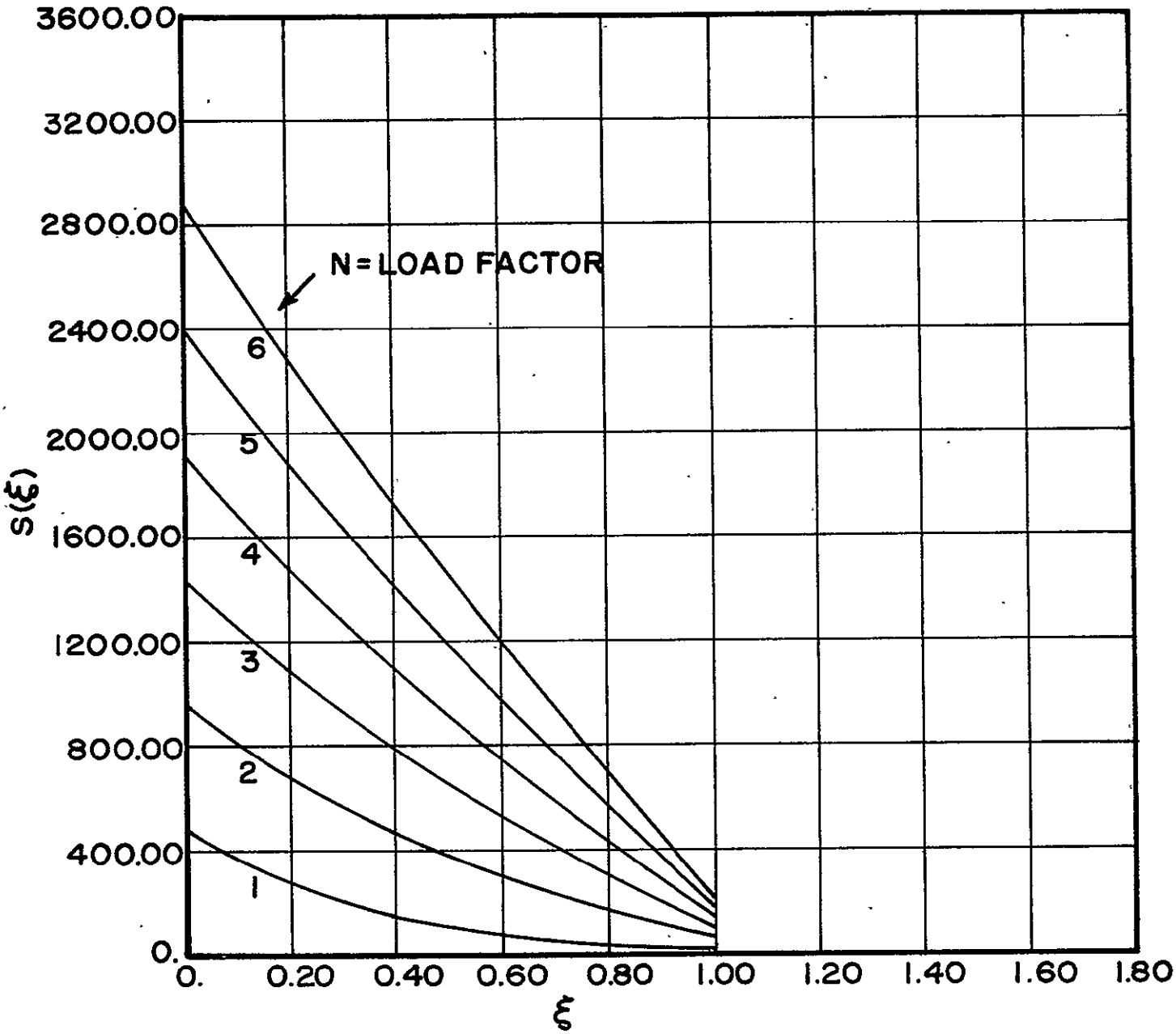

Fig. 45 Elastic wing shear vs. ξ with load factor N as a parameter

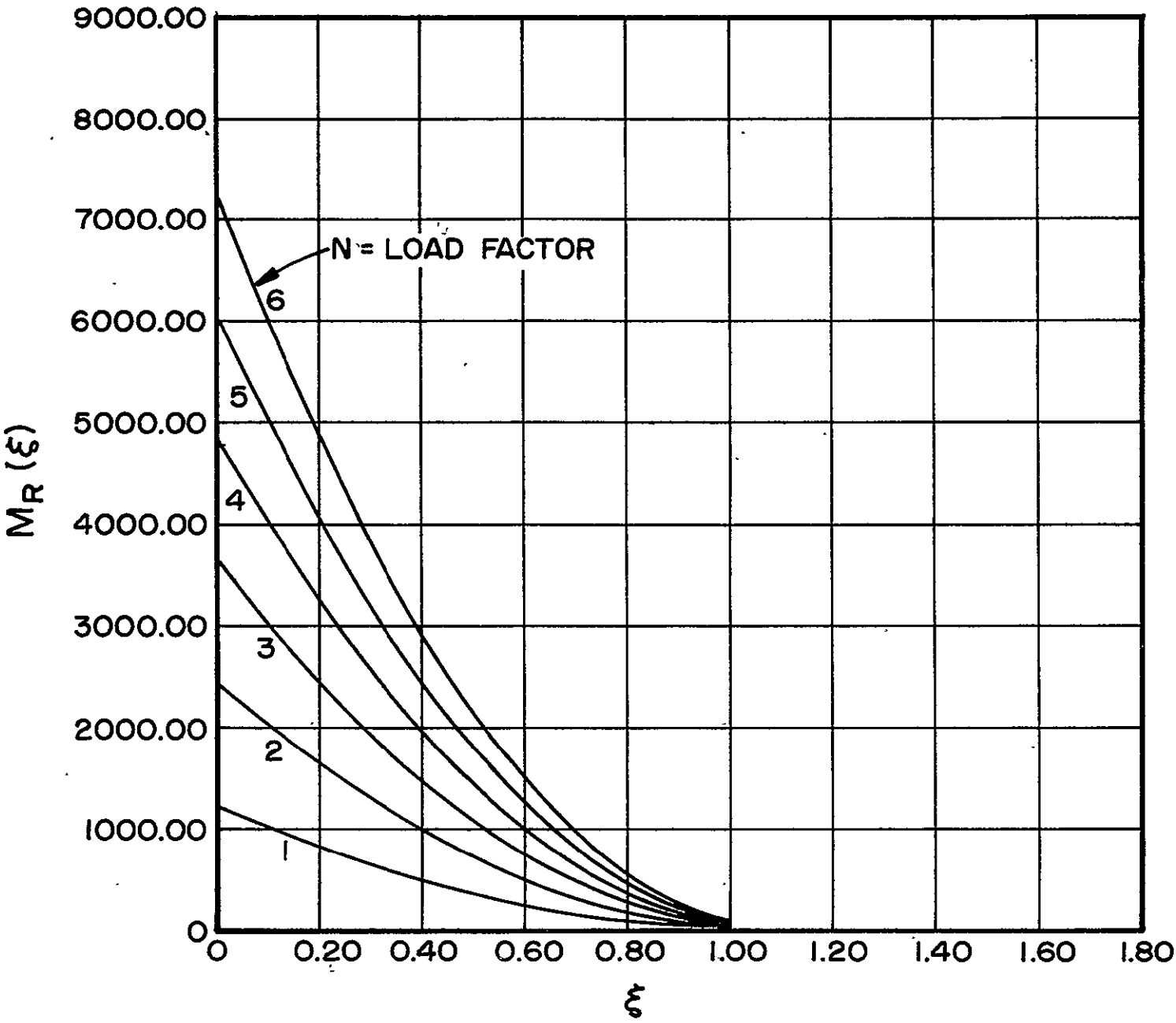

Fig. 46 Rigid wing bending moment vs. ξ with load factor N as a parameter

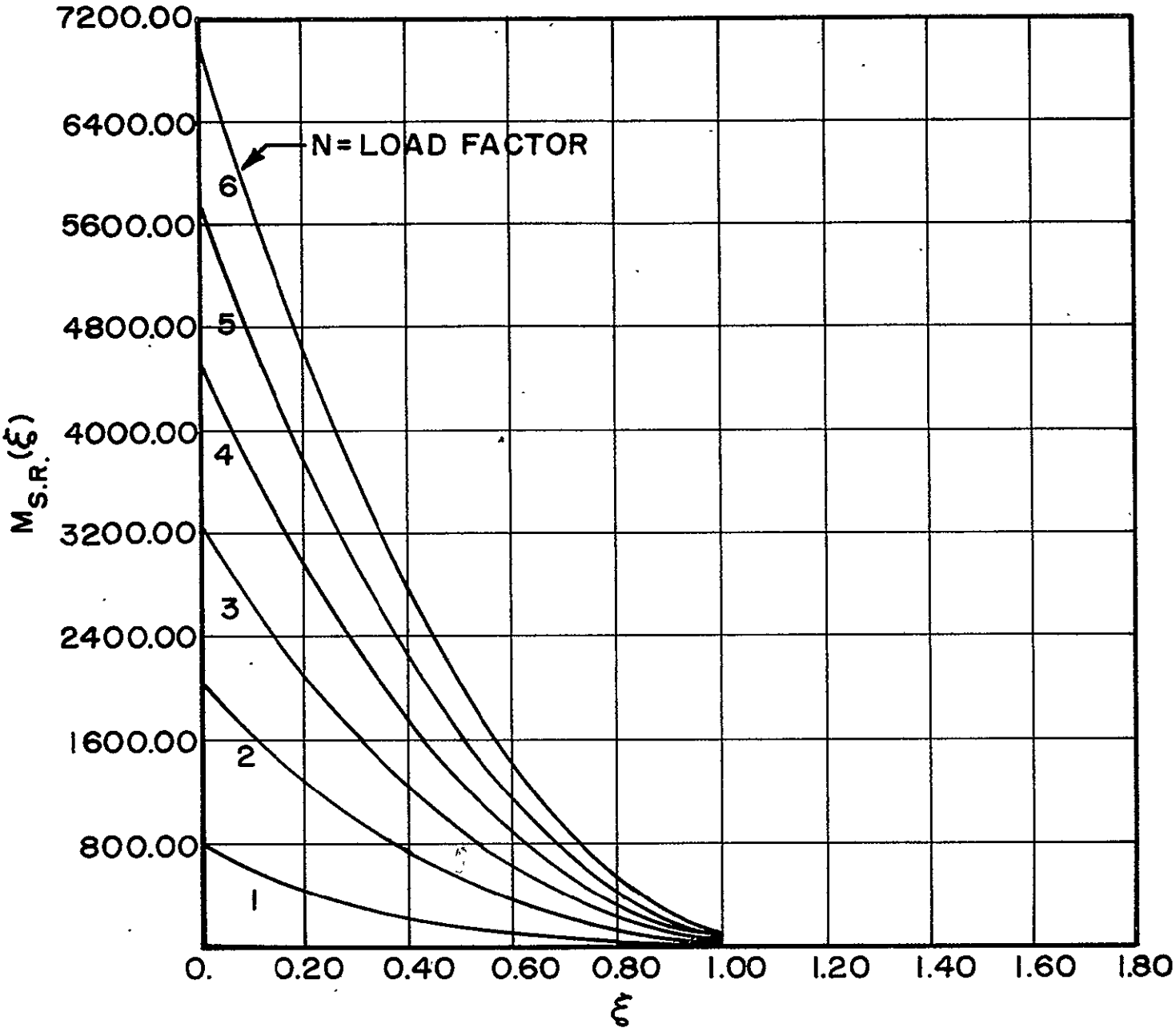

Fig. 47 Semi-rigid wing bending moment vs. ξ with load factor N as a parameter

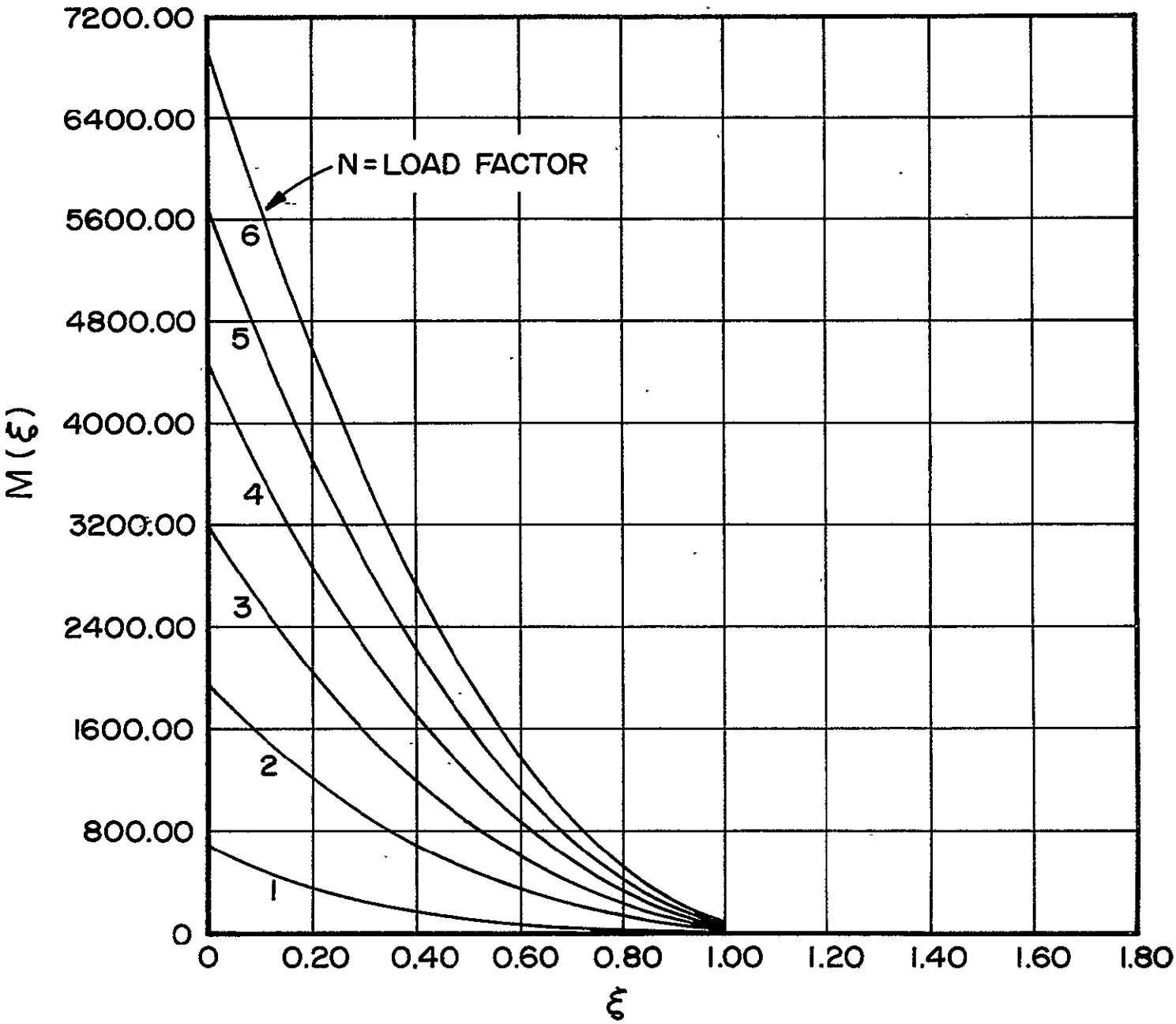

Fig. 48 Elastic wing bending moment vs. ξ with load factor N as a parameter

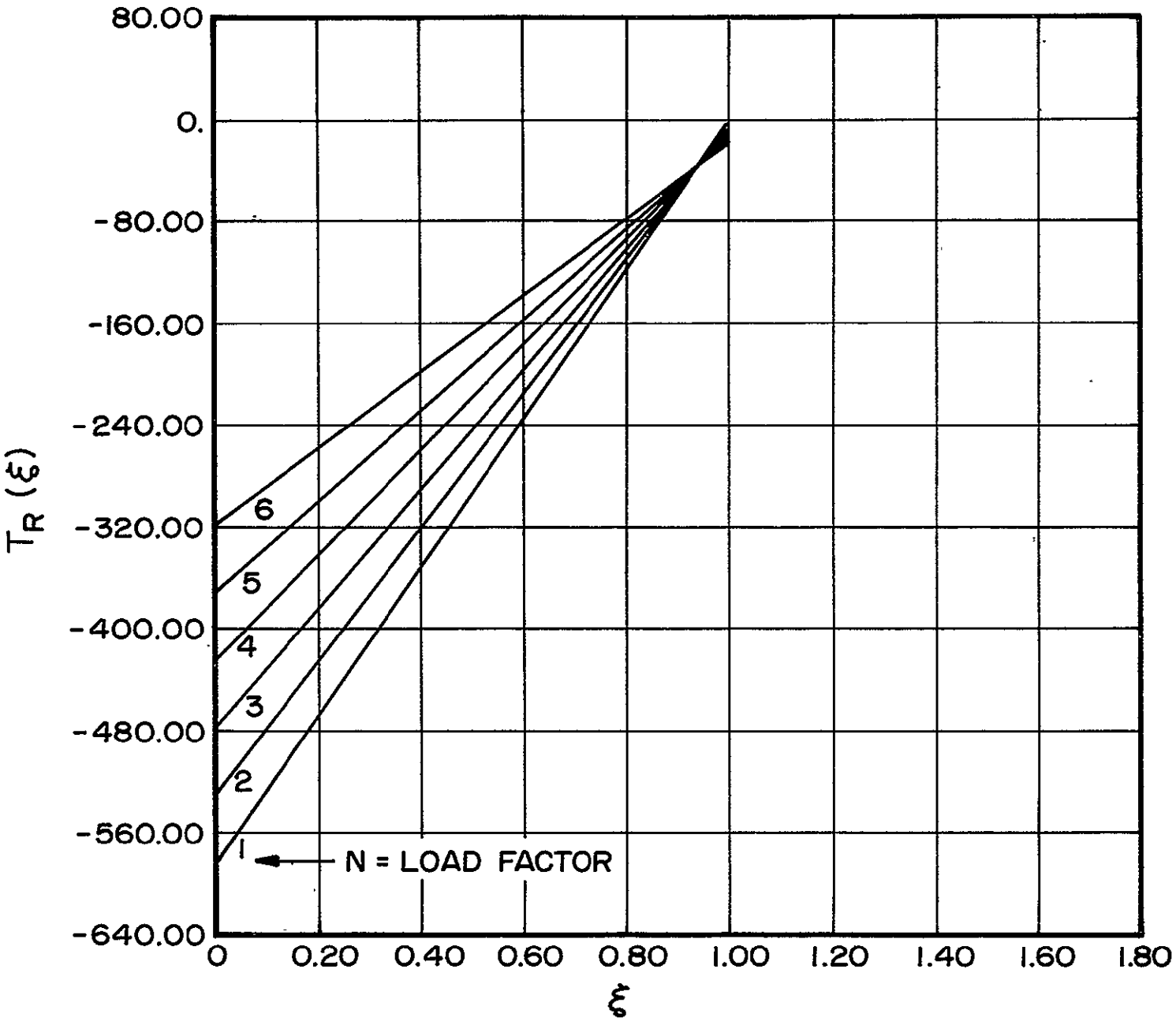

Fig. 49 Rigid wing torque vs. ξ with load factor N as a parameter

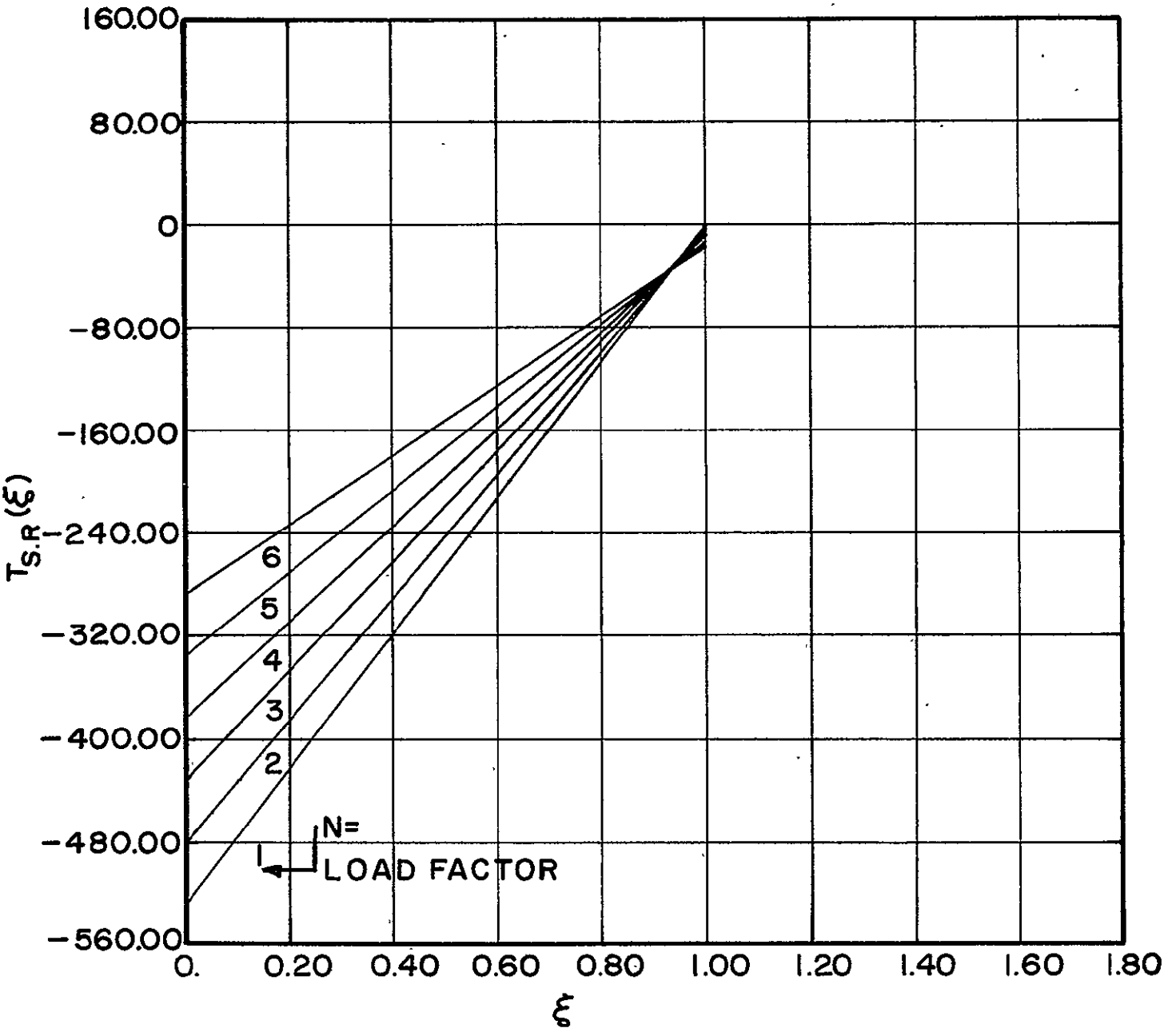

Fig. 50 Semi-rigid wing torque vs. ξ with load factor N as a parameter

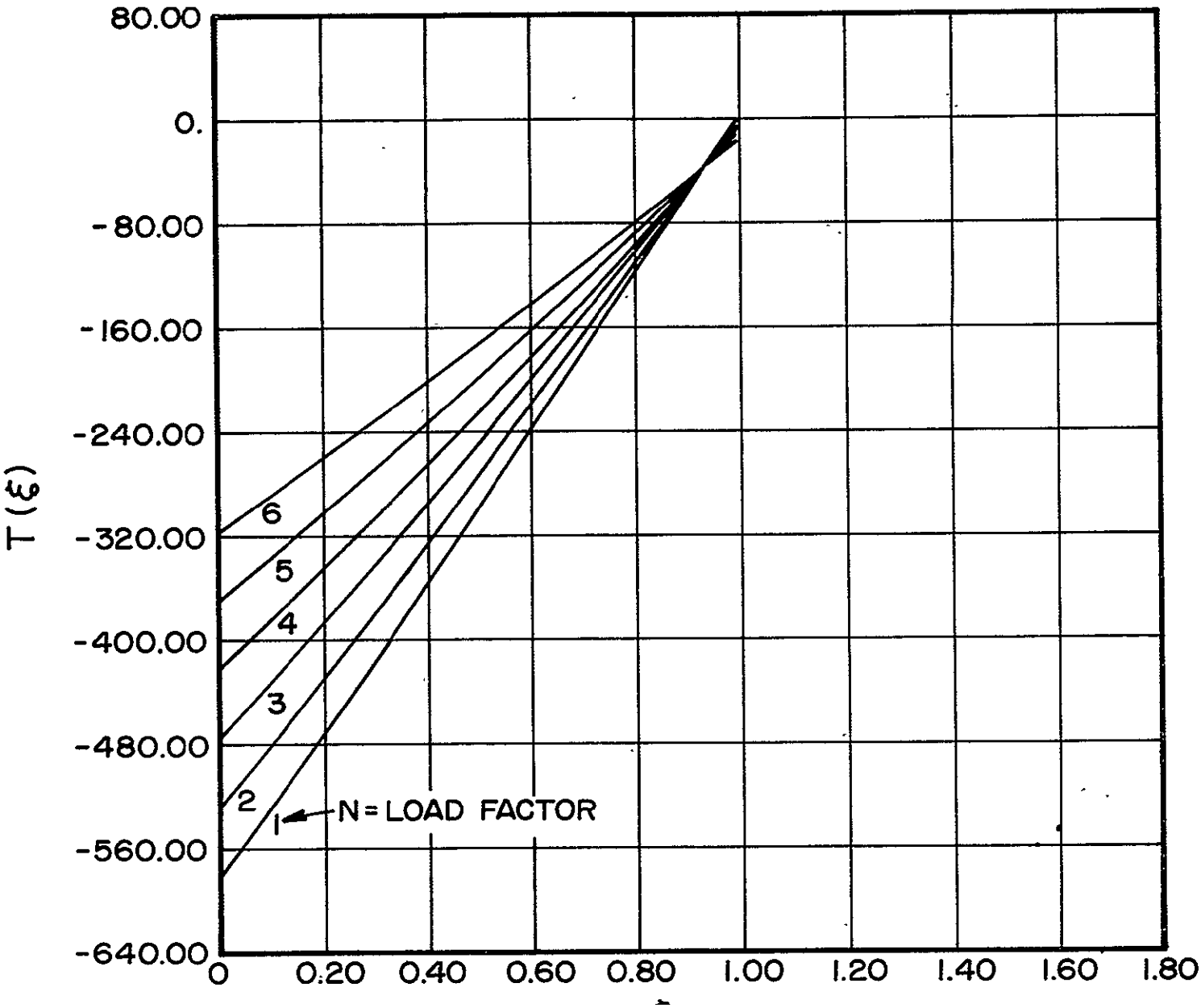

Fig. 51 Elastic wing torque vs. ξ with load factor N as a parameter

In Figures 38 and 39 it is noted that allowing the wing to become fully elastic causes larger negative twist distributions, and that for N = 1 the difference between $\theta(1)_{S.R.}$ and $\theta(1)$ is roughly one-half of a degree. Comparison of the curves in Figures 40 and 41 shows that the outboard sections of the fully elastic wing are less loaded and that (hence) the inboard sections carry more load when compared with the semi-rigid wing. Obviously the center of pressure shifts inboard when the fully elastic analysis is employed. The results of Figures 40 and 41, as well as the corresponding rigid wing angles, are presented in Figure 42. The inboard center of pressure shift is again reflected in the results of the next two series of graphs (Figures 43, 44, 45 and Figures 46, 47, 48) which plot the shear and bending moment distributions for the rigid wing, the semi-rigid wing and the fully elastic wing, respectively.

It is clear from reviewing the results of Figures 38 - 51 and Table VI that a rigid wing analysis gives very erroneous values of all pertinent distribution quantities such as shear, bending moment and torque and presents a very large error in calculating the required root angle (roughly three degrees at load factor N = 1). The distribution quantities are important for their effect on structural integrity and total weight, while the root angle of attack is important because of its relation to the wing-fuselage attachment angle which strongly influences all important

performance quantities (mainly through a non-minimum drag configuration or a non-minimum configuration related to drag and velocity). Further, because of a relatively small value of $\lambda\ell$ (i.e., a torsionally stiff wing and a modest A.C.-E.A. offset distance "e") and a large value of (negative) c_{mac}, the differences between semi-rigid wing and fully elastic wing distribution quantities is generally quite small (and in fact the less rigorous semi-rigid analysis turns out to be a conservative analysis). However, the small differences in $\alpha^r(0)$ and $\alpha^r_{S.R.}(0)$, as well as the distribution differences in $\theta(\xi)$ and $\theta_{S.R.}(\xi)$, should provide different estimates of performance capabilities.

PART III

COMPAD (Computer Aided Design)

COMPAD (Computer Aided Design)
(L. J. Feeser)

The computer aided design portion of the composites project has continued in this reporting period, concentrating for the most part in three separate activities: (a) maintenance and continued enhancement of the finite element computer program, SPAR, (b) initial review of structural optimization programs and (c) preliminary study of the feasibility of the use of array processor technology for improving the speed performance of the program SPAR on our Prime computers.

Considerable effort has been expended on maintaining a working version of SPAR on the Prime computers. Most of this work has been necessary because of updating in the Prime operating system. In addition, a number of students and faculty have obtained hands-on experience in preparing finite element models and coding their input for runs using SPAR. This experience has demonstrated the continued need to keep in close contact with NASA Langley personnel in regard to continued enhancements of SPAR.

The whole area of pre- and post-processing for finite element analysis is moving ahead under the direction of Professor Mark Shephard. Students in his finite element class have been developing individual pieces of a pre-processing system which will be assembled into a trial system during the next six months.

The project has also obtained the documentation of the program ACCESS, a structural optimization program developed by Dr. Lucian Schmidt, under NASA contract. We are evaluating the potential of this program for implementation on our computer systems and for its potential use in structural design related to the composites project.

A preliminary feasibility study has been performed on the potential use of the Floating Point Systems AP120 array processor for speeding up of some of the compute-bound code in SPAR. This preliminary work shows a strong potential for improved speeds. However, the limited study to date has used only the timings from the actual execution of some of the array processor operations and has neglected the transfer times involved in interdevice communications. We have also used only small pieces of code lifted from a number of routines and have not simulated a total SPAR run. The improvements possible in this area are great. We plan to continue these developments as having considerable potential.

PART IV

SUPPORTING RESEARCH

Progress on composites research is reported in the individual write-ups on the succeeding pages in the following areas:

Resin Characterization and Optimization
Moisture Effects on Composite Structural Materials
Optimization of Laminated Plate Design for Shear
Ultrasonic Non-Destructive Testing Developments
Fatigue in Composite Materials
Metal Matrix Composites

The report on Metal Matrix Composites is a final one under this project. While results of interest and high quality are being obtained, they are deemed less appropriate than other investigations as part of the NASA/AFOSR Composite Materials and Structures Research Program at Rensselaer. Accordingly, this work has been concluded under the subject grant.

RESIN CHARACTERIZATION AND OPTIMIZATION

Senior Investigators: G. Diefendorf
C. LeMaistre

A serious problem in the fabrication of composites is the batch-to-batch variation in the properties of resins used as matrix materials. Ideally, provided a particular cure cycle is followed, the cured resin should have reproducible properties. Problems in this regard have been met in the CAPGLIDE program, where difficulties have been experienced with the resin systems. The possibility of incorrect mixing and/or curing has been considered, but the problem has persisted despite close supervision and attention to detail. An examination of the chemistry and related physical properties of commercially available resins has been carried out to see if the present problems can be eliminated.

An additional intent of this investigation is to select an epoxy resin system that produces the optimum composite properties when used as a matrix with carbon fibers. The current wet lay-up practice of using the same epoxy system for glass and carbon fiber reinforcements, while convenient, may not be the best. Investigations of both room temperature and high temperature curing resins have begun.

The resin systems investigated include:

1. Resin Ciba Geigy (Araldite 508 and 509)
   Hardeners XU 224 - Developmental hardener: long pot life (active hydrogen equivalent 143)
   Cure - Room tenperature

2. Resin - Epon 828
   Hardener - Nadi methyl anhydride
   Catalyst - MPDA
   Cure - Up to 150°C

Several analytical methods are being used to characterize the resins in their cured and uncured conditions.

A. High performance liquid chromatography (HPLC):

   Samples of the resins, hardeners and catalysts have been dissolved in tetrahydrofuran (THF) and subjected to HPLC, the initial intention being to obtain a "finger-print" of the currently available resin systems and to use this for comparison with incoming batches of the same resin system. In addition, the mixed but uncured resins have been dissolved in THF and studied with the HPLC as have the cured and semi-cured resins. Initial results have been obtained, and this work is continuing.

B. Infra-red spectroscopy:

   This is under investigation as a tool for determining the species in a resin and the progress of the cure-cycle.

C. Differential scanning calorimeter:

   Epoxy resins during their cure cycle go through an exothermic reaction. The extent of the cure and the effect of additives, etc. can be deduced by noting the occurrence and extent of the exotherm in the "cured" samples. In the case of the Epon 828 system, the

exotherm occurs at approximately 230°C for poorly cured resins. No exotherm is noted for a fully cured resin system.

D. Shear strength:

The shear strength of the "characterized" resins is also under study. In the case of the cured resin without fiber reinforcing, the assembly recommended in ASTM 372 has been fabricated. The cured resin sheet is tested in shear by means of a punch and die assembly. Fiber reinforced systems will be tested by the "short beam" shear test.

As stated in the previous report, the Araldite 509, XU 224 and XU 225 system has an advantage in that, by varying the ratios of XU 224 and XU 225, the gel and pot life of the resin system can be altered. The manufacturer's recommended use of XU 224 and XU 225 to alter gel and pot life is given in Table VII.

TABLE VII
POT LIFE AND GEL TIMES FOR RESIN SYSTEM

Batch	Resin (PBW)[a] A 509	Hardener (PBW) XU 224	Hardener (PBW) XU 225	Pot (hr)	Gel (hr)
1	100	27	30	0.5	0.75
2	100	29	23	1.0	1.25
3	100	34	15	1.5	2.50
4	100	34	9	2.5	3.50
5	100	42	0	3.5	6.00

[a] (PBW) parts by water

The ratio of hardener to resin is calculated on the basis of active hydrogen equivalent. However, there is a variation in the mw of the A 509 (WPE = 189-200) and in the active hydrogen equivalent of XU 224 (AHE = 70-75). The manufacturer's calculations are based on the lowest mw of A 509 (i.e. 189) and highest AHE of XU 224 (i.e. 75) and are thus likely to err on the side of excess hardener additions. These systems are now being analyzed to determine if excess hardener is truly present and if it is the cause of poor cures. The physical properties of the resulting materials are being measured to determine variations whether or not excess hardener is present.

MOISTURE EFFECTS ON COMPOSITE STRUCTURAL MATERIALS

Senior Investigator: S. S. Sternstein

Theoretical studies on the effects of moisture on the physical properties of epoxy resins containing cylindrical fibers have shown that inhomogeneous swelling phenomena may be extremely important in determining internal stresses and strains and moisture gradients. These internal gradients may lead to sufficiently high local stresses as to cause failure of the matrix (precracking). Consideration is presently being given to the problem of defining local instability criteria vis-a-vis our inhomogeneous swelling theory. It appears that there may be critical values of cohesive energy density or crosslink density of the matrix which preclude equilibrium swelling fields from being established. Under such a condition the matrix would literally disintegrate by profuse cracking and chain scission. Such "unzipping" has been known to occur on occasion.

Experimental studies are in progress on the viscoelastic characterization of wet and dry epoxy resins. The purpose here is twofold. First, it is essential to obtain certain data which are needed in the inhomogeneous swelling theory. Second, we intend to obtain a comprehensive and reliable viscoelastic profile of epoxy resins. Several techniques are being utilized, including dynamic mechanical spectroscopy, creep, stress relaxation and thermomechanical analysis.

Temperature ranges from -150°C to 250°C and frequency ranges from 0.1 Hz to 100 Hz are being investigated using several sample geometries and modes of loading, e.g., tension, compression and shear.

OPTIMIZATION OF LAMINATED PLATE DESIGN FOR SHEAR*

Senior Investigator: Y. Hirano

The objective of this program was to apply a mathematical optimization technique (Powell's method) to find the fiber directions in each layer of a laminated plate that give the highest shear buckling stress. The plates considered are laminates of N orthotropic layers whose principal material axes coincide with the plate axes. Each layer is assumed to have the same thickness and an equal number of fibers in the direction of $+\alpha_i$ and $-\alpha_i$ with respect to the plate axes (x-axes).

Shear buckling stresses of the plates were calculated by utilizing Galerkin's method. A computer code, developed by Powell, was rearranged into the code written for the calculation of shear buckling stress. The numerical calculations were made for boron/epoxy plates with length to width ratios, or "aspect ratio", R = a/b = 1, 1.5 and 3. The calculation was first carried out for three-layered plates with a/b = 1. An example of the numerical convergence for this case is shown in Figure 52. In this figure Ψ is defined as $\pi^4/(32\bar{N}xyb^2R^3)$, where $\bar{N}xy$ is shearing force per unit width, b is the width of the plates and R is the aspect ratio of the plates. Next, the calculation was made for the case of

---

* A note related to this work has been accepted for publication in the AIAA Journal.

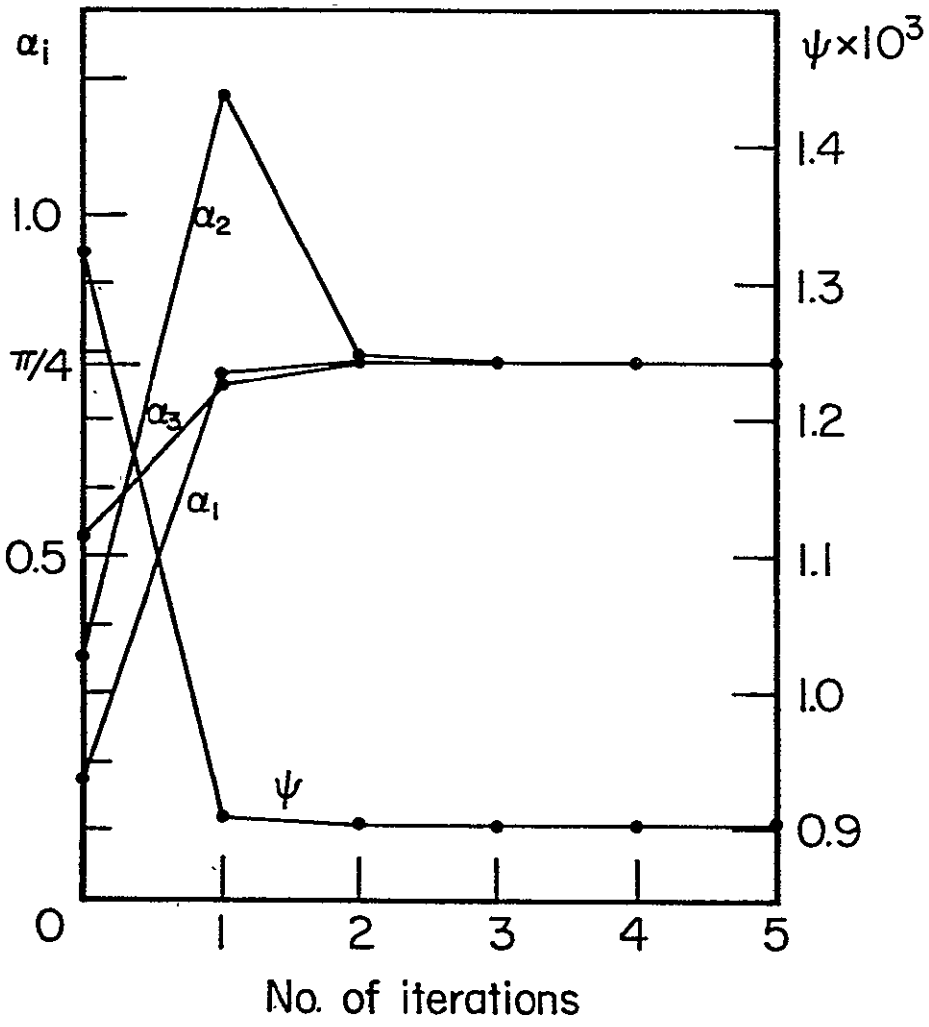

Fig. 52 Variation of α_i and ψ with number of iterations

six-layered plates with a/b = 1, 1.5 and 3. The numerical results for the case a/b = 1.5 are shown in Table VIII. Asterisks in this table indicate that the numerical calculations were stopped because maximum changes in the single variable search did not alter the objective function values.

From Table VIII and from the results for the cases R = 1 and 3, the following conclusions were drawn:

1) An angle-ply laminate gives the highest shear buckling stress with the optimum fiber direction varying with the length to width ratio.

2) The method appears to converge to the optimum with virtually any choice of initial fiber direction.

3) The best fiber directions for the cases R = 1, 1.5 and 3 are ±45°, ±55° and ±60° respectively.

Shear buckling stresses of angle-ply laminated plates with various aspect ratios were calculated, and the results are shown in Figure 53. From this figure we can find the best fiber directions of laminated plates under shear, for aspect ratios from 1.0 to 5.0.

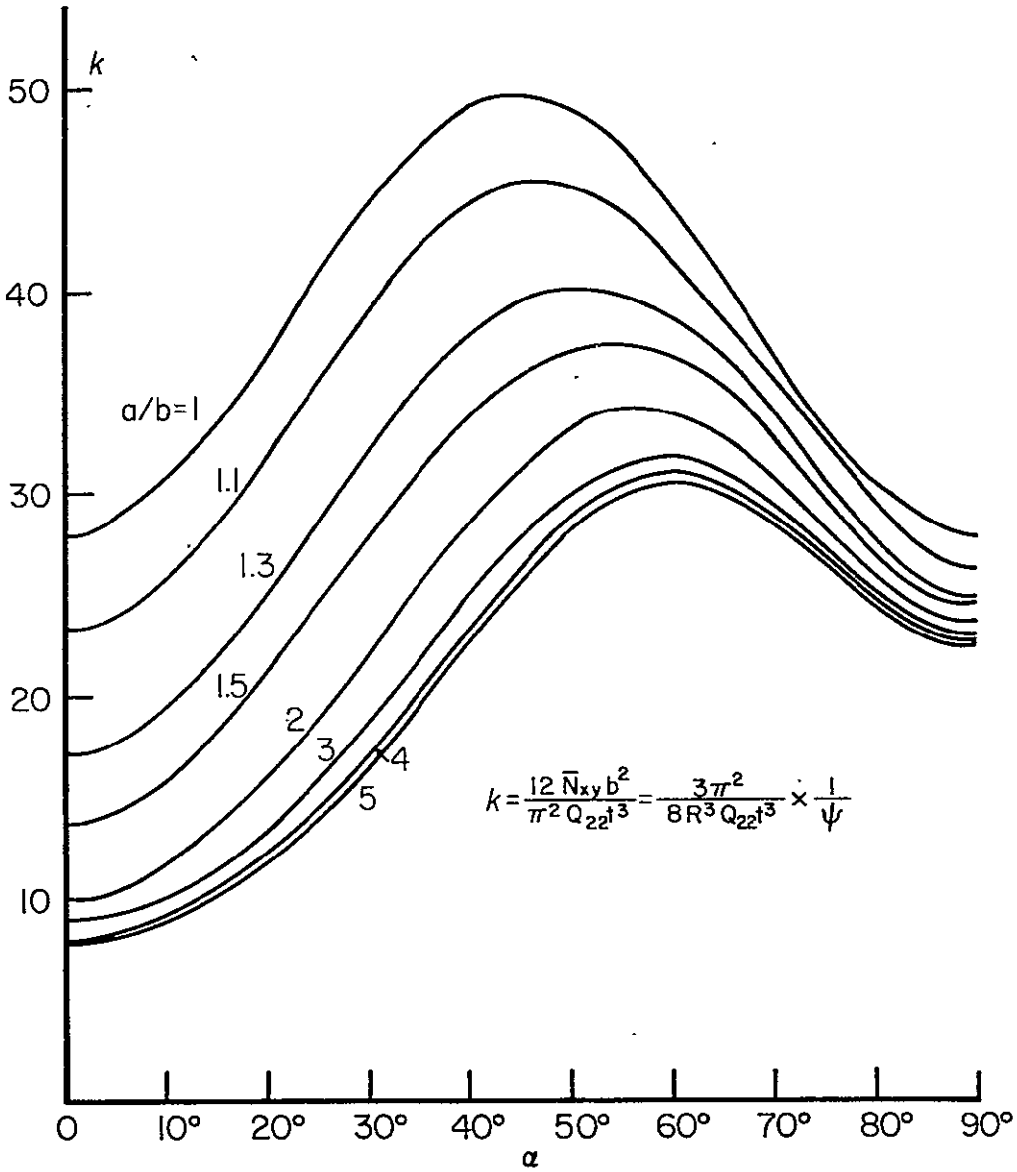

Fig. 53 Shear buckling force of angle-ply laminated plates

TABLE VIII

OPTIMUM FIBER DIRECTIONS FOR 6-LAYERED PLATES WITH a/b = 1.5

Case		Fiber Directions (in degree) α_1	α_2	α_3	α_4	α_5	α_6	$\psi \times 10^5$
1	S	0.0	0.0	0.0	0.0	0.0	0.0	12.279
	F	54.6	54.5	54.4	54.3	54.6	54.5	4.4804
2	S	30.0	30.0	30.0	30.0	30.0	30.0	6.0322
	F	54.7	54.4	54.6	54.6	54.7	54.5	4.4805
3	S	45.0	45.0	45.0	45.0	45.0	45.0	4.6801
	F	54.5	54.7	54.2	54.3	54.8	54.4	4.4805
4	S	90.0	0.0	90.0	0.0	90.0	0.0	6.8648
	F	*	*	*	*	*	*	*
5	S	45.0	45.0	0.0	0.0	45.0	45.0	4.7749
	F	*	*	*	*	*	*	*
6	S	0.0	0.0	45.0	45.0	0.0	0.0	11.516
	F	54.5	54.5	55.2	55.1	54.4	54.7	4.4805
7	S	10.0	20.0	30.0	40.0	50.0	60.0	8.3499
	F	54.6	54.3	54.6	54.1	54.6	54.5	4.4805
8	S	0.0	0.0	45.0	45.0	90.0	90.0	12.486
	F	54.4	64.7	54.1	54.6	125.6	125.5	4.4805
9	S	90.0	90.0	90.0	90.0	90.0	90.0	6.7886
	F	126.0	125.4	90.3	90.4	124.9	126.3	4.5004
10	S	60.0	60.0	60.0	60.0	60.0	60.0	4.5425
	F	54.6	54.4	54.3	54.1	54.4	54.6	4.4805

S: starting values

F: final optimum values

ULTRASONIC NON-DESTRUCTIVE TESTING DEVELOPMENTS

Senior Investigators: H. F. Tiersten
P. K. Das

Since the last report was submitted considerable experimental work has been done in measuring the influence of a tuning inductor on the bandwidth and sensitivity of the trapped energy mode transducer. The inductances employed have been systematically increased to relatively large values, and 3 db bandwidths of the order of 20% of the center frequency have been measured. The inductances have served not only to increase the bandwidth but to increase the sensitivity as well. In fact, in an experiment in which the trapped energy modes are reflected from the surface of the water at normal incidence and detected by the transducer, the ratio of the detected to the applied voltage is less than 20 db.

In the experiments on the monolithic mosaic transducer that have been performed to date, a certain very interesting, hitherto unreported and presently not fully explained phenomenon has been observed. As the frequency is decreased below the point at which ordinary trapping disappears, a very sensitive trapped mode occurs over a very narrow frequency band and then disappears as the frequency is lowered further. With a further decrease in driving frequency a somewhat less sensitive trapped mode occurs, which has a large bandwidth and disappears at a very low frequency. In all cases the existence of energy trapping has been verified by measuring

the mode shape by means of the acousto-optic diffraction of a laser beam. Although at most frequencies the trapped mode shape has a single maximum at the center of the electrode, at certain frequencies the trapped mode exhibits a more complicated shape with two maxima across the electrode and a local minimum at the center.

The computer interfacing for obtaining images from raw transducer data has been significantly improved, and considerably better images are now being obtained. The instrumentation for the excitation and detection of the fundamental extensional and flexural plate waves (surface waves) has been improved.

The analysis of the thickness-extensional trapped energy mode transducer with strip electrodes, in which only the one dominant wave in each region is retained, has been extended to include the coupling with certain other waves that exhibit dispersion curves near that of the dominant wave. The frequency spectrum obtained from the extended analysis is more complicated than the previous one in that a splitting appears, which is caused by the coupling of two independent sets of solutions. When the driving frequency is such that the two split modes exist in a strong coupling region, the aforementioned unusual mode shape with two maxima across the electrodes exists. Under other circumstances the usual mode shape with one maximum at the center exists. Work has been started on determining the lowest complex dispersion curves

for the symmetric extensional waves in an infinite PZT-7A plate for both the unelectroded case and that of the shorted electrodes, which are needed for the explanation of the aforementioned observed behavior of the trapped energy modes in the lower frequency range.

FATIGUE IN COMPOSITE STRUCTURES

Senior Investigator: E. Krempl

Two different uniaxial fatigue test specimen designs were evaluated. A straight sided specimen with thin tabs was shown to be superior to a dog-bone shaped specimen. Static and fatigue tests were performed on unidirectional, cross-ply and quasi-isotropic graphite-epoxy laminates. For the quasi-isotropic laminates, a significant effect of R-ratio* and a significant effect of frequency was observed.

All laminates were made at RPI from HY-E1030 (T300-934) graphite epoxy, manufactured by Fiberite Corporation, using the cure cycle recommended by the manufacturer. Each laminate consisted of twelve graphite plies; unidirectional, cross-ply and quasi-isotropic laminates were made. The stress-strain diagrams of these laminates are shown in Figure 54. The reduction in stiffness and strength with an increase of the number of non-zero degree plies is obvious.

For fatigue testing we considered a dog-bone type and a straight-sided type specimen, as shown in Figure 55. According to ASTM D3039-76, straight-sided specimens show a greater number of failures in the gauge length than the dog-bone type specimens. Accordingly the straight-sided specimens were used for the fatigue studies.

Fatigue tests were performed on symmetric laminates $[0/(\pm 45)_2/90]_S$ and $[90/(\mp 45)/0]_S$. Figure 56 shows that the

* The ratio of alternating to steady stress level.

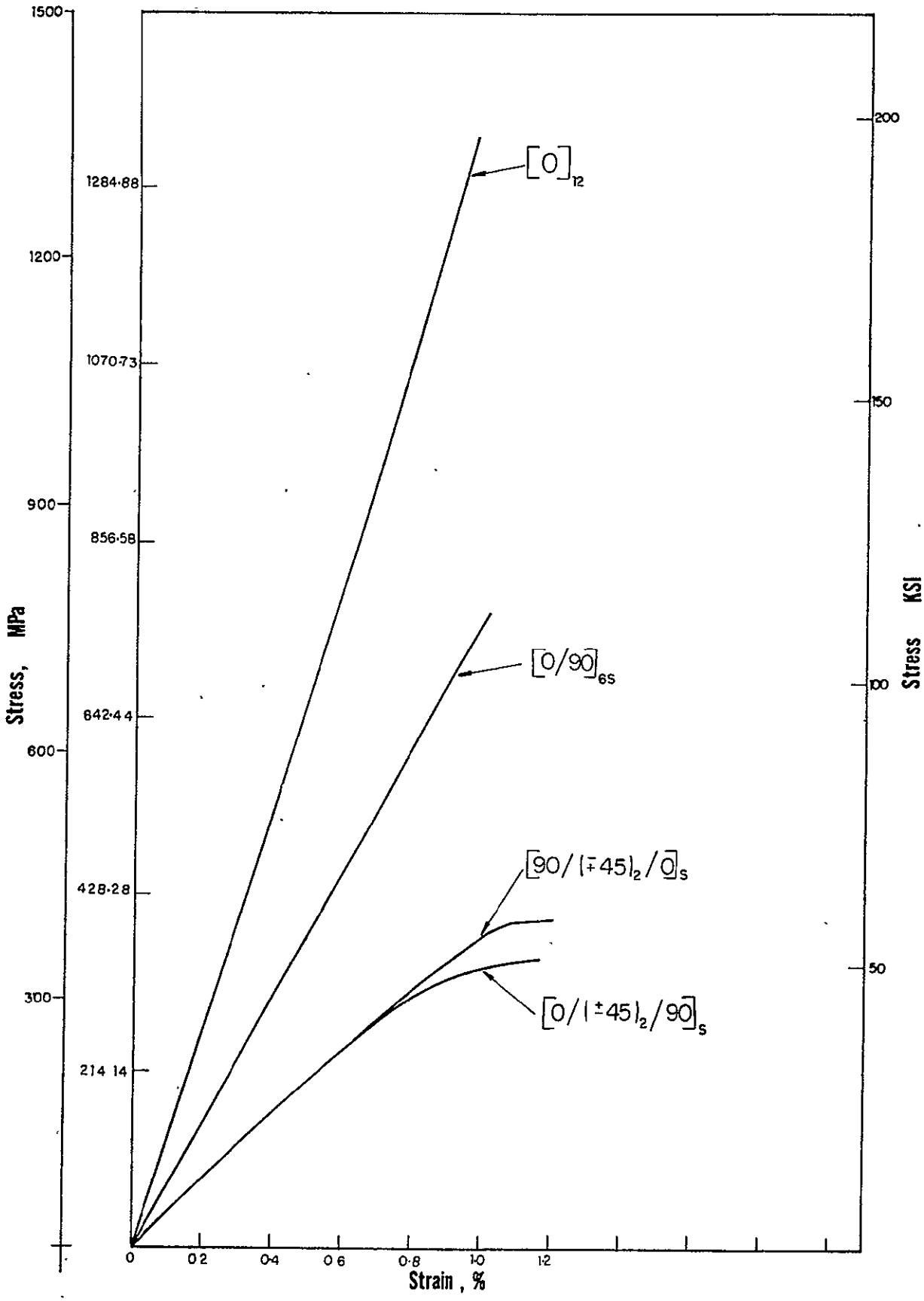

Fig. 54 Stress-strain diagram for unidirectional, cross-ply, and quasi-isotropic graphite-epoxy laminates

SPECIMEN DESIGN

DOG-BONE SPECIMEN

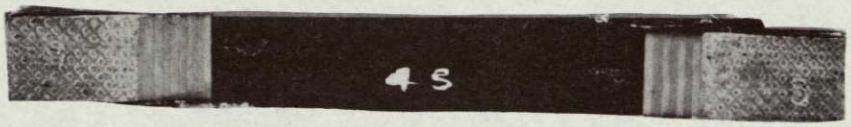

STRAIGHT-SIDED SPECIMEN
ASTM D3039 – 76

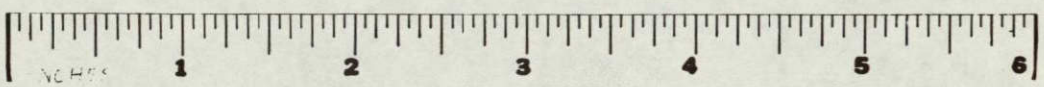

Fig. 55

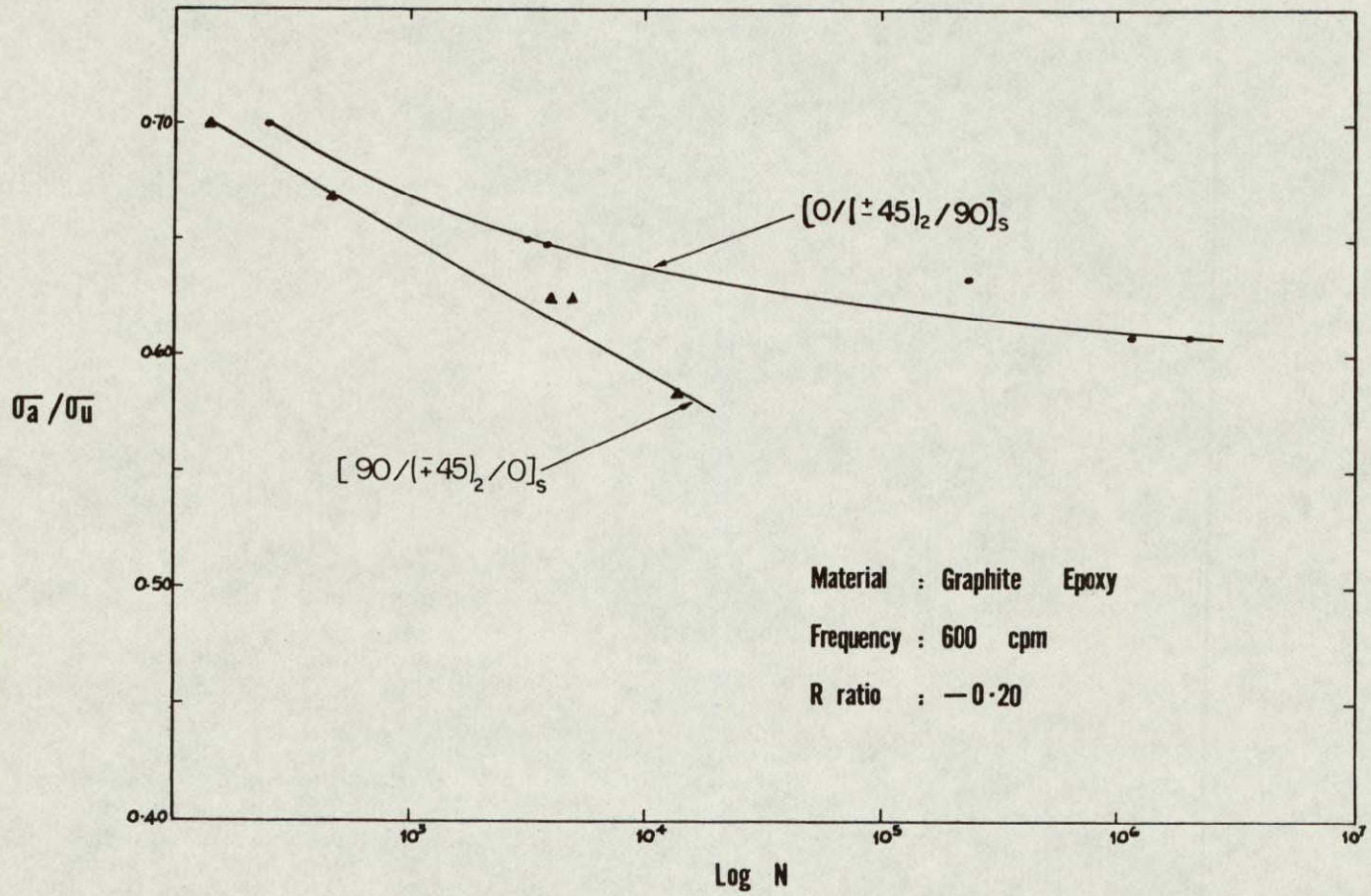
0·70
0·60
0·50
0·40
σ_a / σ_u
$[0/(\pm 45)_2/90]_s$
$[90/(\mp 45)_2/0]_s$
Material : Graphite Epoxy
Frequency : 600 cpm
R ratio : −0·20
10^3
10^4
10^5
10^6
10^7
Log N

Fig. 56

$[0/(\pm 45)_2/90]_S$ has a better fatigue performance than the $[90/(\mp 45)_2/0]_S$ laminate for an R-ratio of -0.20. This R-ratio could be obtained without buckling of the specimens. Photographs of failed specimens are given in Figure 57. The failures in the gauge section are very well visible. The test results, shown in Figure 58, indicate that frequency has a considerable effect on the fatigue life of $[90/(\mp 45)_2 0]_S$ laminates. We find this an effect of considerable significance. Other fatigue tests using approximate R-ratios of .66 produced results with considerable scatter. We also measured the stress-strain diagram of specimens made of $[90/(\mp 45)_2 0]_S$ laminates which we subjected to fatigue cycling but not tested to failure. The stress-strain diagrams of these cycled specimens were different from those obtained on virgin specimens of the same laminates.

We will continue fatigue testing to further explore the effects of R-ratio and frequency on composite structural materials.

TYPICAL FAILURE MODES IN TENSION-COMPRESSION FATIGUE

GRAPHITE - EPOXY COMPOSITE R - RATIO = −0·20

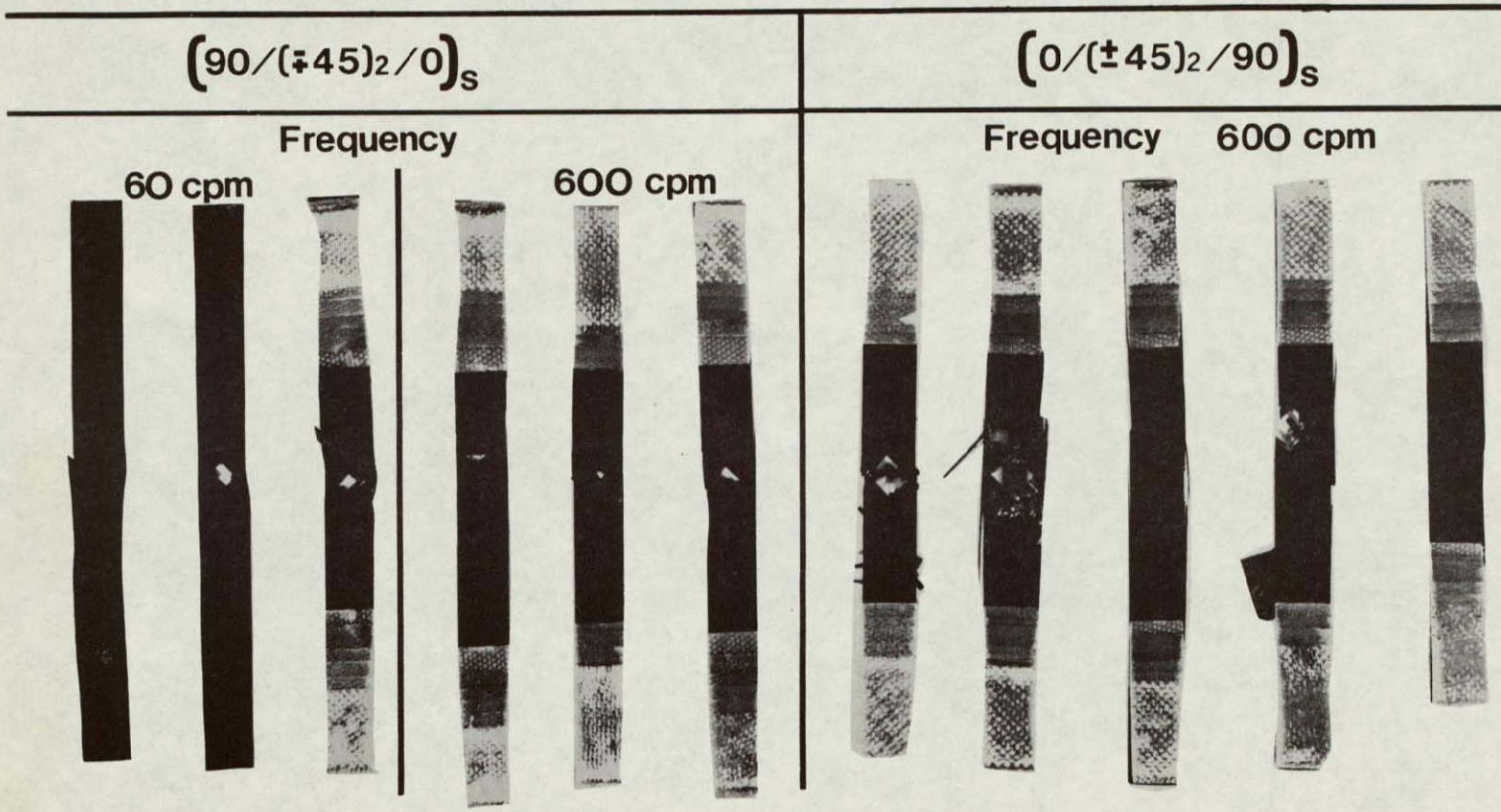

Fig. 57

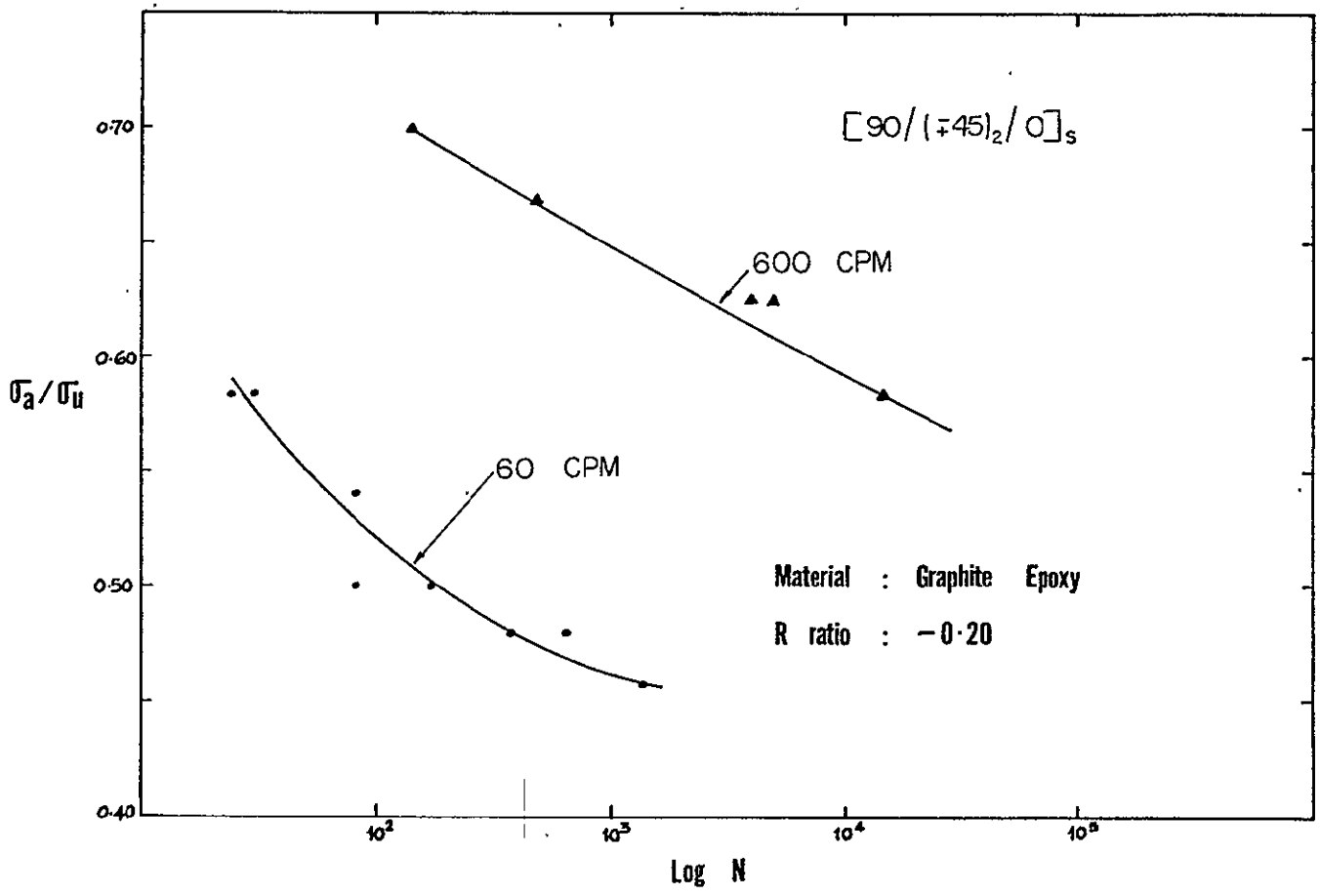
[90/(∓45)2/0]s
600 CPM
60 CPM
Material : Graphite Epoxy
R ratio : −0·20
σa/σu
0·70
0·60
0·50
0·40
10²
10³
10⁴
10⁵
Log N

Fig. 58

METAL MATRIX COMPOSITES

Senior Investigator: N. S. Stoloff

The objective of this program has been to determine those microstructural factors that control the mechanical behavior of advanced metal matrix composites. Since the directionally solidified Ni-Al-Mo eutectic system has good tensile, creep and fatigue properties, it was chosen for study. Mechanical tests have been performed on AG-15 (Ni, 17.7a%Al,16.3a%Mo) and AG-34 (Ni,14.4%Al,20.0%Mo) in the aligned condition.

The room temperature fatigue lives of both alloys were superior in vacuum to properties in air. In testing done at a frequency of 20 hz and a constant minimum stress of 5 ksi, the 10^7 endurance limit of AG-34 was increased from a peak stress of 120 ksi in air, to a peak stress of 140 ksi in vacuum. At 140 ksi the improvement in life was three-fold, whereas, at 160 ksi, the increase was less dramatic (2.5 times). AG-15 showed a ten fold improvement in life for vacuum tests at peak stresses of 130 and 110 ksi.

As reported earlier, fatigue crack initiation occurs at the surface in testing done at room temperature, while initiation at the center of the specimen was evident at 825°C. This indicates that creep plays a significant role in fatigue at 825°C. Additional tests conducted at 725°C have shown that creep processes are minimized at high frequencies. Following a trend established earlier with

tensile properties, the fatigue strength of AG-15 is highest at intermediate temperatures. The life at 110 ksi is fifty times greater at 725°C than at 825°C; it is also six times greater than the life at 25°C. Frequency variations at 725°C in S-N and crack propagation tests will be used to further characterize the creep-fatigue interaction in AG-15.

Initial transmission electron microscopy (TEM) studies on as-DS AG-15 and AG-34 show a predominantly γ' (Ni_3Al) matrix with α (Mo) fibers. AG-15 shows less residual γ (Ni-rich solid solution) due to its higher Al content. Solution-treated and aged specimens of AG-34 show a distribution of fine (0.2μm) γ' in the γ matrix. The as-DS substructure exhibits planar arrays of dislocations in the γ' matrix and looped dislocations in the bcc Mo fiber.

Additional hydrogen embrittlement studies have been carried out on AG-15 and AG-34. Molybdenum fibers, which undergo ductile fracture in unchanged specimens, reveal many brittle-appearing cracks after simultaneous charging and tensile testing. Embrittlement of the fibers by hydrogen seems to be the major cause of embrittlement of the composite.

PART V

PERSONNEL

AUTHOR INDEX

PERSONNEL

Senior Investigators

Brunelle, E. J., Jr., Sc.D. (Aeroelastic and structures design and analysis, CAP-GLIDE)*	Associate Professor of Aeronautical Engineering
Das, P. K., Ph.D. (Non-destructive evaluation, research)*	Professor of Electrical and Systems Engineering
Diefendorf, R. J., Ph.D. (Fabrication, CAPGLIDE; fiber behavior, research)*	Professor of Materials Engineering
Feeser, L. J., Ph.D. (Computer applications and graphics, computer aided design, optimization)*	Professor of Civil Engineering
Hagerup, H. J., Ph.D. (Aerodynamics, configuration, pilot accommodation, CAPGLIDE)*	Associate Professor of Aeronautical Engineering
Helwig, G., Dr.Ing. (Finite element methods, computer aided design, composite structure optimization, CAPGLIDE)*	Research Assistant Professor of Aeronautical Engineering
Hirano, Y., Ph.D. (Structures, composite buckling)*	Visiting Professor of Aeronautical and Mechanical Engineering
Hoff, N. J., Ph.D. (Structural design and analysis, CAPGLIDE)*	John A. Clark and Edward T. Crossan Professor of Engineering
Krempl, E., Dr.Ing. (Fatigue studies, research)*	Professor of Mechanics and Director of Cyclic Strain Laboratory
Sternstein, S. S., Ph.D. (Failure analysis, matrix behavior, research)*	William Weightman Walker Professor of Polymer Engineering

* Fields of Speciality

Stoloff, N. S., Ph.D. (Directionally solidified eutectics, research)*	Professor of Materials Engineering
Tiersten, H. F., Ph.D. (Non-destructive evaluation theory, research)*	Professor of Mechanics

Research Staff

Research Associates

Kenmochi, Kiyoshi, Ph.D.
LeMaistre, Christopher, Ph.D.
Sinha, Bikash K., Ph.D.

Graduate Assistants

Altman, Carl, B.A.
Berg, R. William, B.S.
Chan, Ka-Tung, B.S.
Chen, Lien-Wen, M.S.
Ely, Dale R., B.A.
Fisher, Mark Thomas, B.S.
Hoskote, Mangesh, B.E.
Kim, Wonsub, B.S.
Klein, Leigh, B.S.
Meyer, Bruce, M.S.
Muser, Cristoph, Dipl.Mech.Ing.
Rosenthal, Jay, B.S.
Seagroves, William, B.A.
Shick, D.V., B.S.
Sundaram, Viswanath, M.S.
Talley, S., B.S.
Tartaglia, John M., B.S.
Teferra, Michael, M.S.
Van Shoonveld, H. Garrit, B.S.
Yang, Phillip, B.S.

Undergraduate Assistants - Seniors

Donnelly, J. Patrick
Ezzo, Jeffrey
Lenyo, John S.
Melnyk, Michael S.
Reusch, David
Shaefer, Paul
Shoales, Gregory A.
Speicher, Terrance L.
Weisenger, Norman
Venner, Joseph
Rogers, R. George

* Fields of Speciality

Undergraduate Assistants - Juniors

Borfitz, Michael
Chast, George
Coy, Paul F.
Dearborn, John
Emmel, John
Fallon, William
Flint, Fred
Fortune, James
Gorley, Ronald
Grandon, Albert
Kearns, Thomas
Marchisotto, Paul
Riker, Steven
Schriber, Steven
Schwitter, William
Snyder, Scott
Tavares, Mario
Van Etten, Charles
Wetzel, Eric
Witte, Mark

AUTHOR INDEX

N79-20235

Oversize pages

Do not use

for

Printing

Case file

EXPLODED VIEW

(Muser Design)

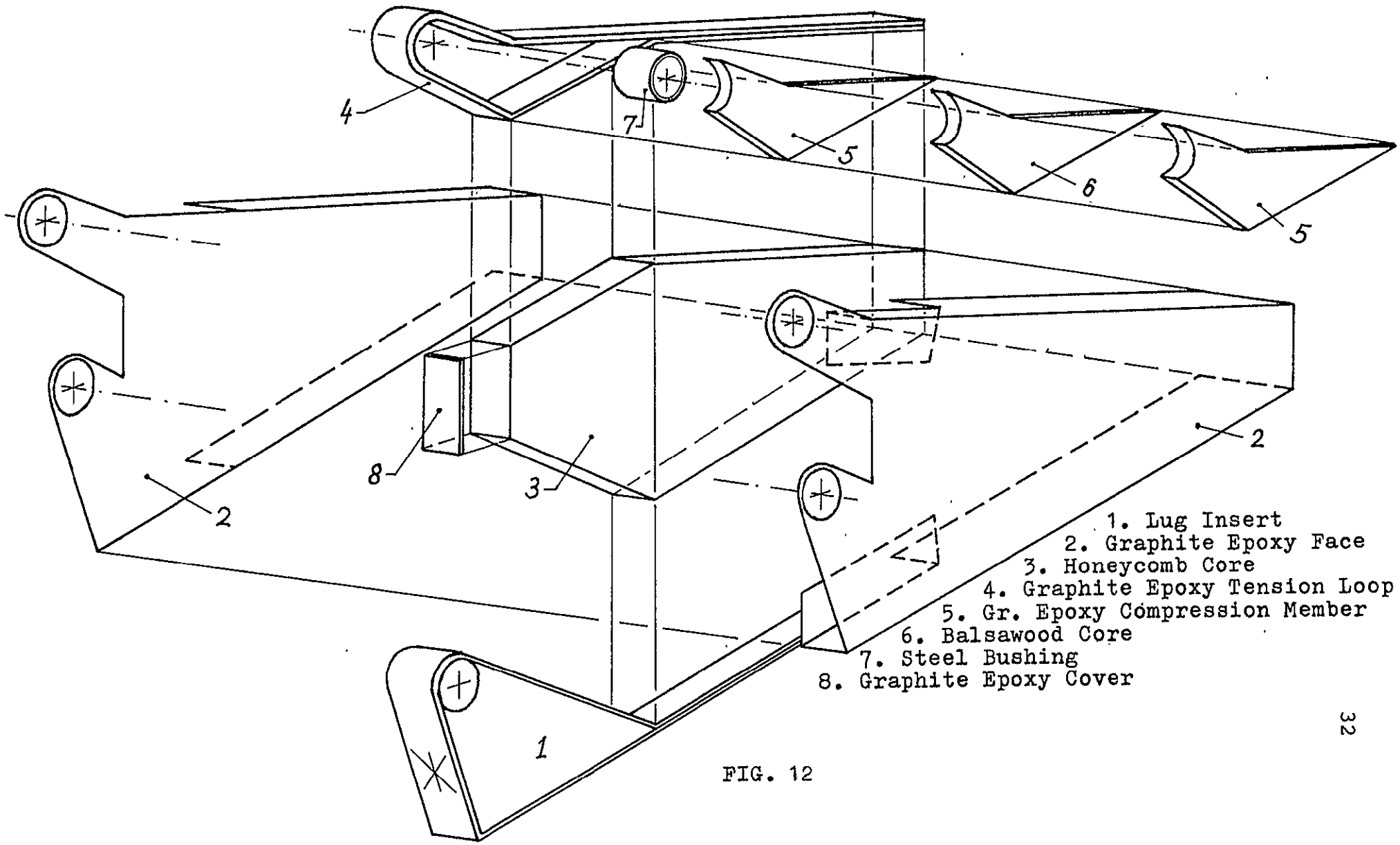

1. Lug Insert
2. Graphite Epoxy Face
3. Honeycomb Core
4. Graphite Epoxy Tension Loop
5. Gr. Epoxy Compression Member
6. Balsawood Core
7. Steel Bushing
8. Graphite Epoxy Cover

FIG. 12

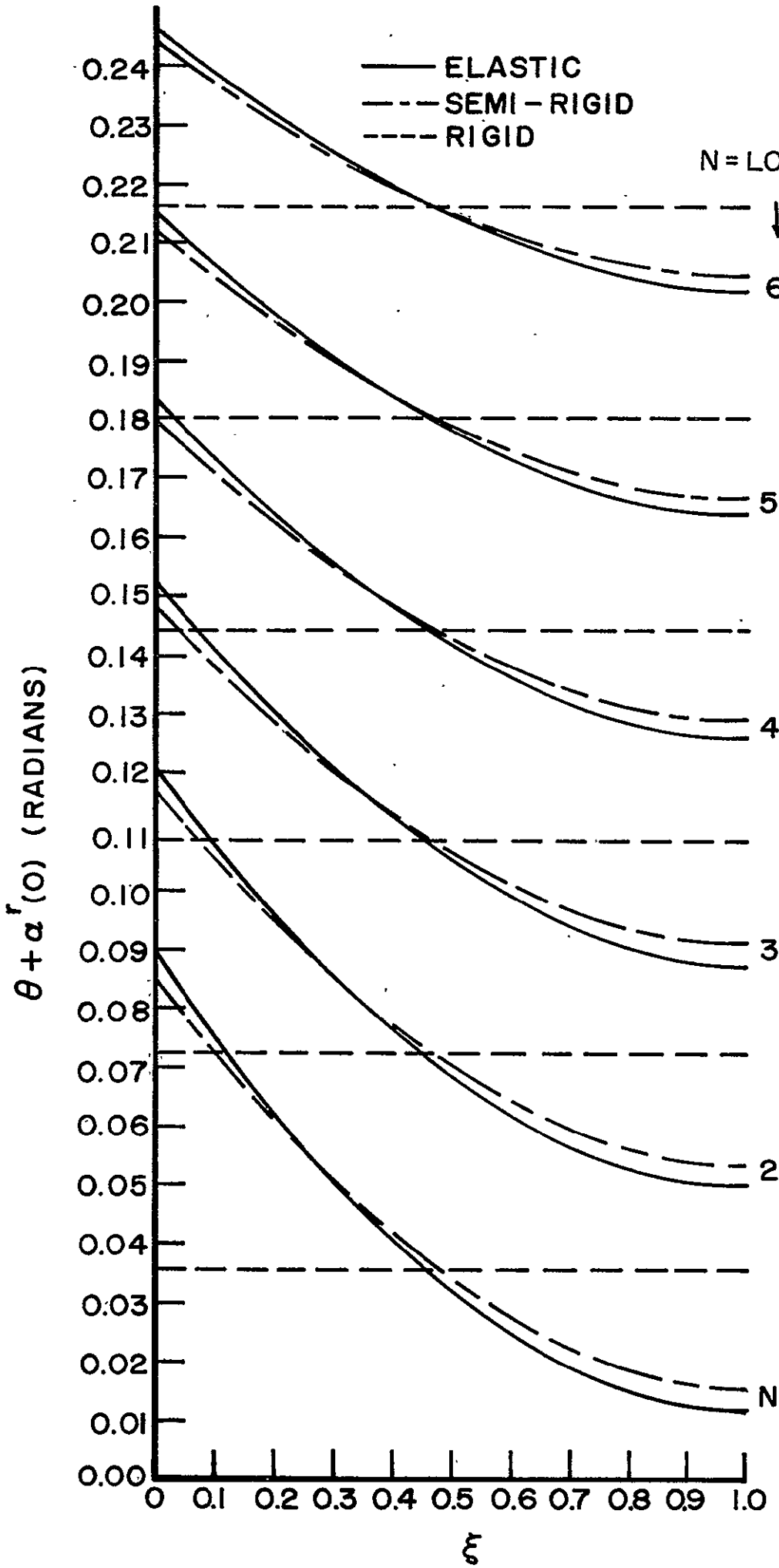

Fig. 42 Total wing angles vs. ξ with load factor as a parameter for the elastic wing, semi-rigid wing, and rigid wing

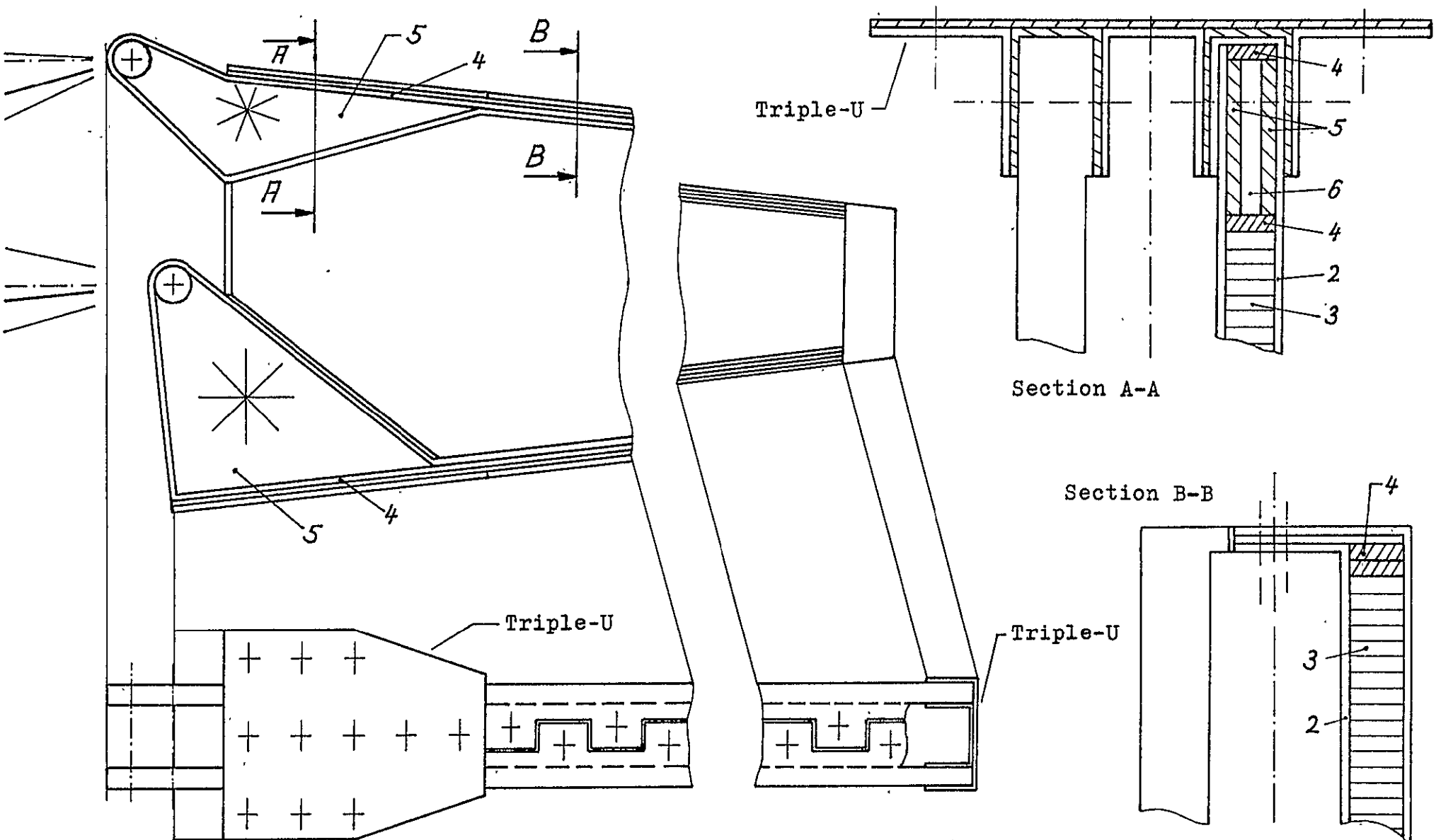

FIG. 13 DETAILS OF THE DESIGN (Muser)